Polymeric and Microrheological Characterization of the *Staphylococcus epidermidis* Biofilm Polysaccharide

by

Mahesh Ganesan

A dissertation submitted in partial fulfillment
of the requirements for the degree of
Doctor of Philosophy
(Chemical Engineering)
in the University of Michigan
2015

Doctoral Committee:

Professor Michael J. Solomon, Chair
Professor Ronald G. Larson
Professor John G. Younger
Professor Robert M. Ziff

To my parents Mrs. Jayashree Ganesan and Mr. Ganesan Baskara Iyer and my wonderful brother Nikhilesh Ganesan

ACKNOWLEDGMENTS

The 2009 Nobel Laureate for Chemistry, Dr. Venkatraman Ramakrishnan, in an award ceremony said – " *…the other lesson I've learnt is, none of us does anything by ourselves. All of them, even natural geniuses, have had amazing chance elements that they have met … as scientists, we have had mentors, we have had people we have randomly connected with that have influenced us in our lives. We never achieve anything by ourselves; we achieve it by a community of people around us…*"

In that spirit, I am immensely obliged to pay gratitude to several people. Acknowledging their support by talking about them in paragraphs, would implicitly impart an ordering about their contribution, or might, convey to the reader that, I have talked about them in an order of importance or respect or magnitude of contribution. Such is not true, for, what I was able to do during graduate school at the University of Michigan, was what I was fortunate to be a part of. I humbly bow down to everyone, in whose journey of life I was fortunate to be a part of, who have helped me at innumerable instances and without whom, graduate school life would not have been possible. I realize that nothing is mine; I am just a part of what is.

If I were to discuss my gratitude to all those who have helped me all along, it would necessitate that I do so by keeping some form a yard stick, with respect to which I would have to comment about their role during this graduate school period. For example – comments such as "…His advice and support to me was the most valuable.." or , "….working with him has been a great

motivating experience for me…" all contain quantifying terms such as "most valuable" or "great experience" etc., which by default, in there very construction, are relative. I concede that I feel incapable of paying such attributes to the people who have helped me. The mere use of the word 'help' implies a sense of quantification, which again, would require a zero point, against which I would say "most helpful" or, "very helpful" etc. The vocabulary in any language that I know fails to even barely describe the mammoth gratitude that I have towards everyone, anyone and all.

In this acknowledgement, I also convey my obligation and lifelong responsibility to give back what I was fortunate to receive. For, Dr. Ramakrishnan finished his speech by saying *"…just as people have helped us along, it's our job to help others achieve their dreams. So thank you very much*."

TABLE OF CONTENTS

LIST OF FIGURES

LIST OF TABLES

ABSTRACT

In this dissertation, we report that the extracellular polysaccharide intercellular adhesin (PIA) present in biofilms formed by *Staphylococcus epidermidis* exhibits self-associations and complexations with proteins in dilute solutions and collectively displays a viscous and elastic response at concentrations found within shaker grown biofilms. Biofilms are naturally occurring viscoelastic soft matter consisting of bacterial aggregates embedded in a self-produced matrix of extracellular polymers (EPS). Biofilms formed by *S. epidermidis* are frequent causative agents of hospital acquired blood stream infections in patients. In such settings, the ability of the biofilm to withstand blood shear stresses and resist host immune responses is primarily attributed to the presence of PIA within the EPS. Here, we aim to understand how PIA contributes towards the viscoelasticity in *S. epidermidis* biofilms.

We use techniques of size exclusion chromatography and multi-angle laser light scattering to measure the molar mass (~ 200 kDa) and radius of gyration (~30 nm) of PIA. We find that the polymer exhibits pH induced self-association and complexation with proteins at all concentrations of PIA greater than 0.3×10^{-2} wt. %. Using diffusing wave spectroscopy microrheology, we identify that PIA exhibits a purely viscous response for concentrations less than 1.6 wt. %, and for concentrations greater than 1.6 wt. %, PIA obeys a zero-shear specific viscosity versus concentration scaling as $\eta_{sp} \sim c^{3.25 \pm 0.62}$, while at concentrations greater than 4.8 wt .%, the loss, G" and the storage, G' modulus of PIA were congruent with a frequency

dependence of G" ≅ G' ~ $\omega^{0.6}$. Furthermore, at PIA concentrations greater than 1.6 wt. %, a polymeric mixture consisting of PIA, bovine serum albumin and λ-DNA, simulating a biofilm EPS, was found to exhibit a 50-fold increase in elasticity than PIA alone. By comparing the rheology of PIA and the entire biofilm EPS at their *in situ* concentrations against microrheological measurements of a biofilm, we identify that these polymers, on their own, do not generate the elasticity as observed in mature biofilms. To better understand the origin of this gap, we report the self-assembly of an artificial biofilm-like construct using planktonic cells and the model polysaccharide chitosan. The artificial constructs exhibited mechanical properties similar to that of naturally occurring biofilms. Specifically, we find that, the elasticity, or the onset of long time plateau in the creep compliance of mature biofilms is mediated by pH induced phase instability of these polysaccharides. Using this finding, we saw that increasing the pH of the solvent environment resulted in softening of a mature biofilm within duration of 3 – 4 hours. Thus, the interactions between the bacterial cells and the extracellular polymers was dependent on the pH of the surrounding environment, which, when changed, resulted in either an onset or dispersal of biofilm viscoelasticity. Collectively, the dissertation provides structural and rheological characterization to support future multi-component modeling of biofilm viscoelasticity. It suggests possibilities for development of biofilm treatment techniques where physical changes to the biofilm growth environment can lead to weakening of the EPS matrix, thus rendering embedded cells vulnerable.

In order to develop medical procedures aimed towards biofilm softening, a primary diagnostic step would be to measure the elasticity of the formed biofilm. We propose that, the technique of cavitation rheometry is a potential *in vivo* diagnostic tool for assaying the elasticity of biological soft materials. Here, we derive a relation between the pressure required to induce

cavitation in soft materials of arbitrary volumes with their elastic modulus. This relation will be shown to extend the scope of cavitation rheometry to measure elasticity of materials of volumes as small as few microliters, similar to biofilms formed in infection sites. Rapid measurements of biofilm elasticity would provide qualitative insight into the maturity and amount of biofilm contamination that supports subsequent therapeutics.

CHAPTER 1

Introduction

In the domain of microbial organisms, the bacterial subdomain has been known to exist and thrive since about 3 billion years ago. In a laboratory setting, bacteria are commonly cultured as suspensions of planktonic cells in shaker flasks, however, in their natural habitat; bacteria often exist in a structurally and mechanically complex phenotype called 'biofilms'. Bacterial biofilms are surface attached, multi-cellular aggregates that encapsulate and protect themselves within a matrix of self-produced extracellular polymeric substances (EPS)[1,2]. The EPS consists predominantly of polysaccharides, in addition to proteins and nucleic acids[3–5]. In this dissertation, we employ techniques of chromatography, light scattering, microrheology, colloidal physics and microbiological assays to measure and correlate the rheology of a biofilm and its EPS polymers. The motivation for such a study is the following.

Bacterial biofilms thrive in a variety of environments such as hydrothermal vents, ship hulls and on the surfaces of medical implants, withstanding detrimental forces like high temperature, shear and antibiotic attack[6]. Amongst them, biofilm contamination of medical implants, such as central venous catheters and orthopedic prosthesis in humans[7,8] is a threatening and expensive harm caused by their growth[9]. In such cases, the presence of the EPS polysaccharides makes the biofilm bacteria resilient to blood shear stresses, host immune responses such as phagocytosis and antibiotic action[3,10–15]. Such resistances makes biofilms chronic resulting in diseases like

septicemia, periodontitis and urinary tract infections[11]. The treatment of biofilm infections has thus necessitated surgical removal of the implant, an expensive procedure[9]. Amongst research efforts directed towards reducing disease burden, studying the composition and significance of EPS polymers in the biofilm life cycle has received much attention in the past decade[16,17]. In this dissertation, we advance the understanding by probing the polymeric and rheological properties of these EPS polymers.

1.1 Importance of the extracellular polymers in the biofilm life cycle

Biofilm formation on medical implants is typically initiated when bacteria enter the host blood stream when a susceptible host, undergoing medical treatment, is prone to cross contamination from the hospital environment[18,19]. Once within the blood stream, presence of extracellular binding proteins[20] enables the bacteria to adhere onto surfaces of artificial implants (Fig. 1.1)[21]. Following attachment, the bacteria reproduce and mature into their biofilm phenotype through secretion of the EPS matrix (Fig. 1.1). The EPS polymers are important for biofilm formation, mechanical properties and antibiotic resistance in the following way: i) the adhesive property of EPS polymers facilitates the tight packing of the biofilm bacteria[22–27]; ii) a mature biofilm's ability to undergo reversible and irreversible deformation and resist premature fragmentation under shear stress is mediated by the polysaccharides in the biofilm matrix[28–30]; iii) the EPS significantly retards the rate of diffusion of antibiotics in biofilms[11,14,31,32] or trap/de-activate the antibodies through charged interactions[11,33] . Furthermore, genetic mutations to inhibit EPS synthesis in bacteria was found to result in softer, less resilient or complete absence of biofilm formation[13,26,34,35]. Following maturation, biofilm may detach into fragments (Fig. 1.1)

that re-enter the blood stream resulting in infection dissemination[2,18,36]. While, detachment is not well understood, current hypotheses involve enzymatic cleavage of the EPS or flow induced fragmentation[37]. In both cases, the properties of the EPS polymers, such as concentration and viscoelasticity, presumably play a role in mediating the propensity to fractionate. It is thus evident that the EPS polymers are crucial for both biofilm maturation and sustenance. We will attempt to quantify the *in situ* concentrations of these EPS polymers, understand how they mediate biofilm rheology and, identify how the cells and polymers interact to generate the mechanics of mature biofilms.

1.2 The structure of a bacterial biofilm

Biofilms are viewed as cellular aggregates, resembling colloidal spheres embedded within the EPS matrix, equivalent to a polymeric hydrogel[36]. The rheology of a bulk biofilm has been measured using techniques such as shear rheometry[38,39], tensiometry[40,41], microrheology[42,43] and microfluidics[44,45]. Biofilms were found to be viscoelastic, with elastic and viscous modulus ranging from 10^{-1} – 10^{2} kPa and 10 – 10^{4} Pa.s respectively[16,46]. By studying the impact of pH, salts, electric fields and destabilizing factors such as ethanol and urea on biofilm structure, the EPS was discovered to be built through hydrogen, hydrophobic or Columbic attraction between the polymers that make up the matrix[3,4,22,23,47–49].

1.3 The role of EPS in mediating biofilm rheology

Despite their importance, understanding the polymeric properties of the EPS in mediating biofilm rheology still remains qualitative, or indirectly demonstrated. For example, from microrheology of biofilms, Chew et al. found that, biofilms of polysaccharide positive strains were 25 fold more elastic than their mutant polysaccharide negative strains[35]. Zrelli et al. identified a dramatic increase in the biofilm compliance upon enzymatic digestion of EPS polymers[50]. Biofilms were found to mediate their resistance to increased shear stresses by escalating the polysaccharide content of their EPS[51]. While, such studies establish the significance of EPS to the rheology of biofilms, they do not reveal fundamental properties such as concentration dependent viscoelasticity of the EPS polymers. The importance for such a measurement is evident from Fig. 1.2. In this view, at ~ 10^{-2} m, the biofilm resembles a homogeneous soft matter and at ~10^{-6} m, biofilms are similar to a colloidal gel. However, at ~10^{-9} m, the mechanics of a biofilm breaks down into that dictated by the hydrogel like EPS, a suspension of spheres and the potential interactions between the two. Thus, the macroscopic stress response of a biofilm is conceptualized as a synergistic response mediated by the extracellular polymers and the cellular aggregates. However, commonly used spring-dashpot models[52] for biofilm rheology neither account for the individual contributions from polymers and cells nor recognize the presence of spatial variation in biofilm mechanics. To predict the stress response of biofilms at short spatiotemporal scales and account for the compositional heterogeneity *in situ*, one approach would be to utilize polymer network theories and multi-component models. For this, we aim to establish experimental data by probing the rheology of a biofilm and its constituent EPS across a wide concentration and frequency range. Such a study could provide insights into the phenomena that generate the EPS viscoelasticity, namely –

physical entanglements or associative interactions. Additionally, we can identify the frequency ranges that are mediated purely by the EPS polymers or by a cell-polymer composite. Mechanical deconstruction of biofilm rheology in this manner is essential for appropriate choice of constitutive models to understand mechanics of biofilm streamers and strain hardening in biofilms.

1.4 *Staphylococcus epidermidis* biofilms

We work with biofilms formed by *Staphylococcus epidermidis*, a pathogen commonly isolated from ~ 70 % of catheter related infections in the US[19]. In *S. epidermidis*, the biofilm formation[13,19], viscoelasticity and eradication[53] is facilitated by the presence of an EPS polymer - polysaccharide intercellular adhesin (PIA)[18,54]. Apart from PIA, the EPS includes matrix binding proteins[20], accumulation associated proteins, extracellular proteins and nucleic acids[34,55]. We work with *S. epidermidis* since; there is a profound gap in the literature on PIA rheology and its role in the viscoelasticity of biofilms formed by this species. A second motivation to work with this species is that, *S. epidermidis* biofilms were found to exhibit interesting rheological properties such as strain hardening[44] and non-monotonic trend in their elastic modulus with increasing osmotic stresses[52]. Thus, we study the polymeric properties of PIA to try and understand if the polymer plays a role in mediating these interesting rheological behaviors of the bulk biofilm.

1.5 Current understanding of the Polysaccharide Intercellular Adhesin (PIA)

PIA is a glycosaminoglycan of β-1,6 linked N-acetylglucosamine (GlcNAc) monomers with ~20% de-N-acetylated moieties ($GlcNH_3^+$)[56]. In addition, about 20% of the total PIA contains anionic ester linked succinates[54]. The presence of positive and negative moieties renders the polymer Zwitter ionic[54]. Furthermore, PIA has a propensity for hydrogen and hydrophobic interactions due to the hydroxyl and alkyl groups respectively. The presence of such interaction sites is of fundamental importance for the adhesive properties of this polymer, as discussed elsewhere[54]. Furthermore, staphylococcal mutants that lack the ability to de-acetylate their PIA resulted in negligible biofilm formation and reduced virulence[13]. This highlights the functional importance of deacetylation in PIA for its role in intercellular adhesion and biofilm formation[54]. The significance of PIA in biofilm virulence, antibiotic resistance and immunogenicity are discussed in detail elsewhere[57,58]. Thus, while the structure, synthesis and immunochemistry of PIA are well studied[54], its extracellular concentration, polymeric and rheological properties are not well understood.

First, measurement of PIA solution properties, namely, its molar mass distribution and radius of gyration have not received much attention. The earliest report of PIA molar mass was in 1990, where, using immunoblotting, Kotilainen et al., estimated a value of 30 kDa[59]. Subsequently, in 1994 and 1995, using gel mobility assays, Arvaniti et al.,[60] and Karamanos et al.,[61] reported values between 20 – 80 kDa. Using methylation analysis, Mack et al.,[56], in 1995, measured PIA molar mass to be 30 kDa. Using a modified PIA isolation technique, Maira-Litran et al.,[57] , discussed that the value of 30 kDa was low, probably, due to protocol induced loss of high molar mass fractions[56]. In 2005, Irina et al.,[62] re-instituted that the molar mass of PIA reported by Mack et al[56] may be incorrect due to depolymeratizaion of the polymer under high

alkaline conditions of methylation reactions. From size-exclusion chromatograms, they proposed the molar mass to be ~ 10^2 kDa. Thus, for more than a decade, quantification of PIA molar mass has had considerable inconsistencies in the literature. On the other hand, the radius of gyration of PIA has received little or no mention. Both molar mass and radius of gyration are fundamental quantities that together mediate the rheological properties of a polymer.

Second, the impact of pH on the solution properties of PIA and its interaction with other matrix components, such as proteins, has not been probed. As consequences of bacterial metabolism, biofilms have pH microenvironments[63]. On the other hand, glycosaminoglycans are known to exhibit varying solution behavior, ranging from isolated coils to aggregates arising from associative interactions as a function of solution pH[64,65]. Thus, it is instructive to investigate if pH has an influence on the structural properties of PIA that could potentially impact both its rheology and the microstructure of the biofilm EPS. Recently, Pavlovsky et al.,[38] attributed the rheology of *S. epidermidis* biofilms to be mediated by interactions between PIA and extracellular proteins. Thus, studying the interaction between PIA and proteins is essential to understand the onset of viscoelasticity in *S. epidermidis* biofilms. Furthermore, understanding the impact of pH and complexation with proteins would provide impetus for developing treatment techniques that could potentially weaken the EPS matrix by nullifying such Columbic interactions.

Third, while the bulk rheology of *S. epidermidis* biofilms has been studied in detail[39,52,66], measurements of PIA viscoelasticity at concentrations within the range present within the biofilm are lacking. The absence of rheological characterization of PIA has restricted the scope of constitutive modeling of *S. epidermidis* biofilms. Currently, the models developed for *S. epidermidis* biofilms are of the spring-dashpot type that do not account for contributions from

molecular level polymeric or colloidal interaction[30,52]. That is, while *S. epidermidis* biofilms are known to be viscoelastic[52] strain hardening[44] solids, very little is known about the microstructure of their EPS matrix, which mediates such complex rheological behavior. Recently, based on experimental data on alginate rheology, *P. aeruginosa* biofilms were modeled using a polymer network theory based on worm like chains incorporated into the Arruda-Boyce eight chain model framework[16]. The authors showed that such a model effectively predicted the viscoelasticy, swelling and stress relaxation in *P. aeruginosa* biofilms. To enable similar high fidelity modeling for *S. epidermidis* biofilms, we lack fundamental micromechanical measurements of PIA chain dimensions and concentration dependent moduli. A foundational understanding in PIA rheology is essential since, these material data are an integral part of more complex simulations such as biofilm growth and detachment studies that serve to understand the onset of viscoelasticity and predict biofilm fragmentations.

1.6 Research Objective

The aim of this thesis is thus to measure the polymeric and rheological properties of a PIA at concentrations relevant to that present within mature biofilms. We will use these measurements to artificially assemble a biofilm like system using planktonic cells and an abacterial polysaccharide similar to PIA in its solution properties. Together, we will utilize these findings to identify a physicochemical factor that mediates the onset and dispersal of viscoelasticity in *S. epidermidis* biofilms. The objectives are summarized here:

1. Using size exclusion chromatography and multi-angle laser light scattering, we will measure the distribution of molar mass and radius of gyration of PIA purified from batch biofilm

cultures, while ensuring negligible loss of high molar mass fractions. The measured values will be validated using batch mode static light scattering. We will use low angle light scattering and spectrophotometry to quantify the influence of pH on PIA solution behavior and intermolecular interactions between PIA and a model protein. The aim is to quantify fundamental polymeric properties of PIA and study its solution behavior at relevant *in situ* conditions.

2. We will measure the microrheology of PIA at concentrations that include the range found within cultured biofilms. Additionally, we will synthesize and measure the rheology of a polymeric composite consisting of PIA and model proteins and nucleic acids that simulates the biofilm EPS. These results will identify if, PIA, by itself, is the dominant contributor to the biofilm mechanical properties, or, alternatively, if it acts synergistically with other components of the biofilm EPS.
3. Using the above findings, we will deconstruct the viscoelasticity of the entire biofilm into its major constituents by measuring and comparing the microrheology of *S. epidermidis* biofilms, the abacterial EPS and PIA. These measurements and the above will be used to construct an artificial biofilm from cells and abacterial polymeric proxies to identify factors that play a role in generating the biofilm morphology and mechanics. We will apply the findings to a naturally occurring biofilm system in the context of understanding biofilm detachment and dispersal.
4. To develop a way to rapidly diagnose elasticity of biological soft matter such as biofilms and tissues, we will provide a theoretical derivation that will serve to extend the scope of a rheological technique called cavitation rheometry to be applicable to materials of volume as low as 1 μL. Cavitation rheometry is the measurement of linear elastic modulus of materials

by measuring the pressure required to induce internal cavitation. Using *ab initio* hyperelastic constitutive modeling, we will derive a relation that relates the critical pressure to the material elastic modulus that takes into consideration the material thickness (or volume).

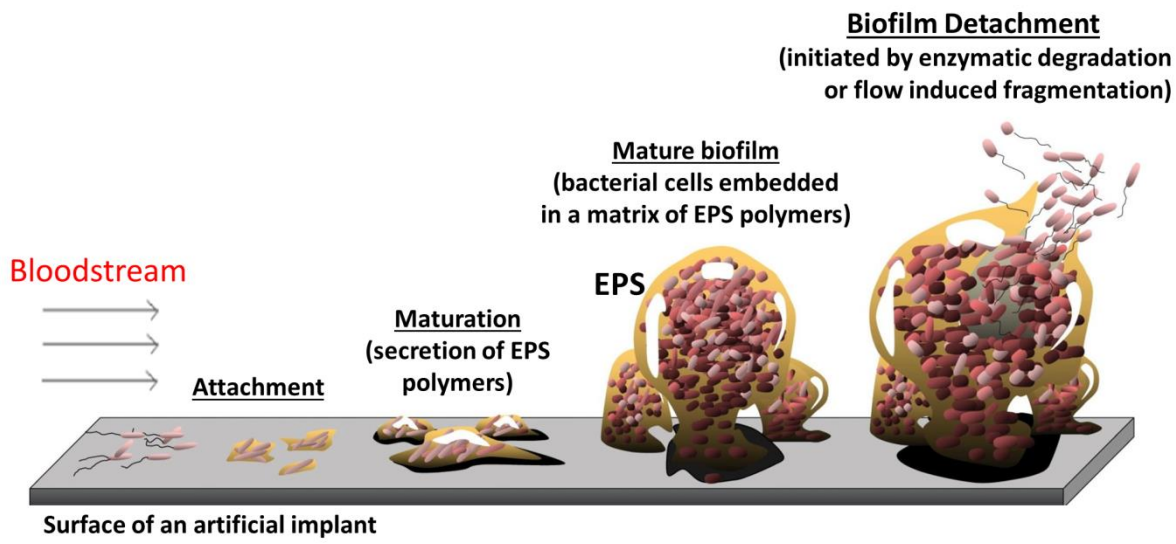

Figure 1.1 Schematic of a biofilm growth on the surface of an implant

(main schematic as reproduced from Monroe[67]).

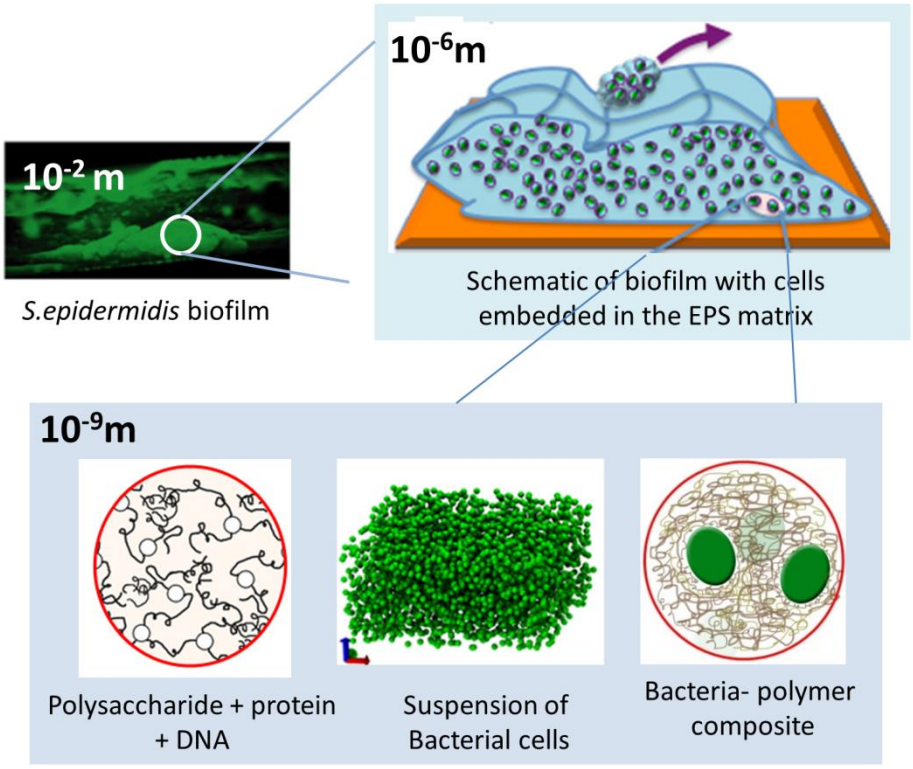

Figure 1.2. Schematic of biofilm mechanics at different length scales

Schematic of breakdown of biofilm mechanics at different length scales from 10^{-2} m down to 10^{-9} m (schematic of biofilm with cells embedded in the matrix is from the lab of Dr. John G. Younger).

1.7 References

1. Watnick, P. & Kolter, R. Biofilm, city of microbes. *J. Bacteriol.* **182,** 2675–2679 (2000).
2. Costerton, J. W. *The biofilm primer*. **1,** (Springer, 2007).
3. Flemming, H.-C. & Wingender, J. The biofilm matrix. *Nat. Rev. Microbiol.* **8,** 623–633 (2010).
4. Lembre, P., Lorentz, C. & Di Martino, P. Exopolysaccharides of the biofilm matrix: a complex biophysical world. *The Complex World of Polysaccharides, InTech* 371–392 (2012).
5. Sutherland, I. W. The biofilm matrix--an immobilized but dynamic microbial environment. *Trends Microbiol.* **9,** 222–7 (2001).
6. Hall-Stoodley, L., Costerton, J. W. & Stoodley, P. Bacterial biofilms: from the natural environment to infectious diseases. *Nat. Rev. Microbiol.* **2,** 95–108 (2004).
7. Lynch, a S. & Robertson, G. T. Bacterial and fungal biofilm infections. *Annu. Rev. Med.* **59,** 415–28 (2008).
8. Costerton, J. W., Stewart, P. S. & Greenberg, E. P. Bacterial biofilms: a common cause of persistent infections. *Science (80-.).* **284,** 1318–1322 (1999).
9. Kiedrowski, M. R. & Horswill, A. R. New approaches for treating staphylococcal biofilm infections. *Ann. N. Y. Acad. Sci.* **1241,** 104–121 (2011).
10. Mah, T.-F. C. & O'Toole, G. A. Mechanisms of biofilm resistance to antimicrobial agents. *Trends Microbiol.* **9,** 34–39 (2001).
11. Hall-Stoodley, L. & Stoodley, P. Evolving concepts in biofilm infections. *Cell. Microbiol.* **11,** 1034–43 (2009).
12. Bridier, a, Briandet, R., Thomas, V. & Dubois-Brissonnet, F. Resistance of bacterial biofilms to disinfectants: a review. *Biofouling* **27,** 1017–32 (2011).
13. Vuong, C. *et al.* A crucial role for exopolysaccharide modification in bacterial biofilm formation, immune evasion, and virulence. *J. Biol. Chem.* **279,** 54881–54886 (2004).
14. Doroshenko, N. *et al.* Extracellular DNA Impedes the Transport of Vancomycin in Staphylococcus epidermidis Biofilms Preexposed to Subinhibitory Concentrations of Vancomycin. *Antimicrob. Agents Chemother.* **58,** 7273–7282 (2014).
15. Mulcahy, H., Charron-Mazenod, L. & Lewenza, S. Extracellular DNA Chelates Cations and Induces Antibiotic Resistance in <italic>Pseudomonas aeruginosa</italic> Biofilms. *PLoS Pathog* **4,** e1000213 (2008).
16. Böl, M., Ehret, A. E., Bolea Albero, A., Hellriegel, J. & Krull, R. Recent advances in mechanical characterisation of biofilm and their significance for material modelling. *Crit. Rev. Biotechnol.* **33,** 145–71 (2013).
17. Guelon, T., Mathias, J. & Stoodley, P. in *Biofilm Highlights* (Flemming, H.-C., Wingender, J. & Szewzyk, U.) **5,** 111–139 (Springer Berlin Heidelberg, 2011).
18. Otto, M. Molecular basis of Staphylococcus epidermidis infections. *Semin. Immunopathol.* **34,** 201–214 (2012).
19. Otto, M. Staphylococcus epidermidis--the "accidental" pathogen. *Nat. Rev. Microbiol.* **7,** 555–567 (2009).
20. Christner, M. *et al.* The giant extracellular matrix-binding protein of Staphylococcus epidermidis mediates biofilm accumulation and attachment to fibronectin. *Mol. Microbiol.* **75,** 187–207 (2010).

21. Flock, J.-I. Extracellular-matrix-binding proteins as targets for the prevention of Staphylococcus aureus infections. *Mol. Med. Today* **5,** 532–537 (1999).
22. Sutherland, I. Biofilm exopolysaccharides: a strong and sticky framework. *Microbiology* **147,** 3–9 (2001).
23. Flemming, H.-C., Wingender, J., Mayer, C., Korstgens, V. & Borchard, W. in *Symp. Gen. Microbiol.* 87–106 (Cambirge University Press, 1999).
24. Cogan, N. G. & Keener, J. P. The role of the biofilm matrix in structural development. *Math. Med. Biol.* **21,** 147–166 (2004).
25. Flemming, H.-C. The perfect slime. *Colloids Surf. B. Biointerfaces* **86,** 251–259 (2011).
26. Vilain, S., Pretorius, J. M., Theron, J. & Brözel, V. S. DNA as an adhesin: Bacillus cereus requires extracellular DNA to form biofilms. *Appl. Environ. Microbiol.* **75,** 2861–8 (2009).
27. Das, T., Sharma, P. K., Busscher, H. J., van der Mei, H. C. & Krom, B. P. Role of extracellular DNA in initial bacterial adhesion and surface aggregation. *Appl. Environ. Microbiol.* **76,** 3405–8 (2010).
28. Peterson, B. W., Busscher, H. J., Sharma, P. K. & van der Mei, H. C. Visualization of Microbiological Processes Underlying Stress Relaxation in Pseudomonas aeruginosa Biofilms. *Microsc. Microanal.* **20,** 912–5 (2014).
29. He, Y. *et al.* Stress relaxation analysis facilitates a quantitative approach towards antimicrobial penetration into biofilms. *PLoS One* **8,** e63750 (2013).
30. Klapper, I., Rupp, C. J., Cargo, R., Purvedorj, B. & Stoodley, P. Viscoelastic fluid description of bacterial biofilm material properties. *Biotechnol. Bioeng.* **80,** 289–296 (2002).
31. Rani, S. A., Pitts, B. & Stewart, P. S. Rapid Diffusion of Fluorescent Tracers into Staphylococcus epidermidis Biofilms Visualized by Time Lapse Microscopy. *Antimi* **49,** 3502–3511 (2005).
32. Stewart, P. S., Davison, W. M. & Steenbergen, J. N. Daptomycin rapidly penetrates a Staphylococcus epidermidis biofilm. *Antimicrob. Agents Chemother.* **53,** 3505–7 (2009).
33. Bagge, N. *et al.* Dynamics and spatial distribution of β-lactamase expression in Pseudomonas aeruginosa biofilms. *Antimicrob. Agents Chemother.* **48,** 1168–1174 (2004).
34. Qin, Z. *et al.* Role of autolysin-mediated DNA release in biofilm formation of Staphylococcus epidermidis. *Microbiology* **153,** 2083–92 (2007).
35. Chew, S. C. *et al.* Dynamic Remodeling of Microbial Biofilms by Functionally Distinct Exopolysaccharides. *MBio* **5,** e01536–14 (2014).
36. Wilking, J. N., Angelini, T. E., Seminara, A., Brenner, M. P. & Weitz, D. a. Biofilms as complex fluids. *MRS Bull.* **36,** 385–391 (2011).
37. McDougald, D., Rice, S. A., Barraud, N., Steinberg, P. D. & Kjelleberg, S. Should we stay or should we go: mechanisms and ecological consequences for biofilm dispersal. *Nat. Rev. Microbiol.* **10,** 39–50 (2011).
38. Pavlovsky, L., Younger, J. G. & Solomon, M. J. In situ rheology of Staphylococcus epidermidis bacterial biofilms. *Soft Matter* **9,** 122 (2013).
39. Di Stefano, A. *et al.* Viscoelastic properties of Staphylococcus aureus and Staphylococcus epidermidis mono-microbial biofilms. *Microb. Biotechnol.* **2,** 634–641 (2009).
40. Aggarwal, S. & Hozalski, R. M. Determination of biofilm mechanical properties from tensile tests performed using a micro-cantilever method. *Biofouling* **26,** 479–486 (2010).

41. Aggarwal, S. & Hozalski, R. M. Effect of strain rate on the mechanical properties of Staphylococcus epidermidis biofilms. *Langmuir* **28,** 2812–6 (2012).
42. Cheong, F. C., Duarte, S., Lee, S.-H. & Grier, D. G. Holographic microrheology of polysaccharides from Streptococcus mutans biofilms. *Rheol. Acta* **48,** 109–115 (2008).
43. Rogers, S. S., van der Walle, C. & Waigh, T. a. Microrheology of bacterial biofilms in vitro: Staphylococcus aureus and Pseudomonas aeruginosa. *Langmuir* **24,** 13549–55 (2008).
44. Hohne, D. N., Younger, J. G. & Solomon, M. J. Flexible microfluidic device for mechanical property characterization of soft viscoelastic solids such as bacterial biofilms. *Langmuir* **25,** 7743–7751 (2009).
45. Mosier, A. P., Kaloyeros, A. E. & Cady, N. C. A novel microfluidic device for the< i> in situ</i> optical and mechanical analysis of bacterial biofilms. *J. Microbiol. Methods* **91,** 198–204 (2012).
46. Shaw, T., Winston, M., Rupp, C. J., Klapper, I. & Stoodley, P. Commonality of elastic relaxation times in biofilms. *Phys. Rev. Lett.* **93,** 98102 (2004).
47. Stoodley, P., DeBeer, D. & Lappin-Scott, H. M. Influence of electric fields and pH on biofilm structure as related to the bioelectric effect. *Antimicrob. Agents Chemother.* **41,** 1876–1879 (1997).
48. Chen, X. & Stewart, P. S. Role of electrostatic interactions in cohesion of bacterial biofilms. *Appl. Microbiol. Biotechnol.* **59,** 718–720 (2002).
49. Mayer, C. *et al.* The role of intermolecular interactions: studies on model systems for bacterial biofilms. *Int. J. Biol. Macromol.* **26,** 3–16 (1999).
50. Zrelli, K. *et al.* Bacterial biofilm mechanical properties persist upon antibiotic treatment and survive cell death. *New J. Phys.* **15,** 125026 (2013).
51. Stoodley, P., Cargo, R., Rupp, C. J., Wilson, S. & Klapper, I. Biofilm material properties as related to shear-induced deformation and detachment phenomena. *J. Ind. Microbiol. Biotechnol.* **29,** 361–367 (2002).
52. Pavlovsky, L., Younger, J. G. & Solomon, M. J. In situ rheology of Staphylococcus epidermidis bacterial biofilms. *Soft Matter* **9,** 122–131 (2013).
53. Itoh, Y., Wang, X., Hinnebusch, B. J., Iii, J. F. P. & Romeo, T. Depolymerization of ␣ -1 , 6-N-Acetyl- D -Glucosamine Disrupts the Integrity of Diverse Bacterial Biofilms †. *Society* **187,** 382–387 (2005).
54. Rohde, H., Frankenberger, S., Zähringer, U. & Mack, D. Structure, function and contribution of polysaccharide intercellular adhesin (PIA) to Staphylococcus epidermidis biofilm formation and pathogenesis of biomaterial-associated infections. *Eur. J. Cell Biol.* **89,** 103–111 (2010).
55. Hussain, M., Herrmann, M. & Eiff, C. V. O. N. A 140-Kilodalton Extracellular Protein Is Essential for the Accumulation of Staphylococcus epidermidis Strains on Surfaces. **65,** 519–524 (1997).
56. Mack, D. *et al.* The intercellular adhesin involved in biofilm accumulation of Staphylococcus epidermidis is a linear beta-1,6-linked glucosaminoglycan: purification and structural analysis. *J. Bacteriol.* **178,** 175–83 (1996).
57. Maira-Litran, T. *et al.* Immunochemical Properties of the Staphylococcal Poly- N -Acetylglucosamine Surface Polysaccharide Immunochemical Properties of the Staphylococcal. *Infect. Immun.* **70,** 4433–4440 (2002).

58. Kropec, A. *et al.* Poly-N-acetylglucosamine production in Staphylococcus aureus is essential for virulence in murine models of systemic infection. *Infect. Immun.* **73,** 6868–6876 (2005).
59. Kotilainen, P. *et al.* Immunochemical analysis of the extracellular slime substance ofStaphylococcus epidermidis. *Eur. J. Clin. Microbiol. Infect. Dis.* **9,** 262–270 (1990).
60. Arvaniti, A., Karamanos, N. K., Dimitracopoulos, G. & Anastassiou, E. D. Isolation and Characterization of a Novel 20-kDa Sulfated Polysaccharide from the Extracellular Slime Layer of< i> Staphylococcus epidermidis</i>. *Arch. Biochem. Biophys.* **308,** 432–438 (1994).
61. Karamanos, N. K. *et al.* Identity of macromolecules present in the extracellular slime layer of Staphylococcus epidermidis. *Biochimie* **77,** 217–224 (1995).
62. Sadovskaya, I., Vinogradov, E., Flahaut, S., Kogan, G. & Jabbouri, S. Extracellular Carbohydrate-Containing Polymers of a Model Biofilm-Producing Strain , Staphylococcus epidermidis RP62A. *Infect. Immun.* **73,** 2007–3017 (2005).
63. Hidalgo, G. *et al.* Functional tomographic fluorescence imaging of pH microenvironments in microbial biofilms by use of silica nanoparticle sensors. *Appl. Environ. Microbiol.* **75,** 7426–7435 (2009).
64. Schatz, C., Viton, C., Delair, T., Pichot, C. & Domard, A. Typical physicochemical behaviors of chitosan in aqueous solution. *Biomacromolecules* **4,** 641–648 (2003).
65. Anthonsen, M., Varum, K., Hermansson, a, Smidsrod, O. & Brant, D. Aggregates in acidic solutions of chitosans detected by static laser light scattering. *Carbohydr. Polym.* **25,** 13–23 (1994).
66. Pavlovsky, L. Novel Methods for the Rheological Characterization of Polymers and Polymeric Biofilms. 129 (2014).
67. Monroe, D. Looking for chinks in the armor of bacterial biofilms. *PLoS Biol.* **5,** e307 (2007).

CHAPTER 2

Molar Mass, entanglement and associations of *S. epidermidis* biofilm polysaccharide

2.1 Abstract

Biofilms are microbial communities that are characterized by the presence of a viscoelastic extracellular polymeric substance (EPS). Studies have shown that polysaccharides, along with proteins and DNA, are a major constituent of the EPS, and play a dominant role in mediating its microstructure and rheological properties. Here, we investigate the possibility of entanglements and associative complexes in solutions of extracellular polysaccharide intercellular adhesin (PIA) extracted from *Staphylococcus epidermidis* biofilms. We report that the weight average molar mass and radius of gyration of PIA isolates are $2.01 \times 10^5 \pm 1200$ *g/mol* and 29.2 ± 1.2 *nm* respectively. The coil overlap concentration, c^*, was thus determined to be $(32 \pm 4) \times 10^{-4}$ *g/mL*. Measurements of the *in situ* concentration of PIA ($c_{PIA,Biofilm}$) was found to be $(10 \pm 2) \times 10^{-4}$ *g/mL* . Thus, $c_{PIA,Biofilm} < c^*$ and the amount of PIA in the biofilm is too low to cause polymer chain entanglements. In the pH range 3.0 to 5.5, PIA was found to both self-associate and to form complexes with bovine serum albumin (BSA). By static light scattering, both self-association and complex formation with 0.5 %(w/v) BSA were found to occur at PIA concentrations of 0.30×10^{-4} *g/mL* and greater, which is about 30 times lower than the measured $c_{PIA,Biofilm}$. These results suggest that the microscopic origin of EPS viscoelasticity is unlikely to be due to polysaccharide entanglements. Furthermore, the onset of self-association and protein

complexation of PIA occurs at concentrations far lower than the native PIA concentration in biofilms. This finding therefore suggests a critical role for those two association mechanisms in mediating biofilm viscoelasticity. (**Text and figures in this chapter is reprinted with permission from Ganesan, M., et al. *Biomacromolecules* 14, 1474-1481 (2013)**[1])

2.2 Introduction

Biofilms are surface adherent aggregates of microorganisms encased within a secreted matrix of extracellular polymeric substance (EPS) [2]. The EPS accounts for about 80% of the biofilm dry mass and thus plays a major role in mediating both the morphology and rheology of biofilms [3]. The EPS is a heterogeneous hydrogel composed predominantly of polysaccharides, proteins and DNA, all of which are contained in the extracellular volume of the biofilm [3–5]. Mechanical properties such as viscoelasticity and cohesiveness of the EPS are thus dependent on the physicochemical properties of the biofilm polysaccharides, such as their molecular weight, radius of gyration, local concentration within the biofilm and their interaction with other EPS constituents [3,5,6]. In this article, we characterize these properties for the case of biofilms formed by *Staphylococcus epidermidis*, an opportunistic pathogen associated with nosocomial blood stream infections [2]. The mechanical stability and the three-dimensional microstructure of the *S. epidermidis* EPS is strongly dependent on a self-produced extracellular polysaccharide called polysaccharide intercellular adhesion (PIA) [2,5,7–9]. While the biochemistry (Fig. 2.1a) and genomic origin of PIA have been well characterized [10], very little has been investigated about the polymeric properties of PIA.

S. epidermidis biofilms are viscoelastic in nature [11,12]. Following [5,6,13,14], PIA chains in the extracellular volume could in theory contribute to biofilm viscoelasticity by one of two mechanisms. In the first, which assumes no specific inter-chain interactions, a high number density of PIA chains produced *in situ* leads to physical entanglements [3,6]. These entanglements induce viscoelasticity in the biofilm matrix (Fig. 2.1b). In the second, associative interactions of PIA with itself and/or other EPS macromolecules such as proteins lead to supra-molecular structures that result in a viscoelastic hydrogel [3,6] (Fig. 2.1c). Since PIA dominates the EPS

microstructure in most strains of this species [5], the purpose of this paper is to establish which physical model is most consistent with the measured molar mass of PIA, local concentration of PIA within *S. epidermidis* biofilms, and its scattering behavior in presence of proteins.

Simple mechanical characterization of bulk biofilm [12,15] is insufficient to distinguish between a material composed of an entangled network of polysaccharide chains and an assembly of strands held together by inter-chain attractions. Rather, what is needed is a determination of the local concentration of polymer within the biofilm ($c_{PIA,Biofilm}$) relative to its *coil-overlap* concentration (c^*, the concentration at which neighboring PIA molecules interpenetrate) and its *critical association concentration* ($c_{critical}$, the concentration above which PIA engages in associative interactions with itself or other EPS macromolecules such as proteins). This paper reports measurements that allow characterization of these three quantities. Consequently, the comparative role of entanglements and associations in PIA is established.

A biofilm in which the extracellular PIA concentration, $c_{PIA,Biofilm}$, is much greater than the overlap concentration, c^*, would acquire viscoelasticity through entanglements of PIA chains (Fig. 2.1b). Here c^* is the overlap concentration, $c^* = \frac{3M_w}{4\pi r_g^3 N_A}$, where M_w and r_g are the weight average molar mass and average radius of gyration of the polymer respectively [16]. Polysaccharide entanglements in biofilm EPS have been invoked as discussions in the literature [6,17–20]; however, little experimental evidence supports their existence.

Likewise, a bacterial community in which $c_{PIA,Biofilm} \geq c_{critical}$ could be viscoelastic due to PIA self-association or inter-molecular complexation with extracellular proteins. These phenomena are driven by hydrogen bond, hydrophobic and/or ion-pair interactions (self-association) [21–23] or electrostatic interactions between oppositely charged groups on two different polymers (complex formation) [24] (Fig. 2.1c). While polysaccharide-protein complexes have been

commonly discussed as prevalent within the EPS [5,13], experimental verification is very limited in the biofilm literature.

The null case in which $c_{PIA,Biofilm}$ is both below the overlap concentration c^* and the critical association concentrations $c_{critical}$ is unlikely because it is inconsistent with the known viscoelasticity of the biofilm EPS. A fourth possibility, in which $c_{PIA,Biofilm}$ is greater than both c^* and $c_{critical}$, is also a potential case.

The aim of this study is thus to measure $c_{PIA,Biofilm} / c^*$ and $c_{PIA,Biofilm} / c_{critical}$ of PIA from *S. epidermidis* biofilms. We use multi-angle laser light scattering (MA-LLS) and size exclusion chromatography (SEC) to quantify M_w, r_g and c^* for PIA recovered from batch cultures. Measurements of extracellular PIA concentration, $c_{PIA,Biofilm}$, were made by quantifying the polymer concentration per biofilm bacteria and bacteria number density *in situ* by biochemical and confocal microscopy methods, respectively. Using pH induced turbidity and low-angle light scattering (LLS) we identify $c_{critical}$ for PIA self-association and complex formation with bovine serum albumin (BSA), representative of one of the most common host proteins likely to be found in any medically important biofilm. We find that the measured $c_{PIA,Biofilm}$ is inconsistent with the formation of polymer chain entanglements but that PIA exhibits signatures of both self-association and complexation at acidic pH. The study therefore suggests that EPS viscoelasticity is generated primarily through associative interactions of EPS macromolecules rather than through polysaccharide entanglements.

2.3 Materials and Methods

2.3.1 Culture conditions and bacterial strains.

S. epidermidis RP62A (ATCC, catalog no. 35984) cultures were grown for 24 h at 37°C in tryptic soy broth media containing 1% (w/v) filtered glucose with a moderate shaking of 60 rpm (Forma Incubated Shaker, Thermo Scientific) [25].

2.3.2 Recovery of PIA isolate from batch cultures.

Recovery of crude PIA was similar to [25] except that isolation was performed in 0.1M $NaNO_3$, the mobile phase for SEC. Flask-adherent biofilm was collected by centrifugation (5000 *g*, 20 min, 4°C), re-suspended, and then sonicated in an ice bath to release the PIA and other extracellular material from cell surfaces (16-19W, 4x30 *s* cycles, Sonic Dismembrator Model 60, Fisher Scientific). After removing insoluble material (such as cell debris) and further clarification (12000 *g*, 10 min), the crude extract rich in PIA was filter sterilized and concentrated using Amicon Ultra-15, centrifugal filter with 10 kDa cut off membrane (Millipore).

2.3.3 Lectin affinity chromatography to obtain high purity PIA

A multi-component elution pattern was observed for crude PIA isolated by sonication (Fig. 2.2a, inset). The SEC trace of the crude isolate shows three peaks. Eluent fractions containing amino sugars were identified using a dot blot technique [26] and the Smith-Gilkerson assay for hexosamines [27]. Eluent fractions corresponding to Peaks 1 and 3 (Fig. 2.2a, inset) showed no GlcNAc content in either assay. Peak 3 was removed using Amicon Ultra-15 filter

with a 30 kDa cut off membrane (Millipore). Figure 2.2a shows that amino sugars are present only in Peak 2, as detected by the colorimetric assay. Peak 1 is a molecule of very high molecular weight ($\geq 10^6$ Da). From the concentration detector signal (blue), this material contributes little to the total mass due to its low concentration. To remove Peak 1, concentrated crude isolates were passed over an agarose bound wheat-germ agglutinin lectin (known to have specific affinity towards N-acetylglucosamine, GlcNAc) bead column (Vector Labs, CA) equilibrated in 20mM Tris-HCl, 0.15M NaCl binding buffer. In this way, we ensure that any contaminants in the crude extract are discarded by means of the flow through from the lectin bead column. Following washing, lectin-bound PIA was eluted using 0.5M GlcNAc in 20mM Tris-HCl, 0.5M NaCl (pH 3.0, AcOH) and washed and concentrated in 0.1M $NaNO_3$ or 0.02μm filtered HPLC Grade water (Fisher Scientific) using Amicon centrifugal filters with 3 kDa cut off membrane (Millipore). Figure 2.2b shows the elution profile of the isolated Peak 2, in which the glucosamine fraction of the isolate is localized. All further plots report data for PIA purified using this protocol. Experiments were performed within a day of sample preparation to avoid any effects due to solvent incompatibility [25].

2.3.4 Size exclusion chromatography (SEC) – Multi-angle laser light scattering (MA-LLS) for Mw and rg measurement.

Waters Ultrahydrogel 2000 and 250 size exclusion columns (Waters Corp., Milford, MA) connected in series were continuously washed at 0.45mL/min with a standard aqueous mobile phase of 0.1M $NaNO_3$, 0.05 %(w/v) NaN_3. The column outlet was connected to a MALLS detector (DAWN EOS, GaAs laser at 690nm, Wyatt Technology, Santa Barbara, CA) and a concentration detector (Optilab DSP refractometric interferometer (RI) detector, Wyatt

Technology, Santa Barbara, CA). The light scattering due to the eluting polymers was analyzed according to the Zimm model to calculate the molar mass distribution [28]. Static light scattering was performed on unfractionated PIA samples of different concentrations at neutral pH using the DAWN EOS. The time averaged angle dependent scattering intensities were then analyzed using the Zimm plot to obtain the z-average r_g [28]. Analysis of light scattering data was done using Wyatt's ASTRA software. Following [29,30], the refractive index increment (*dn/dc*) was taken as 0.162 mLg^{-1}.

2.3.5 Low Angle Light Scattering (LLS).

Static light scattering was performed with a light scattering goniometer equipped with dual detectors (ALV, Langen Germany). The light source was a Coherent Innova 70-C laser (Coherent Inc., Santa Clara, CA) operating at 488 nm. Intensity of scattered light was measured in the range $35° < \theta < 140°$ and extrapolated to the low angle limit as per Zimm theory [28].

2.3.6 Measuring number density of bacterial cells within a biofilm.

S. epidermidis biofilms were grown in Stovall Life Sciences 3-channel flow cells (24 h, 37°C) at constant shear stress (0.01 Pa) in the same media as above. Biofilm cells stained with Syto9 (Invitrogen) were imaged between the adhesion surface and a height of 12 μm using a Leica TCS SP2 confocal laser scanning microscopy (CLSM) with 100x, 1.4 numerical aperture (N.A) oil immersion objective lens. Biofilm beyond that height was not imaged because 12 μm is the maximum working distance (in water) of the high numerical aperture (NA) objective used for microscopy. High NA microscopy was necessary so as to image at a resolution that could uniquely identify individual cells for the cellular density characterization. The excitation

wavelength was 488 *nm*. Image processing was performed on the acquired images to identify bacterial centroids as described previously [31,32]. Number density was computed as the number of cells identified within the total image volume (n_{cell} units: $cells/\mu m^3$). Figure 2.3b shows a confocal image acquired within the biofilm, in a plane parallel to the bottom shear surface of the flow cell. Figure 2.3c is a 3-D reconstruction of the total image volume with the 3-D location of the bacterial cells.

2.3.7 Measuring PIA concentration per biofilm cell (n_{PIA}).

Surface attached PIA from *S. epidermidis* cells was released by incubating cells for 5 min at 100°C in a solution of 0.5M EDTA, pH 8.0 (final volume, 1:50 culture volume) [33]. PIA rich supernatant was collected by centrifugation (9000 *g*, 5min 4°C) and the cell pellet (devoid of PIA) was re-dispersed in PBS. Bacterial cell density was measured using a haemocytometer (Fisher Scientific). The Smith-Gilkerson colorimetric assay for amino sugars [27] was performed on the PIA rich supernatant to obtain the molar concentration of PIA using the knowledge of its M_w (as reported in results). After accounting for dilutions and initial volume, the ratio of PIA concentration to cell density, yielded the number of molecules of PIA per biofilm bacteria (n_{PIA}). A schematic of this procedure is given in Fig. 2.3a.

2.3.8 Average extracellular concentration, $c_{PIA,Biofilm}$, of PIA.

This concentration $c_{PIA,Biofilm}$ is the average number of PIA molecules (n_{PIA}) within the average extracellular volume (V_{PIA}) associated with each biofilm bacterium. That is, $c_{PIA,Biofilm} = n_{PIA}/V_{PIA}$. V_{PIA} is the reciprocal of the local number density of biofilm bacteria (n_{cell} $cells/\mu m^3$ as from the CLSM measurement) less the cellular volume of the bacteria, $V_{bacteria}$. Thus, V_{PIA} =

$V_{total} - V_{cell} = (1/n_{cell}) - \{(4\pi/3)r_{bacteria}^3\}$. From the CLSM measurements, we found $r_{bacteria}$ = 0.32 ± 0.01 μm. This procedure is shown in Fig. 2.3c,d. The CLSM value of bacterial cell radius was consistent with independent characterizations performed by scanning electron microscopy and multi-angle dynamic light scattering.

2.3.9 Preparation of PIA – BSA solutions.

We identify if PIA can form complexes with proteins, which is a normal constituent of the biofilm EPS [3]. Bovine serum albumin (Sigma Aldrich) was used as a model protein for this test. PIA-BSA solutions were prepared by mixing different amounts of PIA with the same initial mass concentration of BSA (0.5 %(w/v)) in 0.02µm filtered HPLC Grade water (Fisher Scientific)) to obtain a series of solutions containing different PIA contents (c_{PIA}: 0.30 x 10^{-4} – 14 x 10^{-4} *g/mL*) [34]. Samples were rolled on a Wheaton Mini Bench Top Roller (WHEATON, Millville, NJ) at 10 RPM for 30 min prior to analysis.

2.3.10 Effect of pH on PIA and PIA-BSA solutions

To select the pH for self-association measurements of PIA, the effect of pH on the scattering intensity at 90° ($I_{\theta=90}$) for dilute solutions of PIA at c_{PIA} = 6.40 x 10^{-4} *g/mL* was measured and is shown in Fig. 2.4. The increase in $I_{\theta=90}$ at pH < 7.5 indicates an increase in size of the scattering specimen, thereby suggesting self-association [21,35]. Figure 2.4 show that self-association occurs in the range 3.0 < pH < 5.5.

To select the pH for protein-induced association of PIA, the effect of pH on absorbance of PIA-BSA solutions containing 0.5 %(w/v) BSA and c_{PIA} = 6.40 x 10^{-4} *g/mL* was measured at 600 *nm* in 1 *cm* path length plastic cuvettes (GENESYS 20, Thermo-Scientific UV Visible

Spectrophotometer) (Fig. 2.5) [34]. Formation of insoluble complexes is characterized by an increase in the absorbance of the specimen [34]. From Fig. 2.5, the range $3.5 \leq pH \leq 5$ favors PIA-BSA complexation. The onset of complex formation occurs at pH_c 5.0 and reaches a maximum at $pH_{c,max}$ 4.5. Thus, to identify critical association concentration, $c_{critical}$, LLS were done for PIA and PIA-BSA solutions at pH 4.9 and 7.5 and $c_{PIA} \leq c_{PIA,Biofilm}$. Scattering experiments were not done at $pH_{c,max}$ to avoid multiple scattering from highly turbid samples.

2.4 Results and Discussion

2.4.1 Molecular Weight Distribution

The angular distribution of light scattering, as reported in the chromatograms in Fig. 2.2b, was analyzed to obtain the molar mass distribution of PIA (Fig. 2.6). The weight average molar mass, M_w, was found to be $2.01 \times 10^5 \pm 1200$ *g/mol* and the number average molar mass, M_n, was $7.14 \times 10^4 \pm 2500$ *g/mol*. The polydispersity of the *S. epidermidis* PIA was thus 2.8 ± 0.1.These results have been averaged over 20 samples purified from separate batch cultures. The accuracy of our result is supported by additional analysis of the isolation and purification process that suggests minimal systematic error due to (i) mechanical damage to the polymer during sonication; (ii) loss to centrifugal filters at each stage [36]. Separately, it was found that environmental conditions such as osmotic stress (due to growth media supplemented with 136 – 770*mM* NaCl [37]) affected PIA yield; however, this change did not significantly affect the measured molar mass distribution of PIA.

The measured value of PIA molar mass is in good agreement with the report of Irina et al.,[25]. While most of the earlier reported values of PIA molar mass are around 30 – 80 kDa [38,39] (Fig. 2.6 a), our protocol has resulted in the isolation of a sizeable fraction of higher molar mass

molecules (> 10^5 Da) as well. We attribute this to our purification protocol, which does not include harsh treatments such as ethanol precipitation, repeated dialysis and filtration or freeze drying as commonly carried out in extracting biofilm polysaccharides [40,41]. These treatment steps could potentially result in considerable sample loss due to precipitation upon frequent solvent changes. The polydispersity indicates that the biofilm EPS contains PIA chains with a distribution of chain lengths. Incubation of crude isolates with Proteinase-K and DNAse I [41], prior to affinity chromatography did not affect our final results.

2.4.2 Radius of Gyration, r_g, and overlap concentration, c^*, of PIA

Static light scattering of unfractionated PIA of different concentrations (1 x 10^{-4} – 15 x 10^{-4} *g/mL*) yielded a Zimm plot as shown in Fig. 2.7. We repeated this experiment four times, and the measured z-average r_g was 29.2 ± 1.2 *nm*. The M_w obtained from the Zimm plot showed a 6.3 ± 0.1 % deviation from that obtained from Fig. 2.6a. This deviation suggests minimal mechanical degradation of the PIA chains within the SEC columns. The second virial coefficient was found to be A_2 = (- 3.4 ± 0.3) x 10^{-4} mol mL/g^2. The negative A_2 indicates poor solvent quality for PIA. Indeed, it was found that PIA precipitated out of aqueous solution at higher concentrations, a phenomena also observed by Irina et al [25]. Thus, experiments were carried out within a day or two of sample preparation to prevent any solvent induced changes in polymer conformation. The leading part of the chromatogram from Fig. 2.2b was analyzed to extract a plot of r_g vs. M_w (Fig. 2.8). This plot shows a scaling of $r_g = 0.01 M_w^{0.60\pm0.01}$ *nm.* The power law exponent is consistent with the behavior of a flexible chain [16]. From the molar mass and radius of gyration, we calculated the coil overlap concentration c^* $\left(c^* = \frac{3M_w}{4\pi r_g^3 N_A}\right)$ to be equal to (32 ± 4) x 10^{-4} *g/mL*.

2.4.3 Average $c_{PIA,Biofilm}$ of PIA in *S .epidermidis* biofilms

The values of cell number density (n_{cell}), V_{total}, V_{PIA} and n_{PIA} are shown in Table 2.1. At the growth conditions studied, the cell number density within the biofilm was found to be 0.19 ± 0.03 *cells/*μm^3. Thus, there is an average of one cell found in a volume of V_{total}= 5.26 ± 0.83 μm^3 within the biofilm. Because $V_{bacteria}$= 0.14 ± 0.01 μm^3, V_{PIA} = 5.12 ± 0.83 μm^3*/cell*. The number of PIA molecules per cell (n_{PIA}) was found to be 1.56 ± 0.2 x 10^4 *molecules/cell*. The ratio of n_{PIA} and V_{PIA}, is the extracellular concentration, $c_{PIA,biofilm}$ (in *molecules/*μm^3), of PIA within the biofilm. Thus, using the value of M_w, $c_{PIA,biofilm}$ = (10 ± 2) x 10^{-4} *g/mL* and the extracellular $c_{PIA,biofilm}/c^*$ of PIA for *S .epidermidis* EPS is 0.31 ± 0.07.

The important result $c_{PIA,Biofilm}/c^* < 1$ shows that the extracellular concentration of PIA produced within the *S. epidermidis* biofilm is in the non-entangled, dilute regime. We remark that the measurement of the PIA $c_{PIA,Biofilm}/c^*$ is an average over the entire biofilm, because the measurements n_{PIA} and V_{total} are themselves taken over the whole cultured biofilm. The measurement thus averages over any spatial fluctuations in local $c_{PIA,Biofilm}/c^*$ within the biofilm. The measurement of $c_{PIA,Biofilm}$ accounts for the excluded volume of cells within the biofilm, and is an accurate measure of the *in situ* PIA concentration for that reason.

Polysaccharide entanglements in biofilm matrices have been thought to occur when the polymer molar mass exceeds a value of 10^5 Da [17,20]. Constitutive models for biofilm mechanics have also been developed under this assumption [20]. Here, we have systematically shown that the molar mass of PIA is well above 10^5 Da; however, even given this high molar mass, the biofilm PIA concentration *in situ* is as such too low to support significant entanglement. Thus, the role of physical entanglements in determining EPS viscosity and viscoelasticity is small.

2.4.4 Associative interactions of PIA

Associative interactions of PIA could be facilitated by its polyelectrolyte chemistry (Fig. 2.1a). Within the biofilm, these interactions could be induced by self-association and/or complex formation with extracellular protein [6]. We address each case in the following sections. To identify $c_{critical}$ for these two kinds of associative phenomenon, the scattering intensity at zero angle ($I_{\theta=0}$) versus c_{PIA} for both PIA and PIA-BSA solutions at pH 4.9 and pH 7.5 was measured.

$c_{critical}$ for self-association of PIA: Figure 2.9 shows significant differences between concentration dependent scattering of PIA at pH 4.9 and 7.5. The difference in scattering intensity is about three orders of magnitude, an indication of microstructural differences in the solutions at these two values of pH. For comparison, the expected scattering of single molecules of PIA is plotted on Fig. 2.9. The curve plotted is based on the measured M_w, r_g and A_2 of PIA, and the Zimm scattering theory [28]. The good agreement between the experimental $I_{\theta=0}$ at pH 7.5 for PIA, and the theoretical scattering behavior for single PIA molecules, indicates that scattering at pH 7.5 is inconsistent with self-association behavior.

On the other hand, at pH 4.9, the scattering intensity is at least 10^3 times greater than that at pH 7.5 for all c_{PIA} values studied. This large change in scattering intensity is consistent with self-association at acidic pH [21,35]. The increase in $I_{\theta=0}$ at pH 4.5 indicates an increase in both the effective (i.e. associative) molar mass and the size of the scattering specimen [21]. Because the large increase in $I_{\theta=0}$ was observed at all PIA concentrations studied, for 0.30 x 10^{-4} *g/mL* and greater, we conclude that any critical association concentration, $c_{critical}$, must be less than 0.30 x 10^{-4} *g/mL*. Consequently, because $c_{PIA,Biofilm}$ = (10 ± 2) x 10^{-4} *g/mL*, the concentration of PIA in the native biofilm is at least 30 times greater than this upper bound on the critical association

concentration. This result provides evidence that one of the mechanisms contributing to the EPS microstructure in *S. epidermidis* biofilm is PIA self-association.

While the self-association reported here is the first report of this kind for PIA, the observed behavior is consistent with literature results for a structurally similar polysaccharide, chitosan. Chitosan is a β-1,4 isomer of PIA. At similar degrees of acetylation, chitosan was also found to exist as self-aggregates in dilute solutions at acidic pH [42,43].

$c_{critical}$ for PIA-BSA complexation: From Fig. 2.9, we find that the scattering behavior of PIA is significantly modified in the presence of BSA. At pH 7.5, the concentration dependent scattering of PIA-BSA solutions is about 10^2 times higher than PIA solutions at the same pH. Here the amount of BSA added to each PIA solution is 0.5 %(w/v). Aqueous solutions of BSA at this concentration were found to scatter negligibly relative to all the curves plotted in Fig. 2.9. Thus, the increase in $I_{\theta=0}$ for PIA-BSA at pH 7.5 is consistent with the formation of a complex comprising of PIA and BSA that is considerably larger in molar mass than either PIA or BSA. The moderate scattering of the PIA-BSA solution at this pH suggests that the size of the complexes is relatively smaller than the self-associated complexes observed at pH 4.9.

On the other hand, at pH 4.9, $I_{\theta=0}$ of PIA-BSA and PIA solutions are comparable. This congruence shows that the incremental effect of PIA-BSA complex formation on scattering at pH 4.9 is small relative to the dominant effect of PIA self-association. Thus, the higher turbidity in PIA-BSA solutions at low pH is due to a combination of both self-association of PIA and complexation with BSA, with a dominant role for the former mechanism. On the other hand, at pH 7.5, complex formation with BSA is the only significant mechanism for PIA driven association. Finally, at both pH values studied, the scattering enhancement linked to association was observed at all concentrations studied ($c_{PIA} > 0.30 \times 10^{-4}$ *g/mL*). Thus, just as for the case of

self-association, we can assign the lower bound of $c_{PIA,Biofilm}/c_{critical}$ to be 30. Consequently, in addition to PIA-self association, the mechanism of PIA-protein complexation could be significant in biofilm EPS. This complexation occurs at both acidic and neutral pH. Its observation here for PIA is consistent with literature results for other polysaccharide-protein systems, including chitosan-BSA/lactoglobulin [34,44], carrageenan-bovine casein [45] and acacia gum-lactoglobulin [46]. Moreover, the functional groups present in PIA chemistry (Fig. 2.1a) are sufficient to support the hydrogen bond, hydrophobic and/or electrostatic interactions that are typical in associating systems [24,44]. Finally, the presence of multivalent crosslinking ions could also impact the complexation behavior, analogous to behavior seen in other associating systems such as pectins and alginates[47].

2.5 Conclusions

In this study, we measured and compared the average concentrations of PIA *in situ for S. epidermidis* biofilms ($c_{PIA,Biofilm}$) to independent measurements of the PIA overlap concentration (c^*) and critical association concentration ($c_{critical}$) for self-association and complexation with proteins. The comparison required measurement of the molar mass and radius of gyration of high purity PIA, as synthesized by *S. epidermidis*. We identified that PIA exhibited pH dependent self-association and complex formation with BSA. While the particular associative behavior of PIA reported here has not been previously discussed, our results are consistent with literature reports for structurally similar polysaccharide systems. Furthermore, it was found that $c_{PIA,Biofilm} / c^* = 0.31 \pm 0.07$ whereas the lower bound on $c_{PIA,Biofilm} / c_{critical} = 30$. Comparison of these two quantities indicates that the viscoelasticity of *S. epidermidis* biofilm EPS is generated

predominantly by associative mechanisms of PIA (Fig. 2.1c), rather than by physical entanglements of the polysaccharide (Fig. 2.1b).

These results suggest the following future directions to better understand the implications of polymer associations in biofilms. First, our findings provide motivation to pursue further studies in which the role of polysaccharide driven association and complexation on biofilm EPS properties is established. For example, results on effects of inorganic multivalent ions, pH, and electric fields on biofilm physical properties such as cohesion and viscosity might be fruitfully explained in the context of these effects [48,49,50]. Second, the presence of pH gradients *in situ* biofilms [51,52] and the pH dependent association of PIA observed in this study together suggest that the EPS microstructure could progressively vary between the interior and exterior regions of the biofilm. This relationship should be examined further because the spatial variation in microstructure could affect the local transport [53] and mechanical properties of biofilms. Third, this paper's evidence of self-association in PIA strongly motivates the use of rheological models developed for associating polymers to characterize biofilm viscoelasticity [54,55], rather than the competing possibility of entanglement modeling. These associating polymer models could be parameterized by, for example, studying the microrheology of the PIA associated system. Work in this direction will address molecular mechanisms responsible for the unusual biomechanics of biofilms; examples of which include their extraordinary resistance to external shear [31,54], their flow-induced fragmentation [56] and the non-monotonic behavior of their elastic modulus with ionic strength of growth media [12].

Lastly, we would offer up one broader interpretation of our findings as they relate to the construction of EPS-based biofilms by microorganisms. Synthesis and cell-wall translocation of large structural polysaccharides for the purpose of establishing a viscoelastic medium in which to

live is a metabolically expensive process but mandatory for survival in such bio-systems. As such, one would expect that selection pressure on biofilm-forming species would yield the most economical means of creating durable extracellular scaffolds, so as to optimize the elastic modulus achieved per unit metabolic energy. The assembly of dense overlapping polysaccharide networks is one possible strategy, but our results indicate at least one competitive alternative: namely the secretion of polymers that are capable of forming elastic networks at concentrations well below their coil overlap concentration by recruiting linking molecules. An idea that warrants further exploration is the possibility that bacteria exploit host proteins for this purpose and therefore generates an additional metabolic savings when forming a safe environment for bacterial proliferation.

Table 2.1 Intra-biofilm properties measured to calculate the extracellular $c_{PIA,Biofilm}/c^*$ of PIA

PROPERTY	VALUE
Cell number density (n_{cell})	0.19 ± 0.03 *cells/*μm^3
V_{total}[a]	5.26 ± 0.83 μm^3
V_{PIA}[b]	5.12 ± 0.83 μm^3
n_{PIA}[c]	1.56 ± 0.20 x 10^4 PIA *molecules/cell*
$c_{PIA,Biofilm}/c^*$	0.31 ± 0.07

[a] V_{total}: reciprocal of cell number density

[b] V_{PIA}: average extracellular volume associated with each biofilm bacterium

[c] n_{PIA}: number of PIA molecules per biofilm bacteria

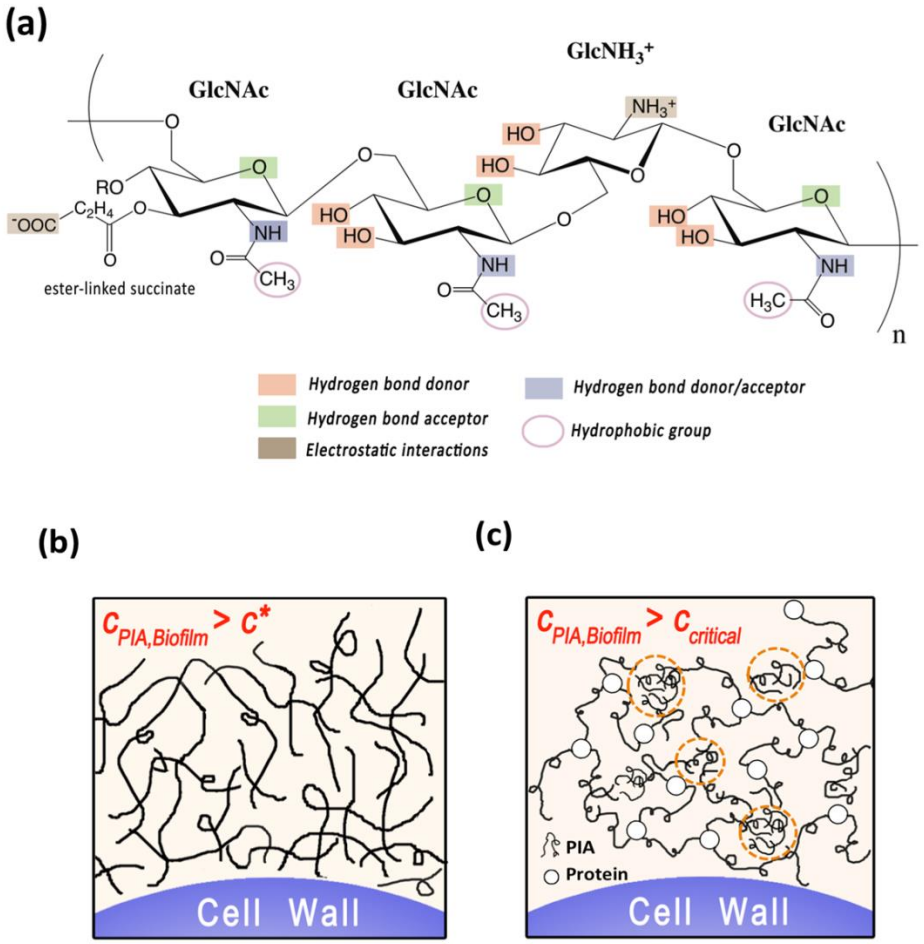

Figure 2.1. Schematic representation of the PIA chain

a) Schematic representation of the PIA chain [9,37]. PIA is a linear homoglycan of β-1,6-linked N-Acetylglucosamine (GlcNAc) residues. About 20% of the monomers are deacetylated, having a cationic free amine group ($GlcNH_3^+$). The chain has a small fraction of anionic O-succinate functional groups rendering the chain zwitterionic. The schematic is a snapshot of a longer molecule; the monomers need not be present in the sequence depicted. Every repeat unit, has potential hydrogen bond participants due to the –OH and acetamido groups. Interactions between chains can therefore occur through the hydrophobic ($-CH_3$), hydrogen bonding (-OH, acetamido), and ionic (deacetylated $-NH_3^+$, and succinyl ester-related $–COO^-$) regions of the polysaccharide backbone. **b)** Schematic representation of the two possible mechanisms of PIA's contribution to *S. epidermidis* biofilm viscoelasticity [2,5]. If $c_{PIA,Biofilm} \geq c^*$, then PIA could form an entangled network of polymer chains [15]. **c)** Alternatively if $c_{PIA,Biofilm} \geq c_{critical}$, then PIA could associate into

a network due to interactions with itself (dotted circles), or due to interactions with protein. See text for definitions of c^* and $c_{critical}$.

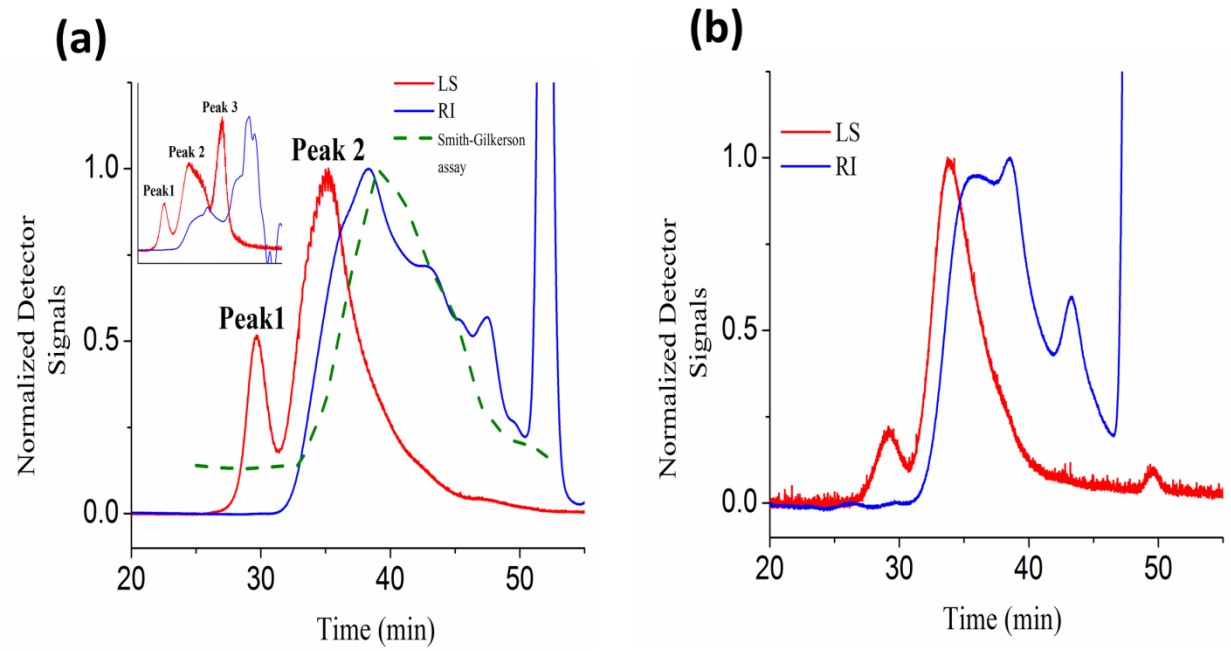

Figure 2.2. Elution chromatogram of PIA

a) Elution chromatograms of PIA isolated by sonication. The chromatograms from the light scattering (LS) detector and from the refractive index (RI) detector are in red and blue respectively. Amino sugars were detected only in Peak 2 (by the Smith-Gilkerson assay) [26]. Eluting fractions beyond 50min are peaks caused by electrolyte in the mobile phase. **b)** The elution chromatogram of isolated Peak 2, containing only amino sugars. This sample represents high purity PIA that was used for all further analysis.

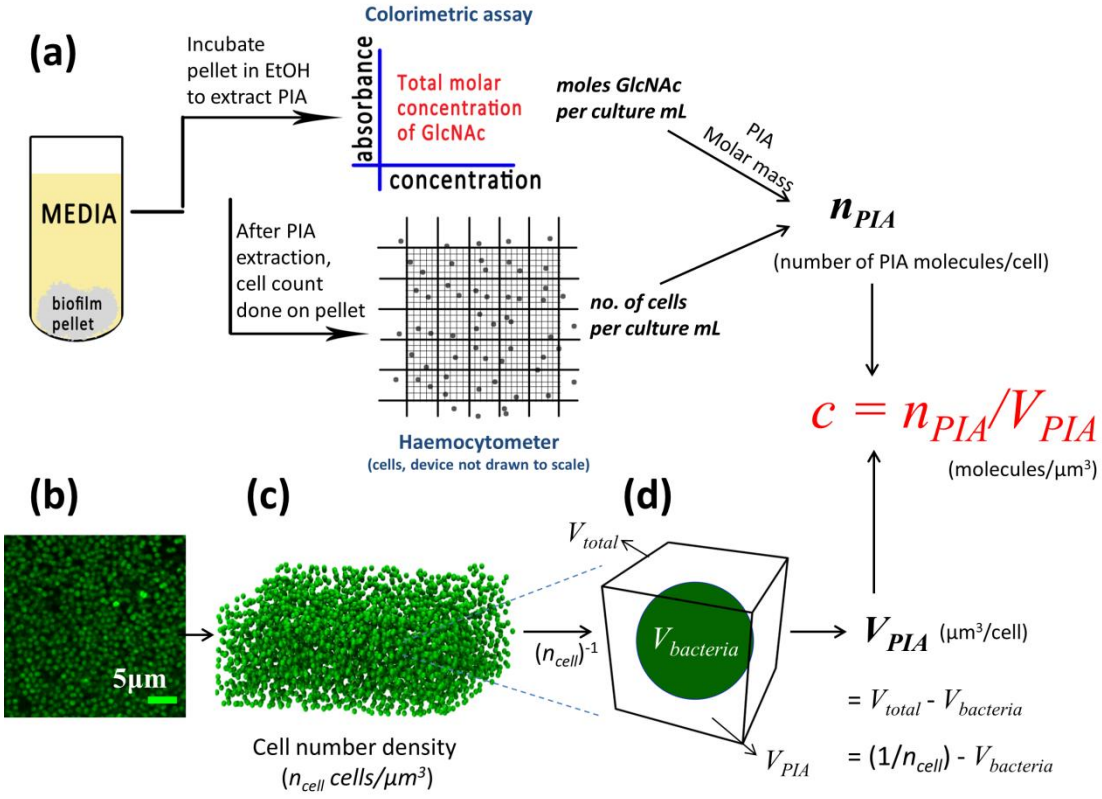

Figure 2.3. Schematic of assay used to calculate average extracellular concentration of PIA

Schematic of assay used to calculate the average extracellular concentration, $c_{PIA,Biofilm}$, of PIA. a) A schematic of the protocol to calculate total number of PIA molecules per biofilm cell (n_{PIA}). b) An x-y CLSM image of bacterial cells (green) within the biofilm. c) A 3-D reconstruction of a biofilm volume using centroid data obtained using image analysis [31]. The number of cells within that volume was taken as local cell number density (n_{cell} *cells/µm*^{3}). c) The reciprocal of the cell number density, $V_{total} = 1/n_{cell}$, is shown. The volume, V_{PIA}, available to PIA molecules per biofilm bacteria (n_{PIA}) was calculated as V_{total} - $V_{bacteria}$ (Table 1). The extracellular PIA concentration within the biofilm, $c_{PIA,Biofilm}$, was then calculated as n_{PIA} / V_{PIA}.

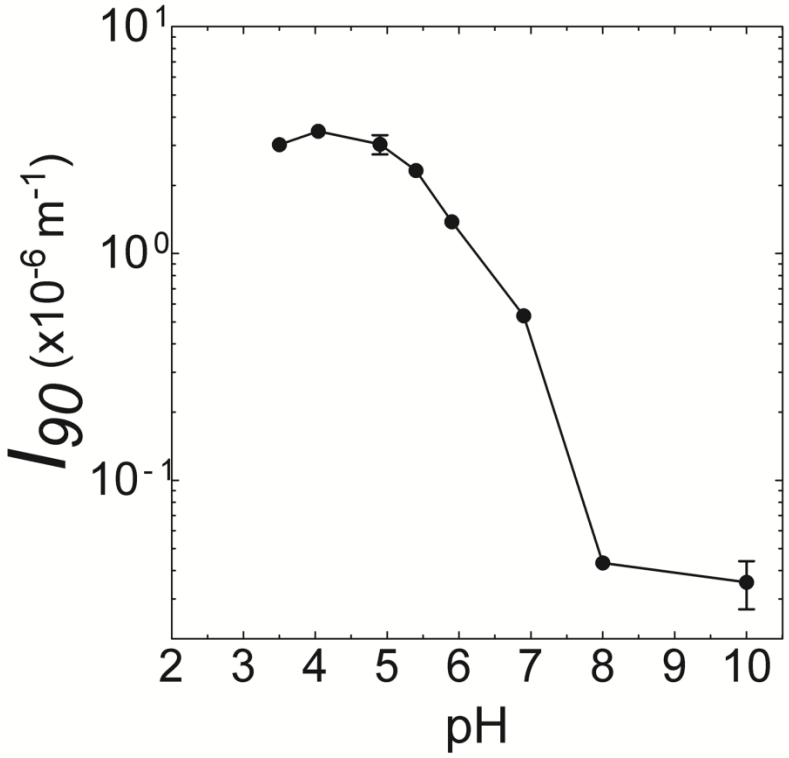

Figure 2.4. Variation of scattering intensity of PIA

Variation of scattering intensity ($I_{\theta=90}$) of PIA solutions at 90° and at c_{PIA} = 6.4 x 10^{-4} *g/mL* versus pH.

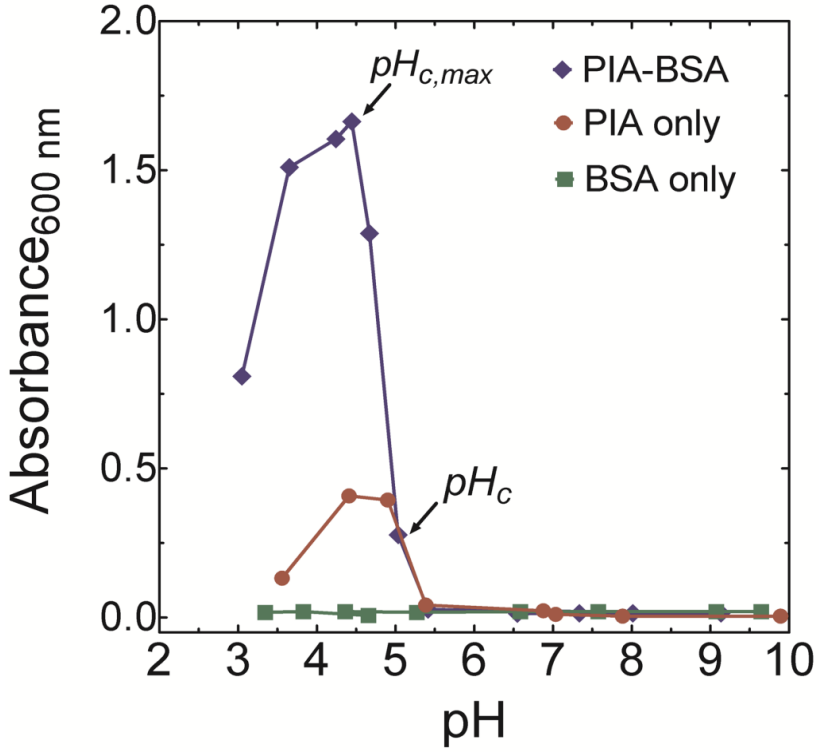

Figure 2.5. Absorbance versus pH for PIA and PIA-BSA solutions

Absorbance (at 600 *nm*) versus pH for solutions of PIA-BSA (6.4 x 10^{-4} *g/mL* PIA, 0.5 %(w/v) BSA) and solutions containing only PIA (6.4 x 10^{-4} *g/mL*) and only BSA (0.5 %(w/v)). The absorbance curve of PIA is consistent with its scattering behavior whereas BSA shows no significant change in absorbance at the concentration studied.

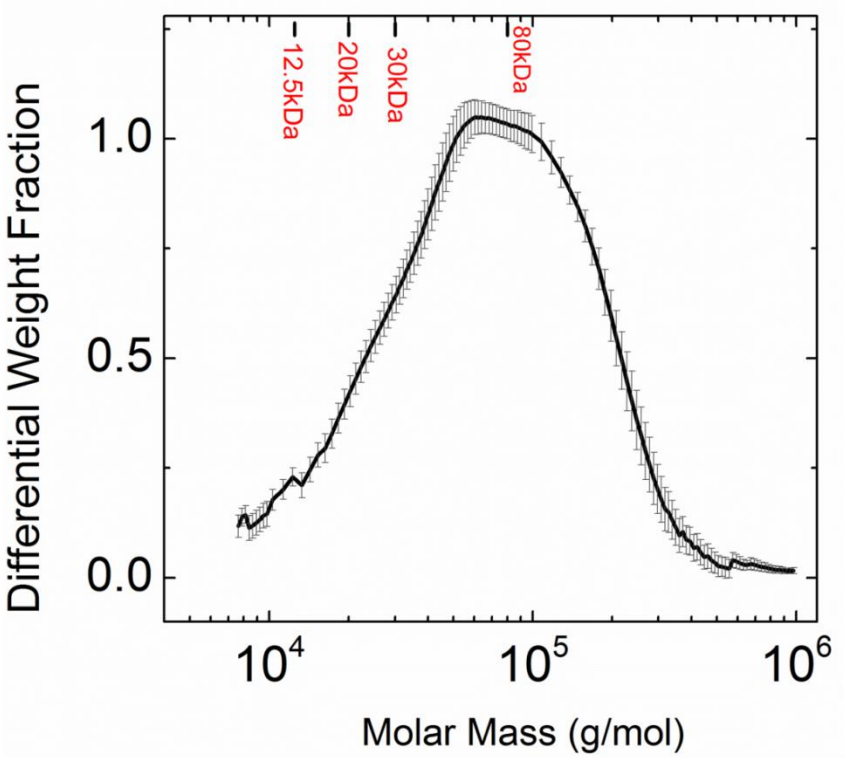

Figure 2.6 Differential molar mass distribution of PIA, indicating PIA molecular weights previously reported in literature [37,38]

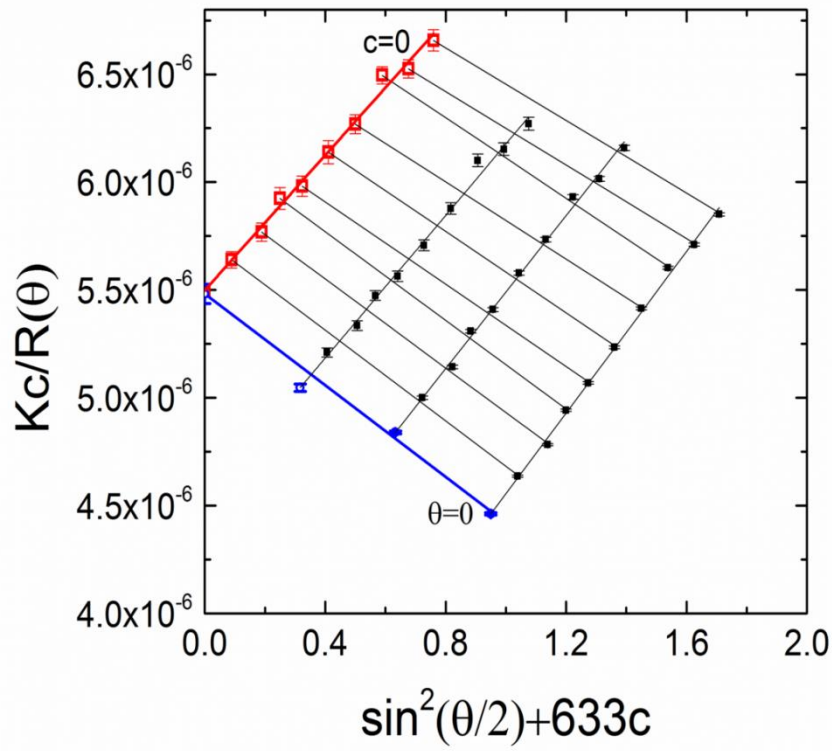

Figure 2.7. PIA Zimm plot obtained by static light scattering

Zimm plot obtained by static light scattering measurement of three different concentrations of PIA (1×10^{-4} *g/mL* – 15×10^{-4} *g/mL* < *c**) at different scattering angles. The weight average molar mass is $1.81 \times 10^5 \pm 3700$ *g/mol* and the z-average r_g is 30 ± 1.6 *nm*.

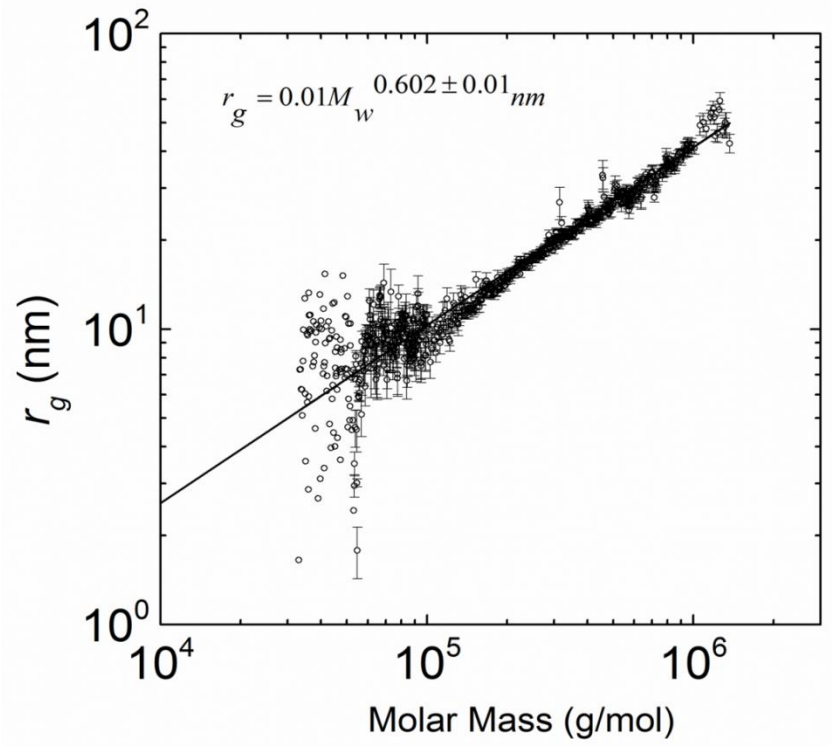

Figure 2.8 Scaling plot of r_g vs M_w for *S. epidermidis* synthesized PIA.

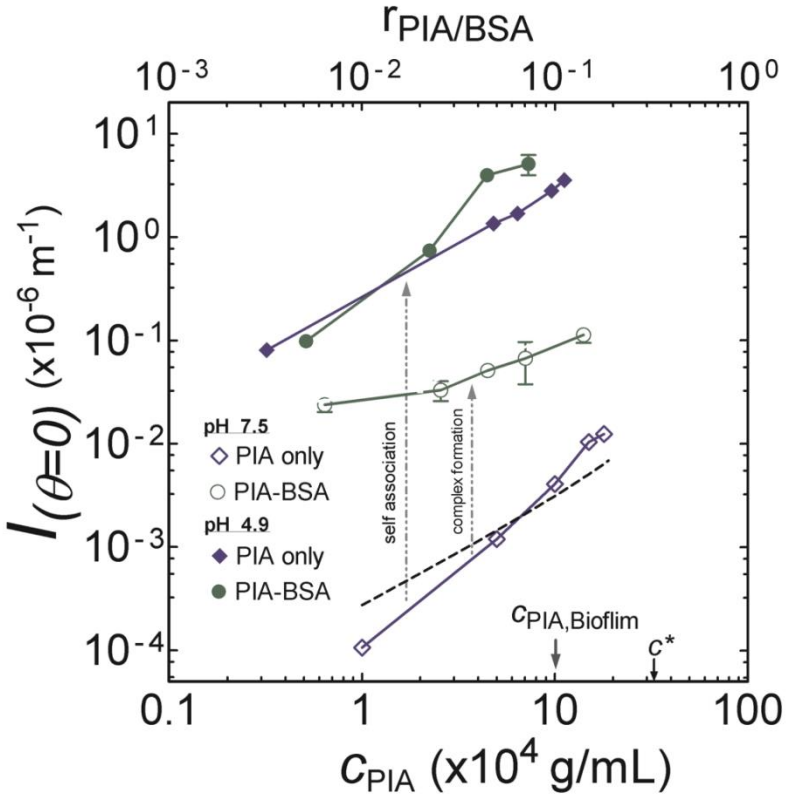

Figure 2.9. Scattering intensity at zero angle versus PIA concentration for PIA and PIA-BSA solutions

Scattering intensity at zero angle ($I_{\theta=0}$) versus PIA concentration (c_{PIA}) at different pH. Solid and empty diamonds indicate solutions containing PIA only at pH 4.9 and 7.5, respectively. Circles indicate PIA-BSA solutions containing 0.5 %(w/v) BSA and varying concentrations of PIA at pH 4.9 (solid circles) and pH 7.5 (empty circles). The dotted line is the theoretical Zimm curve [27] calculated using the M_w and A_2 measured from Fig. 6,7. $c_{PIA,Biofilm}$ and c^* are marked for reference. The upper x-axis denotes the molar ratio of PIA to BSA, $r_{PIA/BSA}$, in each experiment.

2.6 References

1. Ganesan, M. *et al.* Molar mass, entanglement, and associations of the biofilm polysaccharide of Staphylococcus epidermidis. *Biomacromolecules* **14,** 1474–81 (2013).
2. Otto, M. Staphylococcus epidermidis--the "accidental" pathogen. *Nat. Rev. Microbiol.* **7,** 555–567 (2009).
3. Wilking, J. N., Angelini, T. E., Seminara, A., Brenner, M. P. & Weitz, D. a. Biofilms as complex fluids. *MRS Bull.* **36,** 385–391 (2011).
4. Hall-Stoodley, L., Costerton, J. W. & Stoodley, P. Bacterial biofilms: from the natural environment to infectious diseases. *Nat. Rev. Microbiol.* **2,** 95–108 (2004).
5. Flemming, H.-C. & Wingender, J. The biofilm matrix. *Nat. Rev. Microbiol.* **8,** 623–633 (2010).
6. Flemming, H.-C., Wingender, J., Mayer, C., Korstgens, V. & Borchard, W. in *Symp. Gen. Microbiol.* 87–106 (Cambirge University Press, 1999).
7. Rupp, M. E., Fey, P. D., Heilmann, C. & Götz, F. Characterization of the importance of Staphylococcus epidermidis autolysin and polysaccharide intercellular adhesin in the pathogenesis of intravascular catheter-associated infection in a rat model. *J. Infect. Dis.* **183,** 1038–1042 (2001).
8. Vuong, C. *et al.* A crucial role for exopolysaccharide modification in bacterial biofilm formation, immune evasion, and virulence. *J. Biol. Chem.* **279,** 54881–54886 (2004).
9. Otto, M. Molecular basis of Staphylococcus epidermidis infections. *Semin. Immunopathol.* **34,** 201–214 (2012).
10. Rohde, H., Frankenberger, S., Zähringer, U. & Mack, D. Structure, function and contribution of polysaccharide intercellular adhesin (PIA) to Staphylococcus epidermidis biofilm formation and pathogenesis of biomaterial-associated infections. *Eur. J. Cell Biol.* **89,** 103–111 (2010).
11. Di Stefano, A. *et al.* Viscoelastic properties of Staphylococcus aureus and Staphylococcus epidermidis mono-microbial biofilms. *Microb. Biotechnol.* **2,** 634–641 (2009).
12. Pavlovsky, L., Younger, J. G. & Solomon, M. J. In situ rheology of Staphylococcus epidermidis bacterial biofilms. *Soft Matter* **9,** 122–131 (2013).
13. Sutherland, I. Biofilm exopolysaccharides: a strong and sticky framework. *Microbiology* **147,** 3–9 (2001).
14. Mayer, C. *et al.* The role of intermolecular interactions: studies on model systems for bacterial biofilms. *Int. J. Biol. Macromol.* **26,** 3–16 (1999).
15. Guelon, T., Mathias, J. & Stoodley, P. in *Biofilm Highlights* (Flemming, H.-C., Wingender, J. & Szewzyk, U.) **5,** 111–139 (Springer Berlin Heidelberg, 2011).
16. De Gennes, P. G. *Scaling concepts in polymer physics*. (Cornell university press, 1979).
17. Wloka, M., Rehage, H., Flemming, H.-C. & Wingender, J. Rheological properties of viscoelastic biofilm extracellular polymeric substances and comparison to the behavior of calcium alginate gels. *Colloid Polym. Sci.* **282,** 1067–1076 (2004).
18. Körstgens, V., Flemming, H. C., Wingender, J. & Borchard, W. Uniaxial compression measurement device for investigation of the mechanical stability of biofilms. *J. Microbiol. Methods* **46,** 9–17 (2001).
19. Flemming, H.-C. The perfect slime. *Colloids Surf. B. Biointerfaces* **86,** 251–259 (2011).

20. Körstgens, V., Flemming, H. C., Wingender, J. & Borchard, W. Influence of calcium ions on the mechanical properties of a model biofilm of mucoid Pseudomonas aeruginosa. *Water Sci. Technol.* **43,** 49–57 (2001).
21. Esquenet, C. & Buhler, E. Phase Behavior of Associating Polyelectrolyte Polysaccharides. 1. Aggregation Process in Dilute Solution. *Macromolecules* **34,** 5287–5294 (2001).
22. Pedley, a. M., Higgins, J. S., Peiffer, D. G. & Rennie, a. R. Thermodynamics of the aggregation phenomenon in associating polymer solutions. *Macromolecules* **23,** 2494–2500 (1990).
23. Gidley, M. J. Molecular Mechanisms Underlying Amylose Aggregation and Gelation. *Macromolecules* **22,** 351–358 (1989).
24. Turgeon, S. L., Schmitt, C. & Sanchez, C. Protein–polysaccharide complexes and coacervates. *Curr. Opin. Colloid Interface Sci.* **12,** 166–178 (2007).
25. Sadovskaya, I., Vinogradov, E., Flahaut, S., Kogan, G. & Jabbouri, S. Extracellular Carbohydrate-Containing Polymers of a Model Biofilm-Producing Strain , Staphylococcus epidermidis RP62A. *Infect. Immun.* **73,** 2007–3017 (2005).
26. Jefferson, K. & Cerca, N. in *Cell-Cell Interact.* (Colgan, S.) **341,** 119–126 (Humana Press, 2006).
27. Smith, L. R. & Gilkerson, E. Quantitation of Glycosaminoglycan Hexosamine Using 3-Methyl-2-Benzothiazolone Hydrazone Hydrochloride. *Anal. Biochem.* **98,** 478–480 (1979).
28. Podzimek, S. in *Light Scatt. Size Exclusion Chromatogr. Asymmetric Flow F. Flow Fractionation* 207–258 (John Wiley & Sons, Inc., 2011). doi:10.1002/9780470877975.ch4
29. Weinhold, M. X. *et al.* Strategy to improve the characterization of chitosan for sustainable biomedical applications: SAR guided multi-dimensional analysis. *Green Chem.* **11,** 498–509 (2009).
30. Joyce, J. G. *et al.* Isolation, structural characterization, and immunological evaluation of a high-molecular-weight exopolysaccharide from Staphylococcus aureus. *Carbohydr. Res.* **338,** 903–922 (2003).
31. Hohne, D. N., Younger, J. G. & Solomon, M. J. Flexible microfluidic device for mechanical property characterization of soft viscoelastic solids such as bacterial biofilms. *Langmuir* **25,** 7743–7751 (2009).
32. Dzul, S. P. *et al.* Contribution of the Klebsiella pneumoniae capsule to bacterial aggregate and biofilm microstructures. *Appl. Environ. Microbiol.* **77,** 1777–1782 (2011).
33. Vuong, C. & Otto, M. The biofilm exopolysaccharide polysaccharide intercellular adhesin--a molecular and biochemical approach. *Methods Mol. Biol. Clift. Nj* **431,** 97–106 (2008).
34. Guzey, D. & McClements, D. J. Characterization of β-lactoglobulin–chitosan interactions in aqueous solutions: A calorimetry, light scattering, electrophoretic mobility and solubility study. *Food Hydrocoll.* **20,** 124–131 (2006).
35. Lin, W. *et al.* Effect of pH on gelatin self-association investigated by laser light scattering and atomic force microscopy. *Polym. Int.* **51,** 233–238 (2002).
36. Maira-Litran, T. *et al.* Immunochemical Properties of the Staphylococcal Poly- N -Acetylglucosamine Surface Polysaccharide Immunochemical Properties of the Staphylococcal. *Infect. Immun.* **70,** 4433–4440 (2002).
37. Knobloch, J. K. M. *et al.* Biofilm Formation by Staphylococcus epidermidis Depends on Functional RsbU , an Activator of the sigB Operon : Differential Activation Mechanisms Due to Ethanol and Salt Stress. *Infect. Immun.* **183,** 2624–2633 (2001).

38. Mack, D. *et al.* The intercellular adhesin involved in biofilm accumulation of Staphylococcus epidermidis is a linear beta-1,6-linked glucosaminoglycan: purification and structural analysis. *J. Bacteriol.* **178,** 175–83 (1996).
39. Karamanos, N. K. *et al.* Identity of macromolecules present in the extracellular slime layer of Staphylococcus epidermidis. *Biochimie* **77,** 217–224 (1995).
40. Mckenney, D. *et al.* The ica Locus of Staphylococcus epidermidis Encodes Production of the Capsular Polysaccharide / Adhesin. *Infect. Immun.* **66,** 4711–4720 (1998).
41. Vuong, C. & Otto, M. in *Methods Mol. Biol.* (DeLeo, F. & Otto, M.) **431,** 97–105 (Humana Press).
42. Anthonsen, M., Varum, K., Hermansson, a, Smidsrod, O. & Brant, D. Aggregates in acidic solutions of chitosans detected by static laser light scattering. *Carbohydr. Polym.* **25,** 13–23 (1994).
43. Schatz, C., Viton, C., Delair, T., Pichot, C. & Domard, A. Typical physicochemical behaviors of chitosan in aqueous solution. *Biomacromolecules* **4,** 641–648 (2003).
44. Kayitmazer, A. B., Strand, S. P., Tribet, C., Jaeger, W. & Dubin, P. L. Effect of polyelectrolyte structure on protein-polyelectrolyte coacervates: coacervates of bovine serum albumin with poly(diallyldimethylammonium chloride) versus chitosan. *Biomacromolecules* **8,** 3568–3577 (2007).
45. Burova, T. V *et al.* Conformational changes in iota- and kappa-carrageenans induced by complex formation with bovine beta-casein. *Biomacromolecules* **8,** 368–375 (2007).
46. Schmitt, C., Sanchez, C., Thomas, F. & Hardy, J. Complex coacervation between β-lactoglobulin and acacia gum in aqueous medium. *Food Hydrocoll.* **13,** 483–496 (1999).
47. Braccini, I. & Pérez, S. Molecular basis of C(2+)-induced gelation in alginates and pectins: the egg-box model revisited. *Biomacromolecules* **2,** 1089–96 (2001).
48. Brindle, E. R., Miller, D. a & Stewart, P. S. Hydrodynamic deformation and removal of Staphylococcus epidermidis biofilms treated with urea, chlorhexidine, iron chloride, or DispersinB. *Biotechnol. Bioeng.* **108,** 2968–77 (2011).
49. Stoodley, P., DeBeer, D. & Lappin-Scott, H. M. Influence of electric fields and pH on biofilm structure as related to the bioelectric effect. *Antimicrob. Agents Chemother.* **41,** 1876–1879 (1997).
50. Chen, X. & Stewart, P. S. Role of electrostatic interactions in cohesion of bacterial biofilms. *Appl. Microbiol. Biotechnol.* **59,** 718–720 (2002).
51. Vroom, J. M. *et al.* Depth Penetration and Detection of pH Gradients in Biofilms by Two-Photon Excitation Microscopy. *Appl. Environ. Microbiol.* **65,** 3502–3511 (1999).
52. Ganesh, a. B. & Radhakrishnan, T. K. Fiber-optic sensors for the estimation of pH within natural biofilms on metals. *Sensors Actuators B Chem.* **123,** 1107–1112 (2007).
53. Rani, S. A., Pitts, B. & Stewart, P. S. Rapid Diffusion of Fluorescent Tracers into Staphylococcus epidermidis Biofilms Visualized by Time Lapse Microscopy. *Antimi* **49,** 3502–3511 (2005).
54. Klapper, I., Rupp, C. J., Cargo, R., Purvedorj, B. & Stoodley, P. Viscoelastic fluid description of bacterial biofilm material properties. *Biotechnol. Bioeng.* **80,** 289–296 (2002).
55. Chassenieux, C., Nicolai, T. & Benyahia, L. Rheology of associative polymer solutions. *Curr. Opin. Colloid Interface Sci.* **16,** 18–26 (2011).
56. Stoodley, P., Cargo, R., Rupp, C. J., Wilson, S. & Klapper, I. Biofilm material properties as related to shear-induced deformation and detachment phenomena. *J. Ind. Microbiol. Biotechnol.* **29,** 361–367 (2002).

CHAPTER 3

Microrheology of polysaccharide intercellular adhesin (PIA) from *Staphylococcus epidermidis* biofilms as measured by diffusing wave spectroscopy

3.1 Abstract

The rheology of polysaccharide intercellular adhesin (PIA) solutions, the extracellular polymer of *Staphylococcus epidermidis* biofilms, as measured by diffusing wave spectroscopy microrheology, was found to be purely viscous, at concentrations, c_{PIA}, less than 1.6 wt. %, with the zero-shear rate specific viscosity, η_{sp} varying with concentration as $\eta_{sp} \sim c_{PIA}^{1.1 \pm 0.1}$; while for $c_{PIA} \geq 1.6$ wt. %, PIA solutions were viscoelastic with $\eta_{sp} \sim c_{PIA}^{3.25 \pm 0.62}$. At concentrations greater than 4.8 wt. %, the storage and loss modulus of PIA were congruent with $G' \cong G'' \sim \omega^{0.60 \pm 0.06}$. Furthermore, at $c_{PIA} \geq 1.6$ wt. %, a polymeric mixture consisting of PIA, bovine serum albumin and λ DNA, simulating the biofilm extracellular matrix, was 50-fold more elastic than PIA alone. By comparing these measurements to the rheology of a *S. epidermidis* biofilm [Pavlovsky et al., Soft Matter, **9**, 122-131 (2013)], this study provides the insight that, at concentrations found within cultured biofilms, PIA can facilitate the biofilm's overall viscous modulus, however, neither PIA nor the simulated EPS generates the elasticity observed in mature biofilms. Through this study, we extend our earlier work on dilute solution properties of PIA, into the high concentration regime to advance the understanding of the level of contribution of extracellular polymeric components towards the overall viscoelasticity of bacterial biofilms.**(The**

text in this chapter is from the following manuscript – Ganesan, M., Knier, S., Younger, J.G. and Solomon, M.J. *In preparation* (2015))

3.2 Introduction

Biofilms are viscoelastic, surface-attached microbial consortia [1] that are encapsulated in a matrix of extracellular polymeric substances (EPS) [2–4]. The EPS is metabolic excreta, consisting predominantly of polysaccharides, along with proteins and nucleic acids [2]. The EPS accounts for about 90% of the biofilm by dry mass[3]. The presence of the EPS polysaccharides endows the microbes with an increased resistance to high temperature, phagocytosis, and shear stresses [3,5]. While biofilm presence is beneficial in certain settings such as wastewater treatment, their growth often results in undesirable effects such as the clogging of industrial pipelines or an increased drag on ships due to biofilm growth on their hulls [1]. An additional harm of biofilm growth is their contamination of medical implants. This contamination can lead to infections such as sepsis or cystic fibrosis in humans [1]. Their resistance to blood shear stress, host immune attack and antibiotics, makes biofilms resilient, chronic, and difficult to eradicate [3]. In such cases, the importance of EPS polysaccharide in facilitating biofilm viscoelasticity during growth has been recently highlighted [6–9]. For example, stress relaxation and bacterial rearrangement within biofilms when subjected to shear was found to be facilitated due to the presence of the EPS [10]. Biofilms formed by polysaccharide positive wild type strains were 25 fold more elastic and stiffer than that of polysaccharide negative mutants [11]. Biofilms also mediate their resistance to increased shear stresses by escalating the polysaccharide content of their EPS [12,13]. While biofilm compliance persists upon cell death, it rapidly increases following enzymatic digestion of EPS molecules[14].

While the rheology of whole biofilms has been measured [15–18], identification of the specific contribution of the extracellular polysaccharide to bulk biofilm rheology is unavailable. Therefore, quantifying the viscoelasticity of these constituent polysaccharides would help

deconstruct the mechanical properties of the biofilm by identifying the degree to which the polysaccharide, by itself, contributes to the biofilm mechanical properties, or, alternatively, if it acts synergistically with other components of the biofilm EPS to yield the viscoelasticity of whole biofilms.

In this article, we characterize these properties for *Staphylococcus epidermidis* biofilms. *S. epidermidis* is a nosocomial pathogen [19] whose bulk rheology has been previously studied [16,18]. In *S. epidermidis*, biofilm formation is facilitated by the extracellular polysaccharide intercellular adhesion (PIA) [17,20–22]. PIA is a linear polysaccharide, consisting of β-1,6 linked N-acetylglucosamine units with a degree of deacetylation of about 20 % [20] and a molar mass of ~ 200 kDa [23]. The biofilm bulk viscosity and elasticity [16] are thus dependent, at least in part, on the rheology of PIA. Thus, the aim of this study is to measure the concentration-dependent rheology of PIA to understand the extent to which it can contribute to the viscous and elastic modulus of bulk *S. epidermidis* biofilms [16].

However, rheological measurements of PIA solutions pose the following experimental challenges: (i) isolation and separation of surface attached PIA from the biofilm bacteria as well as other EPS macromolecules (primarily protein and nucleic acid); (ii) generation of sufficient quantities to perform rheological characterization. Here we address the first challenge by evaluating four different PIA purification methods available from the literature and selecting the one that generates the highest yield of PIA. The second challenge is addressed by using diffusing wave spectroscopy and applying the generalized Stokes-Einstein equation of microrheology. This measurement requires only ~ 10^2 microliters of specimen.

The four purification protocols evaluated and used are sonication [24], ultracentrifugation [25,26], EDTA extraction [21], and heat treatment [27,28]. To relate PIA rheology to that of the bulk

biofilm, its *in situ* concentration, $c_{PIA,biofilm}$, is characterized for cultured biofilms. Passive microrheology is performed using diffusing wave spectroscopy [29]. In addition to measurements of solutions of PIA, we probe the rheology of a simulated EPS consisting of PIA, a characteristic protein (bovine serum albumin), and a characteristic nucleic acid (λ DNA). The rheological response of these different systems is compared to that of the bulk biofilm [16]. The rheological characterization reported here can support the development of models that use the interactions and microstructure of PIA to predict the rheology of the biofilm EPS. Such polymer models can potentially be used to understand properties of biofilms that are a consequence of their mechanics, including their ability to form streamers [30], to strain harden [31], and to resist flow induced fragmentation [32].

3.3 Materials and Methods

3.3.1 Culture Conditions and Bacterial Strains

S. epidermidis RP62A (ATCC, Catalog No. 35984) batch cultures were grown for 24 h at 37°C with a moderate shaking of 60 rpm (Forma Incubated Shaker, Thermo Scientific, MA) in 1L tryptic soy broth media supplemented with 1 % (w/v) filtered glucose [23,24].

3.3.2 PIA Purification

Physical (sonication and ultracentrifugation) and chemical (EDTA extraction and heat treatment) protocols were used to detach the crude EPS from the cell surfaces.

Sonication [24]: Flask adherent biofilm was collected by centrifugation (4500 *g*, 30 min, 10°C), re-suspended in HPLC water and sonicated in an ice bath (60 % amplitude; 4 x 30 s cycles, Sonic

Dismembrator Model 120, Fisher Scientific, PA) to release crude PIA from the cell surfaces. After removal of insoluble material (10,000 *g*, 25 min), the supernatant was concentrated.

Ultracentrifugation [25,26]: Crude PIA was released from the bacterial material by centrifuging the biofilm in 0.15 M NaCl at 30,000 *g* for 1 h at 4°C. The pellet was re-suspended in 0.1 M phosphate buffer, 0.1 M NaCl and re-centrifuged. Crude PIA from both supernatants was precipitated twice using cold 95 % (v/v) ethanol overnight. The pellet was collected (18,000 *g*, 10min) and re-dissolved in HPLC water. Insoluble material was removed (25,000 *g*, 30min) and the solution containing PIA was concentrated.

EDTA Treatment [21]: Surface attached PIA was released by incubating the homogenized biofilm for 5 min at 100°C in 0.5 M EDTA, pH 8 (1:50 culture volume). PIA rich supernatant was collected (9000 *g*, 30min), dialyzed (2 x 12 h against DI water, 10 kDa cut-off memberane) and washed in HPLC water and concentrated.

Heat Treatment [27]: The culture supernatant was aspirated and the biofilm was incubated at 60°C for 90 min in 0.1 M $MgCl_2$, pH 5.0 (50% (v/v) AcOH) with constant stirring to harvest crude PIA. The supernatant was collected (12,000 *g*, 10min), diafiltered against 5 volumes of DI water, adjusted to 5mM Tris-HCl, pH 8, 2 mM $CaCl_2$, 2 mM $MgCl_2$, diafiltered against 4 volumes separately of 2 M NaCl followed by 25 mM sodium phosphate, pH 2.5, 0.1 M NaCl, followed by 10 volumes of HPLC water and concentrated.

In each protocol, after removing the PIA, the cell pellet was re-dispersed in PBS. The crude PIA was filter sterilized and concentrated to 500 μL (Amicon Ultra-15 30 kDa cut-off centrifugal filters, Millipore, MA [23]).

3.3.3 PIA molar mass distribution and weight average molar mass, M_w

Crude PIA was size fractionated using Waters Ultrahydrogel 2000 and 250 columns (Waters Technology) in series, with a standard aqueous mobile phase of 0.1 M $NaNO_3$, 0.05% (w/v) NaN_3. The eluents were passed through a concentration detector (Optilab DSP refractometeric interferometer (RI), Wyatt Technology, Santa Barbara, CA) and PIA fractions were identified using the Smith-Gilkerson assay [33] and compared against a calibration curve (obtained using polyethylene oxide standards (Polymer Laboratories) of molar mass 1.0×10^3 – 1.5×10^6 g/mol) to obtain the molar mass distribution and M_w (g/mol) as per [34,35].

The analysis steps have been modified in two ways from earlier work [23]. First, we use size fractionation instead of lectin chromatography. Second M_w is obtained using a calibration curve of PEO standard instead of by multi-angle light scattering and the Zimm theory. This modified method is equivalent to our earlier work [23] as evidenced by a less than 5% deviation in the M_w of PIA (purified using the sonication protocol) computed using the above analysis from that measured earlier.

3.3.4 Concentration of PIA *in situ*, $c_{PIA,biofilm}$

$c_{PIA,biofilm}$ represents the number of PIA molecules (n_{PIA}) within the average extracellular volume (V_{PIA}) associated with each biofilm bacterium [23]. Thus, $c_{PIA,biofilm} = n_{PIA}/V_{PIA}$ [23]. For each

protocol studied, n_{PIA} is the ratio of PIA concentration in the final concentrate to the number of bacterial cells in the re-dispersed pellet. PIA concentration is measured using the Smith Gilkerson assay [33] and cell density is measured using a hemocytometer. We compute V_{PIA} from the reciprocal of the local number density of bacterial cells *in situ* minus the volume of a single bacterial cell [23]. The average density of cells within *S. epidermidis* biofilm varies between 0.02 – 0.41 cells/μm^3, depending on the density phenotype of the biofilm [36].

3.3.5 Dependence of M_w and $c_{PIA,biofilm}$ on purification protocol

Figure 3.1 reports the molar mass distribution and weight average molar mass, M_w of PIA, as a function of purification protocol. PIA purified using EDTA spanned the largest molar mass range from 4 x 10^3 - 2 x 10^6 g/mol, while ultracentrifugation resulted in a distribution of relatively small molar mass (Fig. 3.1 *a*). The PIA purified using ultracentrifugation had a relatively lower M_w = 7.0 x 10^4 ± 3000 g/mol. Except ultracentrifugation, the M_w is consistent across the other protocols (Fig. 3.1 *b*) with a deviation < 10 % between protocols and < 6% relative to the earlier measured value [23].

Figure 3.2 reports $c_{PIAbiofilm}$ for the different purification protocols. The result for sonication is consistent with our previous study [23]. Ultracentrifugation results in the lowest $c_{PIA,biofilm}$ with a mean value of 3 x 10^{-2} wt.%. The EDTA protocol yields the highest value for $c_{PIA,biofilm}$; its mean value is 1.6 wt. %. The variation in $c_{PIA,biofilm}$ across protocols reflects differences in their yield. By these different methods, the *in situ* composition of PIA varies from 0.1 wt. % ≤ $c_{PIA,biofilm}$ ≤ 5.0 wt. %. In Fig.3. 2, we have re-evaluated our earlier assessment of $c_{PIA,biofilm}$ in two ways; first by considering its dependence on the choice of purification protocol,

second by incorporating the different cell number densities *in situ* based on the biofilm density phenotype reported by Stewart et al. [36]. Thus, the range of $c_{PIA,biofilm}$ reported here is more complete than the earlier reported value of 0.3 wt. % [23], which was based only on the yield from the sonication protocol and an averaged *in situ* cell number density of 0.19 cells/μm^3. The data in Fig. 3.1 and 3.2 have been averaged over at least 10 biofilm cultures.

For microrheology studies, we use PIA purified using the EDTA protocol due to its high yield and consistent molar mass distribution.

3.3.6 Diffusing Wave Spectroscopy (DWS) Microrheology

For microrheology, PIA solutions were at concentrations, c_{PIA} varying from 0.1 to 20.0 wt. %, at pH = 5. We had earlier proposed that the contribution of PIA to biofilm viscoelasticity is likely through self-associations identified at pH = 5 [23]. Thus, the viscous and elastic modulus of PIA solutions were measured at pH = 5 and compared to that of bulk biofilms [16].

DWS Experiments: Point source transmission mode DWS was performed using a compact goniometer (ALV, Langen, Germany) with an incident Ar^+ laser of wavelength λ_0 = 488 nm (Innova 70 C, Coherent Inc., Santa Clara, CA). Latex microspheres of 0.5 μm diameter (sulfate and carboxylate probes, Invitrogen) at 2% (v/v) were mixed with PIA solutions and rolled (10 rpm, Wheaton Scientific) for 1 h prior to measurement. Rectangular samples cuvettes of path length L = 1 mm (Starna Cells) were chosen so that $L/l^* \sim 8$, which ensures multiple scattering [29]. Here, l^* is the photon mean free path length, calculated using the Mie theory [37]. The horizontally polarized multiply scattered light from the thermally excited probes was collected

through a Glan-Thomspon prism polarizer. The normalized intensity autocorrelation function, $g_2(t)$, of scattered light, was constructed by pseudo-cross correlation with a minimum delay time of 12.5 ns (ALV 5000-E, ALV, Langen, Germany). Measurements of $g_2(t)$ were taken for 3 - 6 h with frequent re-suspension of probes to minimize any effect of possible sedimentation. Results are the average of 3 - 5 independent measurements.

Data Analysis: $g_2(t)$ was converted to the normalized electric intensity autocorrelation function, $g_1(t)$ via the Siegert relationship $g_1(t) = ((g_2(t)-1)/ \beta)^{0.5}$. β is an instrument constant evaluated by averaging the first 30 points of the data [38]. $g_1(t)$, was converted to probe mean-squared displacement (MSD), $\langle \Delta r^2(t) \rangle$, following [29].

Microrheology Analysis: To convert MSD to shear modulus, we follow Dasgupta et al. [39]. The complex shear modulus, $G^*(\omega)$ is computed using the generalized Stokes-Einstein relation (GSER):

$$G^*(\omega) = \frac{k_B T}{\pi a i \omega \mathfrak{F}\{\langle \Delta r^2(t) \rangle\}} \qquad (1)$$

Here $\mathfrak{F}$ is the Fourier transform operator, Γ is the Gamma function, a is the probe radius, T is temperature and k_B is the Boltzmann constant. To compute the Fourier transform, the MSD is approximated locally, around the frequency of interest $t = 1/\omega$ by a second order logarithmic spline as $\langle \Delta r^2(t) \rangle \approx \langle \Delta r^2(1/\omega) \rangle (\omega t)^{\alpha(\omega)+\frac{\beta(\omega)}{2} ln(\omega t)}$ where $\alpha(\omega) = [\partial \ln\langle \Delta r^2(t) \rangle / \partial \ln t]_{t=1/\omega}$ and $\beta(\omega) = [\partial^2 \ln\langle \Delta r^2(t) \rangle / \partial (\ln t)^2]_{t=1/\omega}$ and is incorporated into Equation (1) leading to expressions for G'(ω) and G"(ω) as reported in ref. [39].

3.3.7 Preparing the simulated EPS

Crude biofilm matrix was extracted using the EDTA protocol [21], and total PIA, protein and nucleic acid concentrations were measured using the Smith Gilkerson [33], BCA (BCA Kit, Thermo Scientific) and PicoGreen (Quant-iT, Invitrogen) assay, respectively. Calculations were done on a per cell basis and averaged over 10 biofilm cultures. By these methods, the ratios of PIA to protein and PIA to nucleic acid were measured to be 1:0.5 and 1:0.04, respectively. The simulated EPS was constructed by mixing together PIA, bovine serum albumin (BSA) (Sigma Aldrich) and λ DNA (Invitrogen) at the above ratios. PIA and λ DNA were pre-heated to 50°C, rapidly mixed, and incubated at 37°C for 30 min [40]. BSA (in HPLC water) is then added. The complexation between the macromolecules was verified using agarose gel shift assay and absorbance measurements. Briefly, PIA complexation with nucleic acids was identified by retardation in the mobility of the polymer complex in comparison to both that of naked DNA and of a complex consisting of PIA replaced with a neutral polymer (2×10^5 g/mol polyethylene oxide) [40]. Complexation with proteins was confirmed by observing the onset of turbidity [23].

3.4 Results

3.4.1 DWS study of PIA solutions

Figure 3.3*a* reports $g_2(t)$ of 0.5 μm probes embedded in PIA solutions for c_{PIA} spanning from 0 to 20 wt. %. At low concentrations (< 0.6 wt. %), the $g_2(t)$ curve nearly overlays that of water, indicating negligible influence on PIA on probe dynamics. With increasing PIA concentration, the $g_2(t)$ decay shifts to longer times. This shift indicates retardation in probe dynamics.

Following Weitz and Pine [29], $g_2(t)$ was converted to the probe $\langle \Delta r^2(t) \rangle$, plotted in Fig. 3.3*b*. At $c_{PIA} < 0.6$ wt. %, the MSD of the thermally excited probes are nearly identical their MSD in the absence of any polymer. At PIA concentrations greater than 0.6 wt. %, the displacement of the probes decreased significantly with increasing polymer concentration. These curves can be phenomenologically modeled with the simple scaling $\langle \Delta r^2(t) \rangle \sim t^{\alpha}$. For microrheology, $\alpha = 0$ indicates that the probes fluctuate in a purely elastic medium. The limit $\alpha = 1$ is for probe motion in a purely viscous medium. For a probe in a viscoelastic medium, $0 < \alpha < 1$ [41]. Thus, over the time range measured, at $c_{PIA} < 0.6$ wt. %, the MSD of the probes has a slope on a log-log scale to be ~ 1, indicating a purely viscous response in the polymer. For $c_{PIA} >$ 0.6 wt % the slope change progressively with time. At short times, $\alpha \sim 0.73$, indicating sub-diffusive behavior, while at long times, $\alpha \sim 0.90$, characteristic of diffusive motion. $\alpha < 1$ at short times indicates the presence of an elastic component in the response of the polymer at those concentrations.

To extract the storage and loss moduli of the polymer, we apply the GSER to the measurements of probe diffusion (Fig. 3.3*b*). The quantity $\langle \Delta r^2(t) \rangle a$ must be independent of particle size for this application to be generally valid [38]. The measured dynamics should also be independent of probe chemistry. To evaluate these constraints, $\langle \Delta r^2(t) \rangle a$ of probes of different sizes were compared at $c_{PIA} = 1.6$ wt. % (Fig. 3.4). The results show that the product $\langle \Delta r^2(t) \rangle a$ collapses onto a master curve for probe diameters varying from 0.1 μm to 1.2 μm. Furthermore, the difference in the MSD of 0.5 μm probes which carboxylate and sulfate surface chemistry was

negligible. These results indicate that the continuum viscoelastic approximation of the GSER is satisfied.

3.4.2 Concentration dependent viscoelasticity of PIA solutions

To study the concentration dependence of viscosity, following Colby and co-workers [42], the variation of the zero-shear specific viscosity, η_{sp}, with c_{PIA} is plotted (see Fig. 3.5). Here, $\eta_{sp} = (\eta_0-\eta_s)/\eta_s$ where η_0 is the zero-shear rate viscosity and η_s is the solvent viscosity. η_0 was computed from the data of Fig. 3*b* following Ninomiya [43]. Briefly, $1/\eta_0$ was taken as the intercept at the ordinate of the curve J(t)/t versus 1/t. Equivalently, $\eta_0 = [t/J(t)]_{t\to\infty}$ [38]. J(t) is the creep compliance obtained from MSD by the application of the GSER (Equation 1), following Xu et al. [44]. For $c_{PIA} < 1.6$ wt %, the viscosity followed the scaling $\eta_{sp} \sim c_{PIA}^{1.1 \pm 0.1}$ (see Fig. 3.5). The overlap concentration, c^*, can be estimated as the concentration at which η_0 is twice the solvent viscosity ($\eta_{sp} = 1$) [42]. From Fig. 3.5, we obtain $c^* \sim 0.4$ wt. %, which is comparable to the value of 0.32 wt. % previously reported by static light scattering [23]. At PIA concentrations greater than 1.6 wt. %, we observe a transition in the concentration dependence of viscosity, where η_{sp} increases as $\eta_{sp} \sim c_{PIA}^{3.25 \pm 0.62}$.

Figure 3.6 reports the storage, G'(ω), and loss, G"(ω), modulus of PIA obtained from Fig. 3.3*b* by the method of Dasgupta et al. [39]. We compare it with the bulk storage and loss modulus of *S. epidermidis* biofilms as reported by Pavlovsky et al. [16]. We plot modulus data only for $c_{PIA} > 0.6$ wt. % because at lower concentrations, PIA was inelastic over the frequency range probed. The elastic modulus of PIA (see Fig. 3.6*a*) approached that of bulk, cultured biofilm only at the high concentration of 20 wt. %. At concentrations less than that, the G' of

PIA was less than that of the biofilm by a factor ~10^2. On the other hand, for all concentrations, c_{PIA} > 0.6 wt. %, the viscous modulus of PIA (see Fig. 3.6*b*) was almost comparable to that of the biofilm and was within a factor of ~ 2.5 of the biofilm's viscous modulus. In addition, at a reference frequency of $\omega = 10^4$ Hz, the concentration dependence of the complex modulus was, $G^*(c_{PIA}) \sim c_{PIA}^{1.6 \pm 0.3}$.

We note that, G"(ω) was greater than G'(ω) at low frequencies for all concentrations. This indicates that PIA behaves like an inelastic fluid at those frequencies, as evident from the MSD which has a slope ~ 1 at longer times. For $c_{PIA} \geq 4.8$ wt. %, at higher frequencies, the G"(ω) and G'(ω) curves become parallel, with a frequency dependence of $G' \cong G'' \sim \omega^{0.60 \pm 0.06}$. From the evolution of the loss tangent, $\tan(\delta) = G''/G'$, we find that at concentrations greater than 4.8 wt. %, $\tan(\delta)$ becomes independent of frequency (see Fig. 3.7).

3.4.3 Microrheology of simulated EPS

Figures 3.3-3.7 reported the rheology of aqueous solutions of PIA. Within a biofilm EPS, PIA is often present along with extracellular proteins and nucleic acids [3]. Such simulated EPS mixtures were prepared at four PIA concentrations – 0.1 wt. %, 0.3 wt. %, 1.6 wt. % and 3.2 wt. %, that are within the range of $c_{PIA,biofilm}$ (c.f. Methods).

Figure 3.8 reports the DWS data obtained for a simulated EPS containing PIA at 1.6 wt. %. The evolution in $g_2(t)$ of 0.5 μm probes embedded in solutions containing only PIA, PIA in the presence of BSA, PIA containing λ DNA and PIA in the presence of both BSA and λ DNA

is plotted. With added macromolecules, the decay in $g_2(t)$ shifts to longer times. As a control, BSA and λ DNA were mixed at the same stoichiometric ratios with a neutral polymer of similar molar mass (2 x 105 g/mol, polyethylene oxide). No significant change in the $g_2(t)$ decay was observed for this system (data not shown).

The creep compliance, J(t), of the simulated EPS, as extracted from the measured $g_2(t)$ is plotted in Fig. 3.9*a*. With the addition of BSA, λ DNA and both BSA and λ DNA, the compliance of PIA decreased by 50, 55 and 82 %. In comparison, for the case of polyethylene oxide control, a less than 10 % decrease in compliance was observed in the presence of BSA and λ DNA (data not shown). Therefore, the change in PIA viscoelasticity due to addition of protein and nucleic acid is large relative to the control.

Fig. 3.9 *b,c* further supports this finding. Specifically, without any added macromolecule, PIA, at 1.6 wt. %, has an elastic modulus that is less by a factor of 2×10^2 and a viscous modulus that is less by a factor of 5 than the biofilm. However, the simulated EPS containing proteins and nucleic acids has an enhanced elasticity that is about 50 fold higher than that of PIA alone. The elastic modulus of the EPS was within a factor of 5 from that of the biofilm while its viscous modulus was almost congruent to that of the bulk biofilm.

Figure 3.10 reports the change in zero-shear specific viscosity of the simulated EPS containing different concentrations of PIA. At c_{PIA} = 0.1 wt. %, the viscosity of the simulated EPS was not much different from that of PIA. The samples containing PIA at 0.3 wt. %, 1.6 wt. % and 3.2 wt. % were about ~ 15 times more viscous than PIA alone.

3.5 Discussion

In this study, we probed the concentration dependent viscoelasticity of aqueous PIA at different concentrations and the rheology of a simulated biofilm EPS consisting of PIA, BSA and λ DNA. We first compare rheology of PIA with theoretical and experimental findings reported for similar systems and then discuss these measurements with respect to the contribution of PIA to the overall biofilm viscoelasticity.

At $c_{PIA} < 1.6$ wt. %, the scaling $\eta_{sp} \sim c^{1.1 \pm 0.1}$ is consistent with the Huggins equation for dilute polymer solutions [45]. On the other hand, beyond the transition concentration of 1.6 wt. %, the exponent of 3.25 ± 0.62 is in considerable agreement within its standard deviation, with that predicted for semidilute solutions of entangled non-interacting polyelectrolytes ($\eta_{sp} \sim c^{15/4}$) [46]. We find that, within the concentration rage studied, a clear transition between the dilute to semidilute unentangled regime was however not observed. Thus, the nature of the transition concentration of 1.6 wt. % is unclear. That is, from Fig 3.5, by comparing with theoretical predictions, parametrizing the viscoelasticity of PIA to be due to physical entanglements is unfortunately not forthcoming. However, we note the following consistencies of the scaling exponents reported here with experimental observations for other systems. Morris et al. found that random coil polysaccharides exhibited a scaling of $\eta_{sp} \sim c^{1.4}$ at dilute concentrations and $\eta_{sp} \sim c^{3.4}$ at higher concentrations [47]. Colby and co-workers report that the N-acetylglucosamine containing polysaccharide, hyaluronan, followed a scaling $\eta_{sp} \sim c^{1.2}$ at dilute concentrations, and $\eta_{sp} \sim c^{4.1}$ at higher concentrations beyond a transition point [42].

In our earlier study, we identified self-associations in dilute solutions of PIA [23]. Associative interactions in PIA would be likely hydrophobic in nature due to the presence of alkyl functional groups along the chain [20]. PIA would thus likely represent a multi-sticker associating polymer, which at pH = 5, forms large aggregates [23]. These inter-chain interactions might contribute to viscoelasticity at higher concentrations. To investigate this proposition, we found that at c_{PIA} > 1.6 wt. %, the data in Fig. 3.5, also followed the scaling, $\eta_{sp} \sim \exp(\text{const } (c_{PIA})^{\nu})$, proposed by Semenov and Rubinstein [48] for multi-sticker associating polymers. However, the exponent $\nu = 0.50 \pm 0.15$ identified for PIA with the available data points, is less than their theoretically predicted value of $\nu = 0.87$ [48].

Thus, while c_{PIA} = 1.6 wt. % displays a transition in the viscoelasticity of PIA solutions, at this point, the nature of this transition is unclear. This is because; lack of sufficient rheological data points at intermediate and higher PIA concentrations renders the above scaling exponents inconsistent for comparison with literature. Further experiments are warranted to identify if whether physical entanglements or associative rheology, as proposed by us earlier [23], should be used to describe the viscoelastic properties of PIA. Such experiments could be the following. First, to confirm the presence of associative interactions, the role of destabilizing factors such as urea or guanidine salts that are known to disrupt hydrogen bonding/hydrophobic effects, on the viscoelasticity of PIA solutions is to be studied. Second, measurements to identify if there is an occurrence of shear thickening at intermediate shear rates, which is a common indicator for associative rheology is to be done. Third, while the congruence in frequency dependence of G' and G", as identified here for c_{PIA} greater than 4.8 wt. %, is often attributed to onset of gelation in both physical [49] and chemically cross-linked polymers [50], rheological and

small angle light scattering experiments at higher PIA concentrations are necessary to identify the nature of this phenomena.

From Fig 3.5 – 3.7, we obtain the following insight into the contribution of PIA to the overall rheology of *S. epidermidis* biofilms. From Fig. 3.5, we note that the transition concentration is within the range of $c_{PIA,biofilm}$. At these concentrations, PIA could also complex with proteins and DNA resulting in a composite that has an enhanced elasticity than PIA alone (see Fig. 3.8, 3.9). We thus propose that the contribution of PIA to biofilm rheology is likely to be – i) purely viscous contribution at $c_{PIA,biofilm} < 1.6$ wt.%, ii) viscoelastic contribution on its own or through complexation with proteins and nucleic acids in regions within the biofilm having $c_{PIA,biofilm} \geq 1.6$ wt.%. An average *in situ* concentration (as indicated by the mean in Fig. 3.2 for EDTA) would be 1.6 wt. %. Thus, collectively, the viscous modulus of PIA, both individually and in synergy with proteins and DNA is congruent with that of the biofilm, while its elastic modulus, even in the presence of proteins and nucleic acids, is less than that of a mature *S. epidermidis* biofilm.

3.6 Conclusions

In this study, we report the viscoelastic properties of PIA at concentrations relevant to its composition within shaker grown *S. epidermidis* biofilms. We identified distinct regimes of contribution of PIA towards biofilm viscoelasticity ranging from viscous to viscoelastic mediation on its own or through complexation with proteins and nucleic acids. The study reveals the potential synergistic role of extracellular proteins and DNA in mediating the bulk biofilm rheology. Studying the role of polymer-polymer interactions or agents that are

disruptive to such interactions, such as temperature or presence of salts, on the biofilm rheology is an instructive next step. The extent of $c_{PIA,biofilm}$ and the observed concentration dependent rheological behavior of PIA shows that there could presumably exists regulatory mechanisms *in situ* that tailor PIA concentration locally to enable a rigid or a viscous matrix that facilitates biofilm spreading to suit their colonial life cycles. Since the biofilm bacteria constantly thrive and differentiate into a polymeric continuum that they synthesize, results from the current study coupled with recent insights into biofilm microstructure and rheology enables the structural and mechanical de-construction of biofilm to understand how bacteria control biofilm mechanical properties by regulating their morphology and the EPS composition.

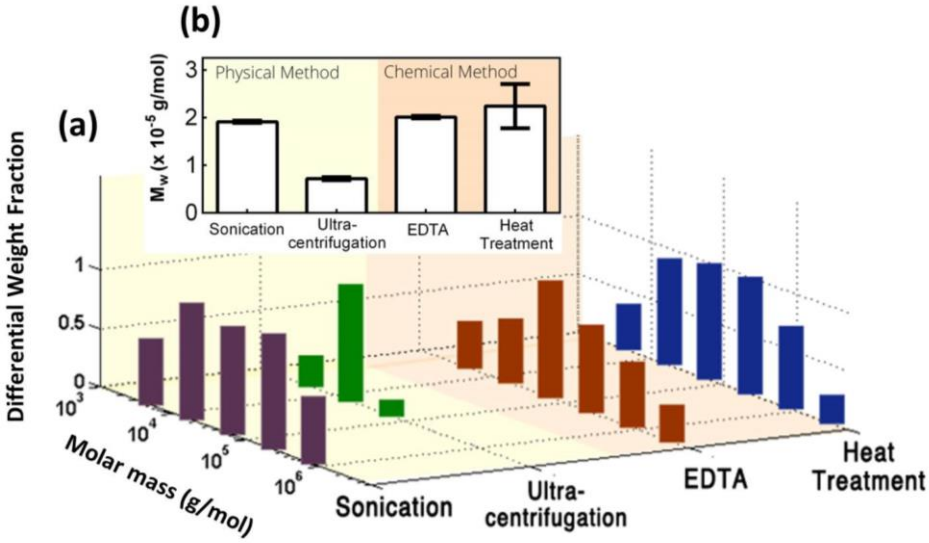

Figure 3.1. PIA Molar Mass dependence on purification protocol

(a) Weight average molar mass, M_w (g/mol) and **(b)** Differential molar mass distribution of PIA obtained using the four different purification protocols.

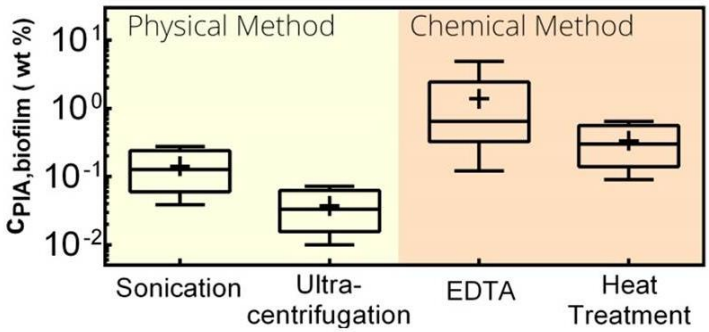

Figure 3.2. Dependence of cPIA,biofilm on the PIA purification protocol used

The whiskers in the box plot extend to the minimum and maximum values. The horizontal line inside the box denotes the median, while the bottom and top boundaries represent the 25th and 75th percentiles respectively. The '+' denotes the mean.

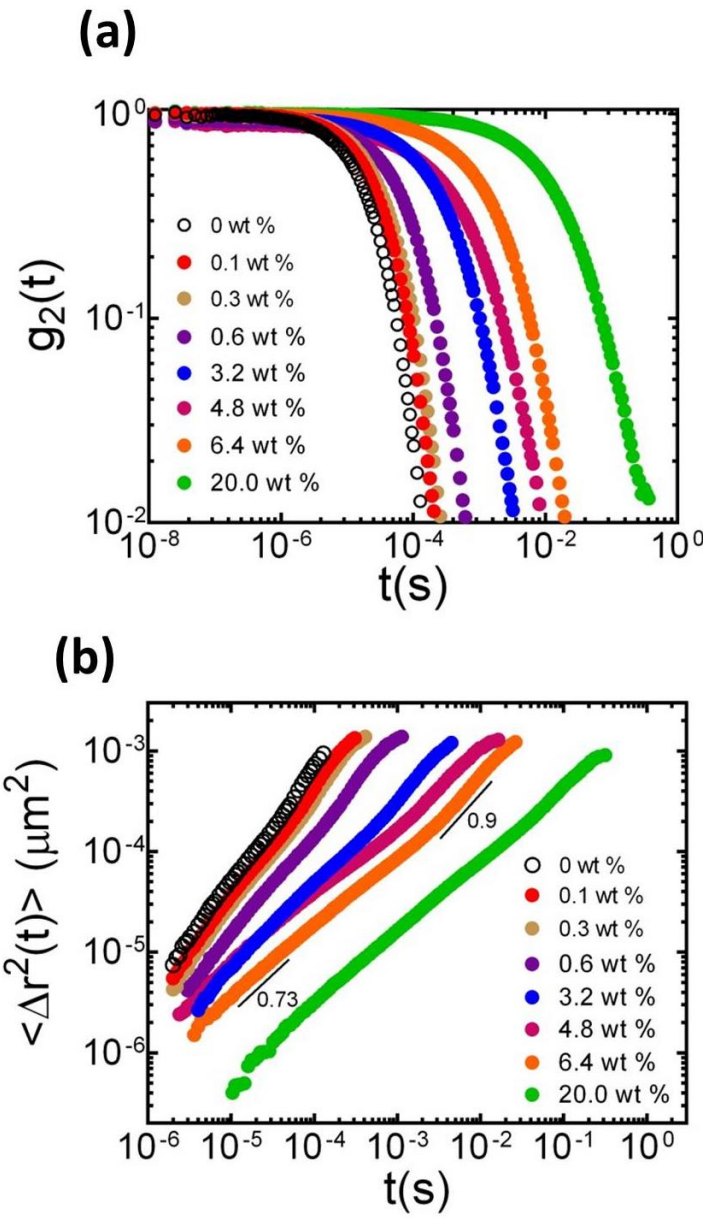

Figure 3.3. DWS analysis of PIA solutions

(a) DWS intensity auto correlation function, $g_2(t)$, and the corresponding **(b)** mean squared displacement ($<\Delta r^2(t)>$) of 0.5μm sulfate probes at 2 % (v/v) in solutions of varying PIA concentrations plotted vs time .

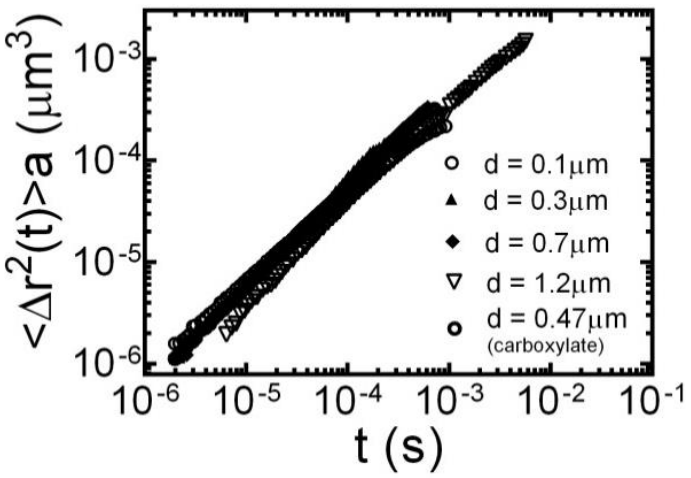

Figure 3.4. Probe size dependence of DWS analysis for PIA

The scaled quantity $<\Delta r^2(t)>a$ for different probe sizes and chemistry plotted vs time at a PIA concentration of 1.6 wt %.

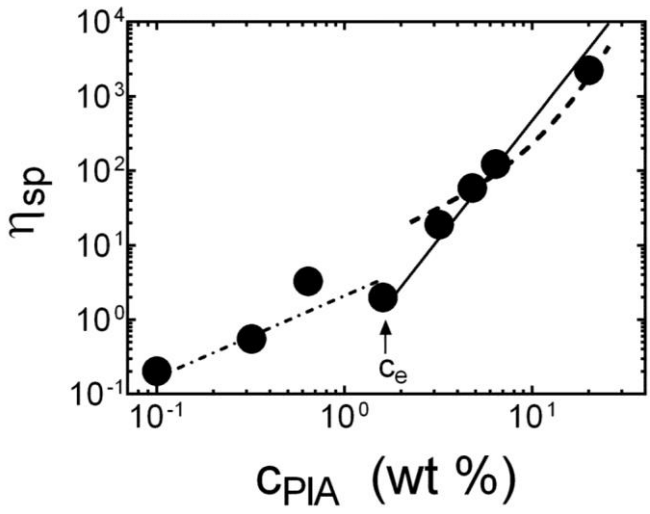

Figure 3.5. Concentration dependence of PIA viscosity

Specific zero-shear rate viscosity (η_{sp}) as a function of PIA concentration. The dot dashed line is a power law fit $\eta_0 \sim (c_{PIA})^{1.1}$, the solid line represents $\eta_0 \sim (c_{PIA})^{3.25}$ and the dashed line is an exponential fit according to Semenov and Rubinstein [48] with $\eta_0 \sim \exp(\text{const}\ (c_{PIA})^{0.50 \pm 1.5})$.

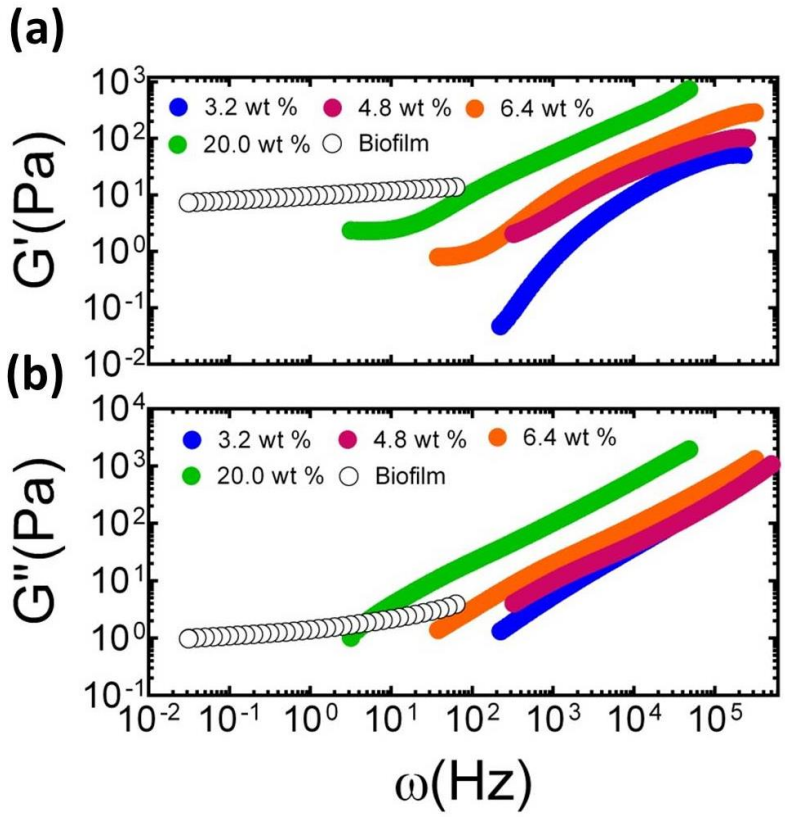

Figure 3.6. Storage, G', and loss, G", modulus of PIA

(a) Frequency dependent storage (G') and **(b)** loss (G") modulus of PIA at different concentrations in comparison with that of a bulk biofilm as reported by(16).

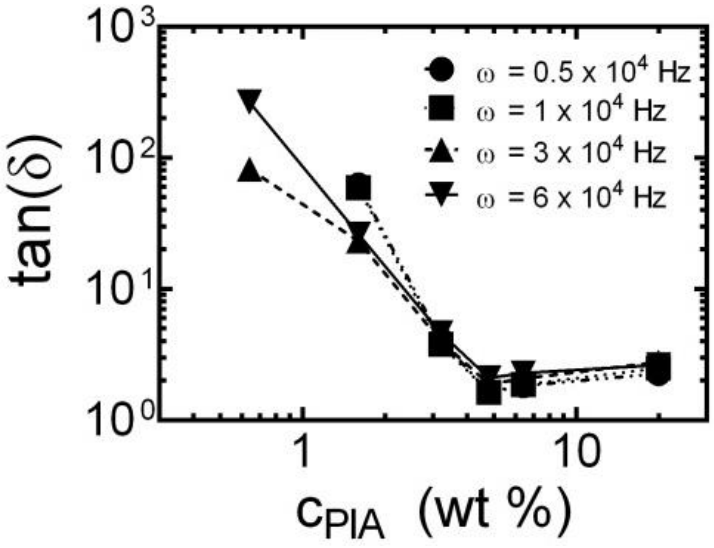

Figure 3.7. Evolution of loss tangent as a function of PIA concentration

Here, loss tangent, tan(δ) = G”/G’.

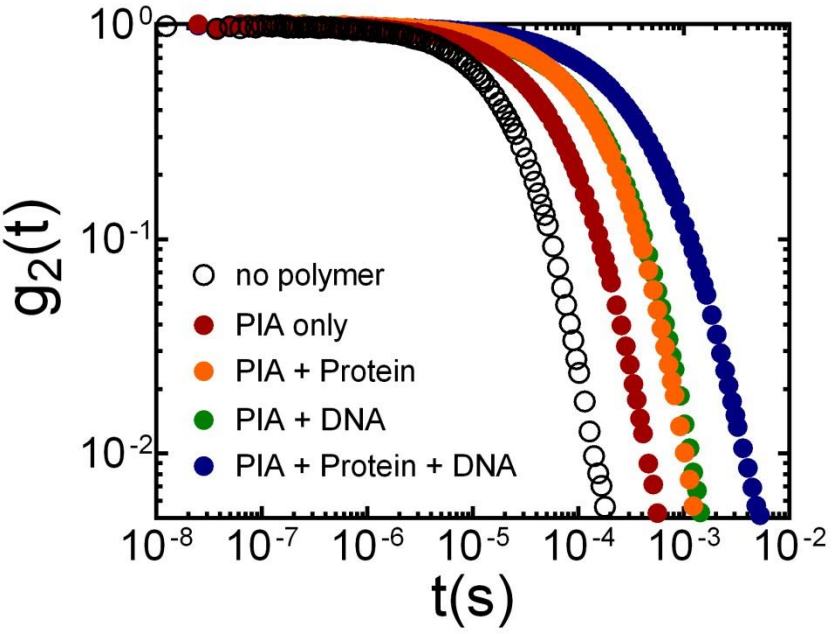

Figure 3.8. DWS analysis of simulated EPS

DWS intensity autocorrelation function, $g_2(t)$, of 0.5μm probes at 2 % (v/v) in solutions containing different components of the simulated EPS mixed at stoichiometric ratios as mentioned in Results. The concentration of PIA is kept fixed at 1.6 wt %.

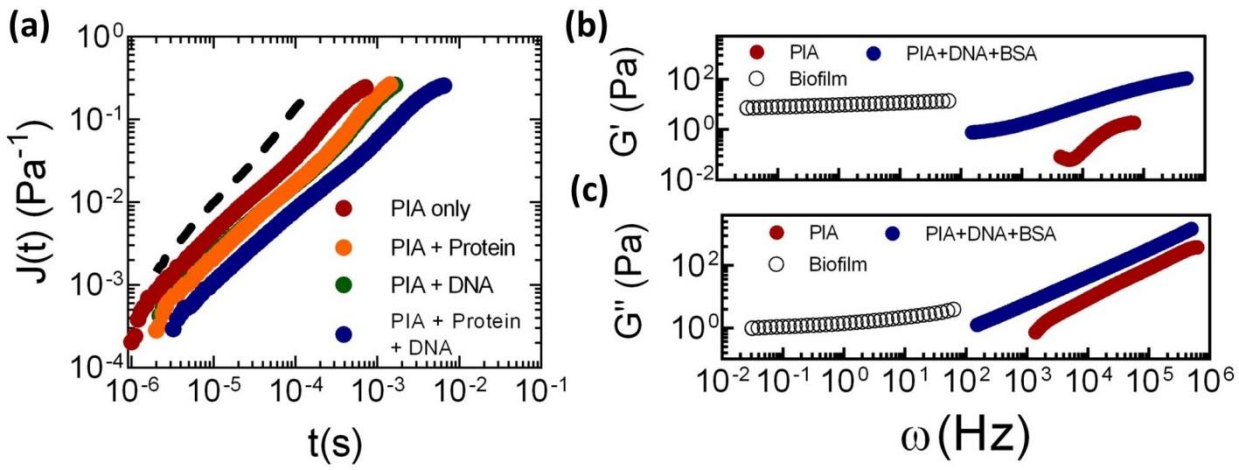

Figure 3.9. Microrheology of simulated EPS

(a) Creep compliance (J(t)) measured by DWS of varying components of the simulated EPS. The dotted line represents the creep compliance of water. **(b)** Storage (G') and **(c)** loss (G") modulus of the simulated EPS and PIA only in comparison to that of the bulk biofilm(16). The concentration of PIA is kept fixed at 1.6 wt % in all solutions.

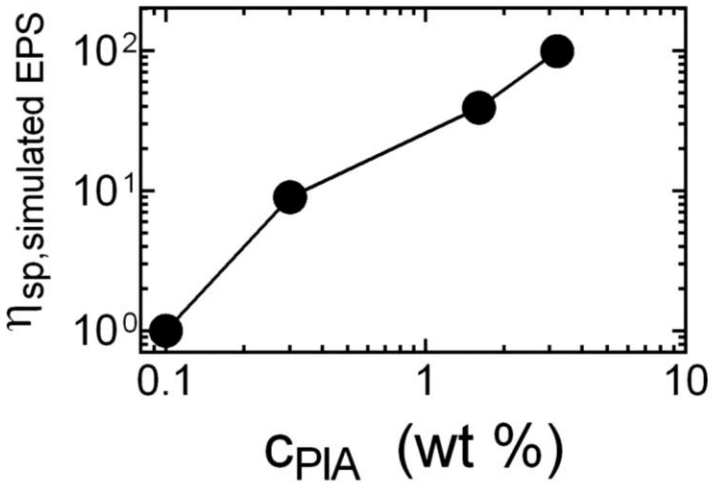

Figure 3.10. Concentration dependence of simulated EPS viscosity

Zero shear specific viscosity of simulated EPS solutions, $\eta_{sp,simulated\ EPS}$, containing different concentrations of PIA.

3.7 References

1. Hall-Stoodley, L., Costerton, J. W. & Stoodley, P. Bacterial biofilms: from the natural environment to infectious diseases. *Nat. Rev. Microbiol.* **2,** 95–108 (2004).
2. Lembre, P., Lorentz, C. & Di Martino, P. Exopolysaccharides of the biofilm matrix: a complex biophysical world. *The Complex World of Polysaccharides, InTech* 371–392 (2012).
3. Flemming, H.-C. & Wingender, J. The biofilm matrix. *Nat. Rev. Microbiol.* **8,** 623–633 (2010).
4. Sutherland, I. Biofilm exopolysaccharides: a strong and sticky framework. *Microbiology* **147,** 3–9 (2001).
5. Sutherland, I. W. The biofilm matrix--an immobilized but dynamic microbial environment. *Trends Microbiol.* **9,** 222–7 (2001).
6. Cense, a W. *et al.* Mechanical properties and failure of Streptococcus mutans biofilms, studied using a microindentation device. *J. Microbiol. Methods* **67,** 463–72 (2006).
7. Körstgens, V., Flemming, H. C., Wingender, J. & Borchard, W. Uniaxial compression measurement device for investigation of the mechanical stability of biofilms. *J. Microbiol. Methods* **46,** 9–17 (2001).
8. Wilking, J. N., Angelini, T. E., Seminara, A., Brenner, M. P. & Weitz, D. a. Biofilms as complex fluids. *MRS Bull.* **36,** 385–391 (2011).
9. Flemming, H.-C., Wingender, J., Mayer, C., Korstgens, V. & Borchard, W. in *Symp. Gen. Microbiol.* 87–106 (Cambirge University Press, 1999).
10. Peterson, B. W., Busscher, H. J., Sharma, P. K. & van der Mei, H. C. Visualization of Microbiological Processes Underlying Stress Relaxation in Pseudomonas aeruginosa Biofilms. *Microsc. Microanal.* **20,** 912–5 (2014).
11. Chew, S. C. *et al.* Dynamic Remodeling of Microbial Biofilms by Functionally Distinct Exopolysaccharides. *MBio* **5,** e01536–14 (2014).
12. Mangalappalli-Illathu, A. K., Lawrence, J. R., Swerhone, G. D. W. & Korber, D. R. Architectural adaptation and protein expression patterns of Salmonella enterica serovar Enteritidis biofilms under laminar flow conditions. *Int. J. Food Microbiol.* **123,** 109–20 (2008).
13. Stoodley, P., Cargo, R., Rupp, C. J., Wilson, S. & Klapper, I. Biofilm material properties as related to shear-induced deformation and detachment phenomena. *J. Ind. Microbiol. Biotechnol.* **29,** 361–367 (2002).
14. Zrelli, K. *et al.* Bacterial biofilm mechanical properties persist upon antibiotic treatment and survive cell death. *New J. Phys.* **15,** 125026 (2013).
15. Guelon, T., Mathias, J. & Stoodley, P. in *Biofilm Highlights* (Flemming, H.-C., Wingender, J. & Szewzyk, U.) **5,** 111–139 (Springer Berlin Heidelberg, 2011).
16. Pavlovsky, L., Younger, J. G. & Solomon, M. J. In situ rheology of Staphylococcus epidermidis bacterial biofilms. *Soft Matter* **9,** 122–131 (2013).
17. Di Stefano, A. *et al.* Viscoelastic properties of Staphylococcus aureus and Staphylococcus epidermidis mono-microbial biofilms. *Microb. Biotechnol.* **2,** 634–641 (2009).
18. Aggarwal, S. & Hozalski, R. M. Effect of strain rate on the mechanical properties of Staphylococcus epidermidis biofilms. *Langmuir* **28,** 2812–6 (2012).
19. Otto, M. Staphylococcus epidermidis--the "accidental" pathogen. *Nat. Rev. Microbiol.* **7,** 555–567 (2009).

20. Rohde, H., Frankenberger, S., Zähringer, U. & Mack, D. Structure, function and contribution of polysaccharide intercellular adhesin (PIA) to Staphylococcus epidermidis biofilm formation and pathogenesis of biomaterial-associated infections. *Eur. J. Cell Biol.* **89,** 103–111 (2010).
21. Vuong, C. *et al.* A crucial role for exopolysaccharide modification in bacterial biofilm formation, immune evasion, and virulence. *J. Biol. Chem.* **279,** 54881–54886 (2004).
22. Brindle, E. R., Miller, D. a & Stewart, P. S. Hydrodynamic deformation and removal of Staphylococcus epidermidis biofilms treated with urea, chlorhexidine, iron chloride, or DispersinB. *Biotechnol. Bioeng.* **108,** 2968–77 (2011).
23. Ganesan, M. *et al.* Molar mass, entanglement, and associations of the biofilm polysaccharide of Staphylococcus epidermidis. *Biomacromolecules* **14,** 1474–81 (2013).
24. Sadovskaya, I., Vinogradov, E., Flahaut, S., Kogan, G. & Jabbouri, S. Extracellular Carbohydrate-Containing Polymers of a Model Biofilm-Producing Strain , Staphylococcus epidermidis RP62A. *Infect. Immun.* **73,** 2007–3017 (2005).
25. Rinker, K. D. & Kelly, R. M. Growth Physiology of the Hyperthermophilic Archaeon Thermococcus litoralis: Development of a Sulfur-Free Defined Medium, Characterization of an Exopolysaccharide, and Evidence of Biofilm Formation. *Appl. Environ. Microbiol.* **62,** 4478–85 (1996).
26. Bozzi, L., Milas, M. & Rinaudo, M. Characterization and solution properties of a new exopolysaccharide excreted by the bacterium Alteromonas sp. strain 1644. *Int. J. Biol. Macromol.* **18,** 9–17 (1996).
27. Joyce, J. G. *et al.* Isolation, structural characterization, and immunological evaluation of a high-molecular-weight exopolysaccharide from Staphylococcus aureus. *Carbohydr. Res.* **338,** 903–922 (2003).
28. Karamanos, N. K. *et al.* Identity of macromolecules present in the extracellular slime layer of Staphylococcus epidermidis. *Biochimie* **77,** 217–224 (1995).
29. Weitz, D. A. & Pine, D. J. Diffusing-wave spectroscopy. *Dyn. Light Scatt.* 652 (1993).
30. Rusconi, R., Lecuyer, S., Autrusson, N., Guglielmini, L. & Stone, H. A. Secondary Flow as a Mechanism for the Formation of Biofilm Streamers. *Biophys. J.* **100,** 1392–1399 (2011).
31. Hohne, D. N., Younger, J. G. & Solomon, M. J. Flexible microfluidic device for mechanical property characterization of soft viscoelastic solids such as bacterial biofilms. *Langmuir* **25,** 7743–7751 (2009).
32. Byrne, E., Dzul, S., Solomon, M., Younger, J. & Bortz, D. M. Postfragmentation density function for bacterial aggregates in laminar flow. *Phys. Rev. E* **83,** 41911 (2011).
33. Smith, L. R. & Gilkerson, E. Quantitation of Glycosaminoglycan Hexosamine Using 3-Methyl-2-Benzothiazolone Hydrazone Hydrochloride. *Anal. Biochem.* **98,** 478–480 (1979).
34. Shortt, D. W. Differential molecular weight distributions in high performance size exclusion chromatography. *J. Liq. Chromatogr. Relat. Technol.* **16,** 3371–3391 (1993).
35. Podzimek, S. *Light scattering, size exclusion chromatography and asymmetric flow field flow fractionation: powerful tools for the characterization of polymers, proteins and nanoparticles*. (John Wiley & Sons, 2011).
36. Stewart, E. J., Satorius, A. E., Younger, J. G. & Solomon, M. J. Role of Environmental and Antibiotic Stress on Staphylococcus epidermidis Biofilm Microstructure. *Langmuir* **29,** 7017–7024 (2013).

37. Hulst, H. C. & van de Hulst, H. C. *Light scattering: by small particles*. (Courier Dover Publications, 1957).
38. Lu, Q. & Solomon, M. Probe size effects on the microrheology of associating polymer solutions. *Phys. Rev. E* **66,** 1–11 (2002).
39. Dasgupta, B., Tee, S.-Y., Crocker, J., Frisken, B. & Weitz, D. Microrheology of polyethylene oxide using diffusing wave spectroscopy and single scattering. *Phys. Rev. E* **65,** 1–10 (2002).
40. Mao, H.-Q. *et al.* Chitosan-DNA nanoparticles as gene carriers: synthesis, characterization and transfection efficiency. *J. Control. Release* **70,** 399–421 (2001).
41. Squires, T. M. & Mason, T. G. Fluid mechanics of microrheology. *Annu. Rev. Fluid Mech.* **42,** 413 (2009).
42. Krause, W. E., Bellomo, E. G. & Colby, R. H. Rheology of Sodium Hyaluronate under Physiological Conditions. *Biomacromolecules* **40,** 65–69 (2001).
43. Ninomiya, K. An extrapolation method for estimating steady-flow viscosity and steady state compliance from creep data. *J. Phys. Chem.* **67,** 1152 (1962).
44. Xu, J., Viasnoff, V. & Wirtz, D. Compliance of actin filament networks measured by particle-tracking microrheology and diffusing wave spectroscopy. *Rheol. Acta* **37,** 387–398 (1998).
45. Huggins, M. L. The viscosity of dilute solutions of long-chain molecules. IV. Dependence on concentration. *J. Am. Chem. Soc.* **64,** 2716–2718 (1942).
46. Dobrynin, A. V, Colby, R. H. & Rubinstein, M. Scaling theory of polyelectrolyte solutions. *Macromolecules* **28,** 1859–1871 (1995).
47. Morris, E. R., Cutler, A. N., Ross-Murphy, S. B., Rees, D. A. & Price, J. Concentration and shear rate dependence of viscosity in random coil polysaccharide solutions. *Carbohydr. Polym.* **1,** 5–21 (1981).
48. A N, S. & Rubinstein, M. Dynamics of Entangled Associating Polymers with Large Aggregates. *Macromolecules* **35,** 4821–4837 (2002).
49. Larsen, T. H. & Furst, E. M. Microrheology of the liquid-solid transition during gelation. *Phys. Rev. Lett.* **100,** 146001 (2008).
50. Winter, H. H. & Chambon, F. Analysis of Linear Viscoelasticity of a Crosslinking Polymer at the Gel Point. *J. Rheol.* **30,** 367–381 (1986).

CHAPTER 4

Microrheology of a biofilm and synthesis of bacterial-chitosan constructs that establish the role of physical self-assembly in biofilm formation †

4.1 Abstract

The microrheology of a biofilm and its extracellular polymer substances (EPS) are compared over a frequency range of 10^{-1} – 10^{5} Hz, as measured using diffusing wave spectroscopy. Biofilms are structured communities of bacteria that are enclosed within a self-produced polysaccharide rich EPS matrix. We found that, biofilms formed by *Staphylococcus epidermidis* displayed a viscoelastic solid like creep response with a long time plateau consistent with shear rheometry data of Pavlovsky et al[1]. However, the EPS, at their *in situ* concentrations, had a purely viscous creep compliance with zero shear viscosity, storage and loss moduli ~ 10^{2} fold less than that of the biofilm. To understand this gap between the EPS viscoelasticity and that of a mature biofilm, bacterial constructs with biofilm-like microstructural and mechanical properties were self-assembled by exploiting interactions that were exclusively physicochemical rather than genetic in origin. Although the EPS synthesis pathways and microstructure of biofilms have been previously studied, how the cells and the EPS together generate the biofilm mechanics is largely unclear. We find that it is physical interactions that drive the self-assembly of EPS components and bacterial cells resulting in the long time plateau in creep compliance observed in mature, naturally occurring biofilms. Specifically, pH conditions that induce phase instability of polysaccharides yield artificial biofilms whose rheology match those of natural

biofilms. Thus, during the biofilm lifecycle, genetic processes regulate EPS synthesis, which are purely viscous, but self-assembly with surrounding bacteria then generate the elasticity observed in a mature biofilm. We demonstrate an implication of pH-induced stabilization of the EPS towards understanding biofilm disassembly, a finding relevant for treating medical device contaminations. (**Part of the text here is reprinted with permission from Stewart, E.J., Ganesan, M., et al.** ***(manuscript submitted)***)

† Elizabeth J. Stewart performed all the confocal microscopy and image processing presented in this chapter, and is a co-first author of this work

4.2 Introduction

Bacterial biofilms are multi-cellular structured communities encapsulated in an extracellular polymeric substance (EPS) of polysaccharides, proteins, and DNA[2,3]. As soft materials, they are viscoelastic, with elastic modulus of 10^{-1} – 10^{2} kPa, essential for resilience against high shear[1,4,5], and a viscous modulus of 10 – 10^{4} Pa.s that prevents pre-mature fragmentation and enables spreading of young biofilms[4,6]. Biofilms display structural, mechanical and physicochemical heterogeneity across multiple length scales, with spatially varying EPS composition, morphology[7–9], mechanical properties[10,11] and pH microenvironments[12].

The formation of biofilms is commonly viewed as the consequence of genetically controlled synthesis and export of EPS components[13]. Genetic encoding of EPS, factors affecting its kinetics and implications on biofilm's life cycle has been studied in detail[14,15]. On the other hand, bulk rheology of biofilms has been probed using a variety of measurement[4,5] and simulation[16] techniques. In the first part of this chapter, we identify the presence of a profound gap between our understanding of these genetically mediated synthesis and export operations on biofilm formation and the complex rheology that is achieved by mature biofilms. In the second part, we then address the process through which EPS components interact with the cells to generate the observed mechanical properties in biofilms, a finding that serves to bridge the above gap.

We work with biofilms formed by *Staphylococcus epidermidis*, whose rheology has been studied in detail. The viscoelasticity of *S. epidermidis* biofilms is mediated by the EPS, whose primary component is a glycosaminoglycan polysaccharide intercellular adhesin (PIA). Ganesan et al. (see Chapter 3) recently measured the concentration dependent microrheology of PIA.

From cell number densities reported by Stewart et al.,[7] they establish a range for PIA, protein and nucleic acid concentration within the biofilm. Thus, when deformed, the biofilm relaxation behavior would be mediated, atleast in part, by the *in situ* concentration and rheology of PIA and other EPS macromolecules. However, a study comparing the rheology of the biofilm, PIA, and EPS (containing PIA, extracellular proteins and DNA) at corresponding frequencies and relevant *in situ* concentrations is unavailable. Mechanical deconstruction of the biofilm in this way helps identify appropriate constitutive models to understand unique rheological features of biofilms such as strain hardening and their ability to form streamers. Alternatively, it can serve to elaborate how the EPS polymers mediate rheological properties of a biofilm.

In the second part of this chapter, (*work done in collaboration with E. J. Stewart*), we construct an artificial biofilm using planktonic cells and abacterial EPS proxies to identify the phenomena that generates the observed morphology and elasticity of biofilms. The idea of exopolymers mediated depletion aggregation of biofilm bacteria contributing to biofilm formation has been introduced[17,18]. Other descriptions of biofilm formation include integrated genetic pathways involved in expression of the EPS that are controlled by cellular signaling such as quorum sensing and response factors[15,19]. In *S. epidermidis*, the synthesis and export of PIA is encoded by a pathway operated by the *ica*ADBC operon[14]. Growth factors such as pH, salt concentration and shear stresses trigger the activity of a variety of stress response genes, which then cascades via a complex pathway to mediate the synthesis and export of PIA[14,20,21]. Thus, the extracellular concentration of PIA in a mature biofilm is, in part, mediated by a chain of genetic signaling. However, these phenomena do not inherently contain explanations for the mechanical properties observed in biofilms. While depletion interaction seems plausible; it only accounts for the aggregation of biofilm bacteria, but precludes a description for onset of viscoelasticity.

Furthermore, these explanations do not account for solvent induced physicochemical forces, such as pH, that could mediate polymer-polymer (as identified in PIA[22]) and cell-polymer interactions, which might be important for biofilm mechanics and microstructural properties.

Here, using microrheology, we report the high frequency viscoelastic properties of *S. epidermidis* biofilms and its EPS. We find that the biofilm exhibits a viscoelastic response, with a long time elastic plateau in creep, while the EPS, at its *in situ* concentration exhibits a purely viscous response at all times observed. The viscosity and complex moduli further indicate that the EPS, on its own, cannot generate the rheology observed in a mature biofilm. We hypothesize that there is a phenomena apart from genetic processes that drives aggregation of polymers and cells into viscoelastic volumes. Here we show that physical self-assembly of cellular and polymeric components, utilizing the pH induced phase instability of these polymers, can, in the absence of any bacterial regulatory control, produce the morphology and mechanics of biofilms. Therefore, we identify of a gap in our current rheological understanding of biofilms and institute that cell-polymer self-assembly bridges this gap. The essential role of self-assembly in the formation of biofilms is demonstrated as a strategy for biofilm mechanical remediation.

4.3 Materials and Methods

4.3.1 Extraction and quantification of biofilm polymers

Extracellular polymeric substances (EPS) and high purity PIA was isolated from *S. epidermidis* cultures as per[22,23]. The concentration of glycosaminoglycans, proteins and nucleic acids was measured using the Smith Gilkerson[24], BCA and PicoGreen assay respectively. The concentrations of PIA, protein, and nucleic acids within *S. epidermidis* biofilms were calculated by obtaining the total concentration of EPS polymers per biofilm cell (the latter is quantified as total cell density per culture using a hemocytometer), computing the average extracellular

volume available per biofilm cell (from measurements of *in situ* cell number density of Stewart et al.,[7]) and dividing the two to obtain the total average *in situ* concentration of the macromolecules as done earlier[22]. The calculated values, averaged over at least 10 different batches are reported in Table 4.1.

4.3.2 Particle tracking microrheology of polymers and biofilm using diffusing wave spectroscopy (DWS)

Transmission mode DWS was performed as per ref[25,26]. Briefly, a mode-locked vertically polarized Ar^+ laser of wavelength λ = 488 nm (Coherent Innova 70-C, Coherent Inc.), was focused using a converging lens onto the face of the sample contained in a rectangular cuvette made of optical glass of path length L. The scattered light from thermally diffusing probes embedded in the sample was collected through a Glan-Thomspon prism polarizer set to transmit only horizontally polarized light and sent to a pseudo cross correlator (ALV/5000 multi tau correlator, ALV, Langen Germany). The detector arm was position at 2°. The probes used were 0.5 μm sulfate latex beads (Invitrogen). To ensure multiple scattering, probe concentration was chosen such that $L/l^* > 8$, where l^* is the mean free path of scattered light[26]. The latter depends on the probe diameter and concentration and was computed using Mie theory[26–28]. Biofilms for DWS were cultured directly in 1 mm rectangular cuvettes by using *S. epidermidis* colonies to inoculate the growth media; the probes were added during inoculation. This method of probe addition during inoculation was carried out by Birjinuik et al., recently[10]. At 488 nm, the biofilm had a transmittance ~ 30 times that of latex spheres at multiple scattering concentrations. Thus, the scattered light collected is due to probe scattering with minimal contribution from the biofilm bacteria. The mean squared displacement (MSD) of probes in PIA,

EPS and biofilm was computed from their normalized intensity autocorrelation function, $g_2(t) = \langle I(0)I(t)\rangle/\langle I(t)\rangle^2$, where I(t) is the scattering intensity at time t and $\langle\ \rangle$ is the time average operator, as per ref[26,28]. Briefly, the longtime plateau in $g_2(t)$ due to laser fluctuations were fit to an exponential and subtracted from the correlation function [29]. The field autocorrelation function, $g_1(t)$ was obtained from the subtracted data using the Siegert relationship $g_1(t) = ((g_2(t)-1)/\beta)^{0.5}$. The constant β was calculated by averaging the first 30 data points[25]. Using the relationship of Weitz and Pine[28], MSD was computed from $g_1(t)$ by using an iterative minimization routine. The material storage, G'(ω) and loss, G"(ω) modulus, zero shear viscosity,η_0, and creep compliance, J(t), were obtained as per[25,30–32] (described in detail in Chapter 3). A probe size and surface chemistry study of PIA and EPS solutions indicated no local heterogeneity and no probe-polymer interaction. DWS of the biofilm however exhibited significant probe size and surface chemistry dependence as discussed in Results.

4.3.3 Chitosan preparation

Stock solutions of 1 wt. % chitosan, with manufacturer reported molar mass of 190 – 300 kDa and a degree of deacetylation of ~75-85 % (Sigma Aldrich, St. Louis, MO), were dissolved in 0.3 M AcOH (pH = 3.0). For imaging, chitosan was labeled using 10 μg/mL Wheat Germ Agglutinin (WGA), AlexaFluor® 633 (Life Technologies, Grand Island, NY).

4.3.4 Bacterial strains and culture conditions

S. epidermidis RP62A (ATCC 35984) was grown overnight in a 250 mL Erlenmeyer flask in 50 mL tryptic soy broth with 1 wt. % added glucose (TSBG) media at 37°C, 200 RPM. 1 mL of pre- culture was added to 50 mL TSBG and grown to desired OD_{600}. *S. aureus* SH1000

colonies were cultured on tryptic soy agar (TSA). Bacteria were stained with 2.5 μM Syto9 for imaging.

4.3.5 Bacterial-chitosan constructs and polymer phase stability

To simulate the biofilm solvent environment discussed in most reports on staphylococcal biofilms, TSBG was used as the solvent for making the constructs[23]. For each *S. epidermidis* cellular OD_{600} value (0.5, 1.0, 1.4), we created bacterial constructs with chitosan concentrations of 0, 0.05, 0.1, 0.2, 0.25, and 0.3 wt. %. Chitosan dilutions were done by adding from stock directly to 200 μL *S. epidermidis* cells in TSBG. This step implicitly introduced pH dependence. Constructs were equilibrated for 2 hours. In Fig.4.4 and 4.5, high density constructs correspond to constructs with OD_{600} = 1.4 and 0.3 wt. % chitosan, while low density constructs were made from OD_{600} = 1.0 cells and 0.05 wt. % chitosan. The dynamics observed in the other constructs was intermediate to planktonic or the arrested state. Constructs were let to equilibrate for 3 hours after pH change. The phase stability of chitosan and *S. epidermidis* EPS in TSBG was studied by tracking changes in absorbance (λ = 600 nm, GENESYS 20, Thermo Scientific) with pH. The transition to an unstable phase was marked where a five-fold increase in absorbance was observed. The pH range 4.5 - 6.7 studied here are within range *in situ S. epidermidis* biofilms (4.5 - 7.5)[33–35].

4.3.6 Biofilm growth conditions

Biofilms with heterogeneous density phenotypes were grown as per ref[7]. *S. epidermidis* RP62A and *S. aureus* SH1000 biofilms used to investigate the effect of pH changes on biofilm mechanics were grown in 400 μL TSBG in Nunc™ Lab-Tek™ II Chambered Coverglass dishes (Thermo Scientific, USA) for 18 hours at 37°C, 60 RPM. Biofilm were stained with 4 μM Syto9

and 25 μM Propidium Iodide (Molecular Probes, Inc.,). To induce pH changes to biofilms, growth media was replaced with TSBG with pH adjusted to desired value. After pH change, the biofilm was equilibrated at room temperature for 4 hours.

4.3.7 Confocal laser scanning microscopy (CLSM) and image analysis (performed by E.J. Stewart)

CLSM imaging of bacterial-chitosan constructs and biofilms grown in flow cells and culture wells was done as per[7]. Imaging and analysis to compute mean squared displacement of bacteria within constructs and biofilm was done as per[7,36].

4.4 Results and Discussion

4.4.1 Microrheology of a biofilm – effect of probe size and chemistry

We studied the effect of probe size and surface chemistry on the DWS of cuvette grown biofilms. This was done to verify that the measured biofilm mechanical properties were independent of probe size and that the DWS autocorrelation function was not affected by probe aggregation or adherence/sequestration within biofilm clusters.

The biofilm was cultured in 1 mm cuvettes with sulfate latex probes of diameters 0.1 μm, 0.3 μm, 0.5 μm, 0.7 μm and 1.2 μm embedded in it. The concentrations of probes was chosen such that their respective l^* was < 1/8 mm[27,28]. Figure 4.1 shows the DWS, $g_2(t)$-1, of probes in the biofilm. Probes larger than the size of *S. epidermidis* cells (> 0.5 μm) exhibited nonergodic dynamics, as characterized by a $g_2(t)$ intercept << 1 [37], presumably because of entrapment within or between biofilm clusters and were therefore not analyzed further. Probes of size equivalent to that of the bacterial cells – 0.5 μm diameter – exhibited decay in $g_2(t)$ that was consistent with

thermally induced random motion. The $g_2(t)$ of probes smaller than the cellular diameter (< 0.5 μm) did decay to zero at infinite time; this behavior is indicative of restricted concentration fluctuations (i.e. localization), because of entrapment of the smaller probes within biofilm clusters. The biofilm J(t) as a function of probe size is shown in Fig. 4.2. We found that the short time response ($t < 10^{-3}$s) was independent of probe size while the cross over into the viscoelastic regime was found to be strongly dependent on probe size. Probes of size 0.5 μm – a dimension equivalent to the size of a *S. epidermidis* bacterial cell – resulted in a J(t) that matched mechanical rheometry[38].

To study probe aggregation, DWS autocorrelation functions were measured for 0.5μm probes of different surface chemistry embedded in the biofilm. Using CLSM and a MATLAB image processing routine, we identified that carboxylate and amine probes strongly associated with the biofilms (fraction of aggregated or stuck probes > 70%), while sulfate probes showed weaker aggregation of < 15%. Thus, carboxylate and amine probes were not used further. We show that the presence of < 15 % aggregation in sulfate spheres has minimal impact on the decay of the DWS correlation function. Probe aggregation or binding to the biofilm induces a dynamical heterogeneity in the scattering media. Thus, the decay in the DWS $g_2(t)$ is now due to thermally diffusing probes and probes that are aggregated/stuck to the biofilm[39]. This has consequences on the static and dynamic property of scattered light. First, the effective mean free path, l^*, of scattered light, becomes a function of spatial correlation between the aggregated particles[28]. Second, since DWS represents an ensemble averaging, the contribution from the aggregated spheres does not probe microrheology following Langevin dynamics, which requires all the spheres to be Brownian. Thus, their contribution has to be addressed to validate the use of the Generalized Stokes Einstein equation to obtain material moduli. The probes used were

0.5μm sulfate spheres at 2% (v/v) in 1mm cuvettes. To address the change in l^*, we consider the two species the following way. The non-aggregated probes are considered to be Brownian (~ 85%) and their l^* is computed as per[25,28]. The fraction of stuck probes (< 15%) modeled as correlated media following an attractive potential. For interacting particles, the effective diffusivity is also a function of the hydrodynamic interaction[28]. Following Kaplan et al.,[40] at low volume fractions (< 0.1), we neglect the contribution of hydrodynamic interaction. We compute the l^* for the stuck probes following Weitz and Pine[28] and using the structure factor formulation for colloidal aggregates[41,42]. Next, we compute the effective l^* and the MSD of this binary system. Pine et al.,[39] outline a method to analyze the correlations of multiply scattered light from a polydisperse medium of species with different diffusion coefficients. In this framework, the reciprocal of the effective mean free path is then a reciprocal sum of the mean free path of the individual scattering elements. We find that, the difference between this effective l^* and the l^* of free particles was less than < 1 %. Similarly, the effective MSD will be a sum of the contributions from the free and stuck probes weighted by the relative concentration of species and by its scattering strength, as expressed by its scattering cross section. The deviation of the effective MSD was < 6% of the MSD of the free particles. Thus, we conclude that the small fraction of aggregated probes has negligible effect on the decay of the observed $g_2(t)$ and the measured MSD can be directly used in the microrheology formulation to extract material properties.

4.4.2 Microrheology of a biofilm and its constituent extracellular polymers

We assessed the mechanical properties of the primary components of *S. epidermidis* biofilms. Figure 4.3 compares the creep compliance (J(t) Pa^{-1}), zero shear viscosity (η_0 Pa.s), storage (G'(ω) Pa) and loss (G" (ω) Pa) moduli of PIA, EPS and the biofilm across a range of

10^{-1} - 10^{6} Hz. The creep compliance, of a mature *S. epidermidis* biofilm is characteristic of a viscoelastic solid with an elastic modulus of ~ 3 Pa.s, as obtained from its plateau value (Fig. 4.3A). The finite plateau at long time is collinear with shear rheometry measurements of Pavlovsky et al.,[1]. The progressive increase in J(t) at long times was attributed by Pavlovsky et al.,[1] to a long-term creep phenomena. The reason for this is yet unclear. In Fig. 4.3A, using DWS microrheology, we extend the biofilm creep response to short times scale responses.

The extracellular polymers synthesized by *S. epidermidis* – either PIA or the entire acellular EPS – show only a viscous response at their *in situ* stoichiometry, as seen from their linear creep response over the time scales probed (Fig 4.3A). PIA, exhibits a viscous creep while the EPS exhibits a relatively delayed creep with viscosity ~ 10^{-2} Pa.s. Thus, in the presence of proteins and DNA, the deformation of PIA is significantly retarded, highlighting the synergistic response of these polymers. The short time ($t < 10^{-3}$ s) creep of the biofilm was congruent with that of the EPS up to a finite compliance of ~ 10^{-2} Pa^{-1}. For $t > 10^{-3}$ s, we find a transition from a purely viscous to a viscoelastic response. While the transition region was found to depend on the amount of biofilm growth, the factors mediating this transition regime between 10^{-3} s < t < 10^{-1} s is unclear. At $t > 10^{-1}$ s, the biofilm creep exhibits a plateau (see Fig. 4.3A). The biofilm deformation can therefore be approximated as a viscous, polymer mediated response in parallel with a cell-polymer mediated elastic response. It is however evident that the EPS do not contribute towards either the transition or the elastic plateau.

Other measures, such as η_0 Pa.s (Fig. 4.3B), G'(ω) and G" (ω) (Fig. 4.3C, 4.3D) confirm that neither PIA nor EPS exhibit the rheology of a mature biofilm. From Fig. 4.3C, D we note that the DWS measurements of biofilm microrheology are congruent with the bulk rheometry data of Pavlovsky et al[1]. This confirms the validity of the technique. We find that, at all

frequencies measured the complex moduli of PIA and EPS are atleast ~10^2 fold less than that of the biofilm. . Importantly, at time scales on the order of bacterial growth, the onset of elasticity (or the long time plateau) in the biofilm rheology is unclear. This is contrary to the idea that exopolymers determine biofilm mechanics[43].

The synthesis of these EPS components and their extracellular concentration is presumably mediated by a hierarchy of genetic signaling, however, Fig 4.3A-D indicates that, such a mechanism, solely, results only in a viscous polymer matrix and does not account for elasticity seen in a biofilm. To explain this gap between the EPS and biofilm rheology we hypothesize that, there is, a phenomena that mediates an interaction between these secreted polymers and the multi-cellular microbial communities that results in a viscoelastic composite. However, the driving force behind this polymer-cell coupling is unclear. Experiments conducted with mature biofilms do not yield themselves to understanding this phenomenon mediating the interactions of biofilm components due the limited ability to control concentrations of both cells and matrix materials.

4.4.3 Self-assembly of a bacterial-chitosan construct[††]

Self-assembly is the process by which individual constituents organize into structures as a result of their physical interactions. We hypothesize that biofilm viscoelasticity emerges from the physical self-assembly of its constituent cellular and polymeric components. This self-assembly – independent of genetic control – induces self-organization of multi-cellular volumes. Particularly, we will show that this complex mediates the long time plateau observed in the creep compliance. Biofilm morphology and viscoelasticity are then the consequence of processes akin to those of attractive colloids, whose self-organization yields viscoelastic structures[43,44].

To test this, planktonic bacterial cells and abacterial proxies for the polysaccharides, proteins, and DNA were mixed at *in situ* stoichiometry (Table 4.1) to create artificial biofilms (Fig. 4.3E) in TSBG. The abacterial proxies eliminated genetic regulation as an explanation of the artificial biofilm mechanics. In place of PIA, we used the N-acetylglucosamine glycan chitosan that is a product from crustacean shells, which differs from PIA only in glycosidic linkages[21,45]. Solution properties of PIA and chitosan such as molar mass, self-associations at acidic pH[22,46], complexation with proteins and nucleic acids[22,47,48] are nearly equivalent. We varied chitosan concentration between 0.05 and 0.3 wt. %, representative of *in situ* PIA. By using TSBG as the solvent, we implicitly introduced pH variation in the assemblies simulating pH microenvironments (c.f. Methods). Bovine serum albumin and λ-DNA replaced biofilm extracellular proteins and DNA, however, their impact in mechanics of the assemblies was negligible.

By mixing together initially dilute planktonic suspensions of cells with appropriate volumes of chitosan, we constructed assemblies of varying microstructure and rheology.

Artificial high cellular density constructs were self-assembled using chitosan at 0.3 wt. % at pH=4.3 ± 0.02 (Fig. 4.4A, Fig. 4.4B) in TSBG that resembled naturally occurring high density biofilms (Fig. 4.4C, Fig. 4.4D). Low cellular density constructs (Fig. 4.4E, 4.4F) were created from 0.05 wt. % chitosan at pH = 5.3 ± 0.1. These constructs were qualitatively more clustered were similar to low-density phenotype biofilms (Fig. 4.4G, 4.4H).

The morphology resemblance of the high and low density constructs to equivalent high and low density phenotype biofilms was further established by showing similarity in cellular number densities, volumetric rendering and radial distribution functions between the two. These measures quantify the microstructure in terms of space spanning and fractal dimensions. Figure 4.4 shows that the microstructure of biofilms is not necessarily mediated by genetic processes alone, as shown by self-assembly of an abacterial polymer component and cells to create microstructures similar to natural biofilms. Self-assembly has not been accounted for in previous studies on biofilm formation and mechanics. Since our concentration ranges are within *in situ* conditions, the finding in Fig. 4.4 is of relevance to naturally occurring biofilms.

The mean squared displacement, $\langle \Delta x^2(t) \rangle$, of cells in the bacterial-chitosan construct characterizes its rheology[49]. We found that cells within the high density construct exhibit retarded mobility, but the near-linear increase in $\langle \Delta x^2(t) \rangle$, over the time scales probed, indicates viscous behavior for the construct (Fig. 4.5A). At corresponding times, natural biofilms however exhibit a plateau in their $\langle \Delta x^2(t) \rangle$, characteristic of a purely elastic behavior (as derived from their creep response (Fig. 4.3A)). Cells in the low density construct show nearly time independent $\langle \Delta x^2(t) \rangle$, consistent with an elastic modulus ~ 2.6 Pa (obtained as $G' \propto k_B T/(\pi r_{bacteria} \langle \Delta x^2(t) \rangle_{t \to \infty})$[50]). Similarly, *S. epidermidis* biofilms have an elastic modulus of ~ 3.7 Pa (Fig. 4.3A).

It is remarkable that the cells in the low-density construct (containing 0.05 wt. % chitosan) are localized, consistent with an elastic behavior, while cells in the high-density construct (with 0.3 wt. % chitosan) are not localized representing a viscous fluid. However, there is no indication of this dynamical difference in the microstructure reported in Fig 4.4. By studying the microstructure and MSD of constructs synthesized using varying cell and chitosan concentration, we found that cellular localization and elasticity of the bacterial-chitosan constructs are correlated neither with increased cell density nor chitosan concentration.

Instead, we found that it is the pH of the artificial biofilm that controls its rheology. When pH of the high cellular density construct was increased from 4.3 to 7.3, the $\langle \Delta x^2(t) \rangle$ transitioned from viscous diffusion to elastic localization (Fig. 4.5B). Analogously, when pH of the low-density bacterial construct was decreased from 5.3 to 4.4, the mobility of cells increased and approached that of free bacteria (Fig. 4.5B). J(t) of both high and low-density constructs at pH= 4.4 was just below that of free bacteria (Fig. 4.5C). When the pH is 5.3 and 7.4 for the low- and high-density constructs, respectively, J(t) approximates that of native biofilms (Fig. 4.5C). Thus, a key finding is that, changing the pH of the environment rapidly changes the dynamics of the construct from a viscous to an elastic material. Furthermore, this indicates that the observation in Fig. 4 is different from purely depletion induced aggregation.

Visualization of chitosan within the arrested and mobile constructs reveals the effect of pH (Fig. 4.5D, 4.5E). At pH = 5.3, chitosan formed a stringy network between the bacterial cells that visibly spanned the image volume (Fig. 4.5D), while at pH=4.3, the stringy chitosan network was absent, due to the molecular-level dispersion of chitosan (Fig. 4.5E). Thus, the high-density construct, at pH 4.3, does not induce instability of the form seen in the low density case which in turn results in the observed fluid like compliance of the high density construct. For the low-

density construct, the solvent pH mediated chitosan phase instability yields polymer aggregation (Fig. 4.4D) that then dynamically arrests the cells, and generates biofilm-like viscoelasticity. We attribute the onset of instability to the non-ideality in solution properties of chitosan in TSBG. While the constituents of the growth media are known to supplement microbial growth, their role in mediating solution properties of extracellular polymers has been not been recognized (see Appendix A). Figure 4.4 and 4.5 support the central role of self-assembly in producing biofilm structure and mechanics. Furthermore, the MSD in Fig. 4.5 show that the long term plateau in biofilm J(t) in Fig. 4.1A is mediated by a cell-polymer composite, the formation of which is through physical self-assembly.

If chitosan phase instability is critical to the construct viscoelasticity, then EPS phase instability might control the viscoelasticity of naturally occurring biofilms. Figures 4.6A, 4.6B compare the pH dependent absorbance of chitosan and *S. epidermidis* EPS in TSBG. Chitosan showed a significant increase in turbidity at pH ~ 7, marking a transition from a stable phase at low pH to an unstable phase at high pH. In the *S. epidermidis* EPS, the effect of pH on stability is reversed; the EPS is stable at high pH and unstable at low pH, with a transition at pH ~ 7. The pH dependent solution behavior of EPS can be attributed to variations in the intermolecular interactions between PIA, extracellular proteins and DNA that are present in it. Polysaccharide-protein interactions are known to show strong pH dependence in their absorbance. Furthermore, considering that EPS predominantly has PIA, the pH at which we see an increase in absorbance is consistent with the pKa of the amine groups, which is ~ 6.2. That is at pH < 6.2, the PIA is positively charged that can interact with anionic nucleic acids and amino acid groups resulting in turbidity. In TSBG, the onset of this turbidity is further enhanced due to peptides, that are present at relatively large concentrations in this growth media.

This generates a non-trivial prediction for *S. epidermidis* biofilm viscoelasticity, namely, that a change in natural biofilm pH from low to high will result in a loss of biofilm viscoelasticity. Figure 4.6C, 4.6D tests this prediction. When the pH of a natural *S. epidermidis* biofilm was increased from 5.0 to 6.1, the biofilm bacteria remained arrested (Fig. 4.6C); however, at a pH of 7.3, mobility increased and approached that of planktonic bacteria (Fig. 4.6C). This change in biofilm mechanics occurs at a pH where the EPS absorbance is low, consistent with thermodynamic stability of the EPS.

A matrix of 0.3 wt. % chitosan becomes unstable at pH = 7.1, consistent with the transition from a mobile to an arrested construct between pH = 5.6 – 7.3 (Fig. 4.6D). When EPS is the matrix, it transitions between stable and unstable phases at pH 7. High-density *S. epidermidis* biofilms transition from their native arrested state to a viscous mobile state between pH= 6.2 - 7.0. The antipodal pH dependence of the artificial constructs and natural biofilms is conserved in both their matrix stability (as measured by absorbance) and their mechanics (as measured by $\langle \Delta x^2(t) \rangle$).

Staphylococcus aureus biofilms secrete the same EPS polysaccharide as *S. epidermidis* (31). When *S. aureus* biofilm pH was increased from 4.6 to 6.9, the creep compliance of the biofilm increased by a factor of four, as seen similarly for *S. epidermidis* (Fig. 4.6E), just as for *S. epidermidis*, which shows that our finding holds true in multiple species of biofilms.

Therefore, Fig. 4.6 findings introduce self-assembly as a factor in both biofilm formation and dispersal. The correlation between the EPS phase stability and the mechanics of the construct indicates that the viscoelasticity of biofilms is not just an additive effect of the individual mechanics of polymers and cells, but instead includes cross contributions generated by associations between polymeric species that are mediated by the state of the solvent

environment. Thus, in bridging the gap in our rheological understanding identified earlier, we institute the following. The instantaneous creep response of the biofilm is mediated predominantly by the EPS polymers at their *in situ* concentration. While, the longtime plateau in the biofilm creep is indeed mediated by a self-assembled system of cells and EPS polymers. The presence of pH microenvironments within biofilms[12] and the self-association of PIA at low pH[22] indicate that bacteria produce polymers that exhibit poor solvent behavior in their growth environment. Particularly, the presence of pH microenvironments and the connection of pH to EPS phase stability could facilitate microbial survival by promoting either the formation or breakdown of biofilm elasticity. Second, the presence of high and low density phenotypes that span viscous to elastic mechanics depending on local pH offers a possible explanation for the recently observed spatial variation of the compliance within bacterial biofilms[11]. pH variation within the biofilm can be a consequence of metabolism; the role of pH in mediating biofilm elasticity presents an interesting coupling between metabolism and mechanical properties.

†† Data presented in this section was performed in collaboration with Elizabeth J. Stewart

Table 4.1. Average extracellular concentrations, as defined by Ganesan et al. (28) of PIA, protein and DNA within *S. epidermidis* biofilms.

Component	**Concentration (g/mL) x 10^2**
PIA	2.0 ± 0.5
Total Protein	1.0 ± 0.4
Total DNA	0.1 ± 0.07

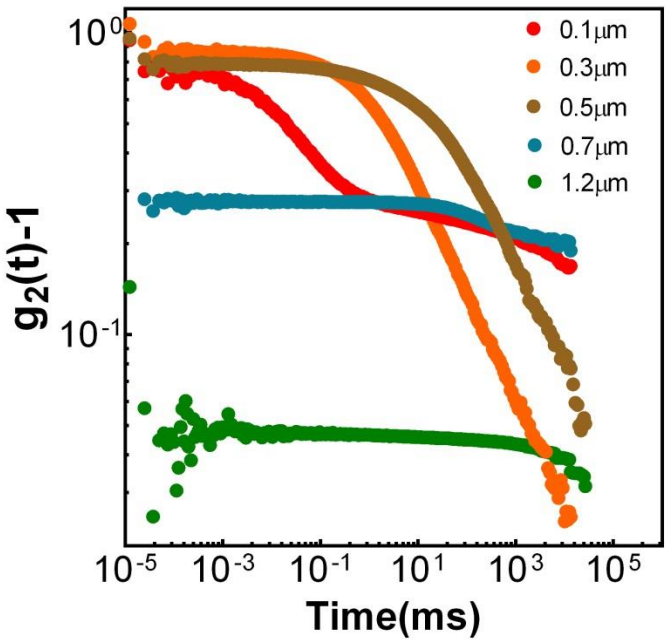

Figure 4.1. DWS probe study for biofilms

DWS intensity autocorrelation function, g2(t)-1 of the thermal motion of sulfate probes of different diameters embedded within *S. epidermidis* biofilms cultured in 1 mm path length rectangular cuvettes.

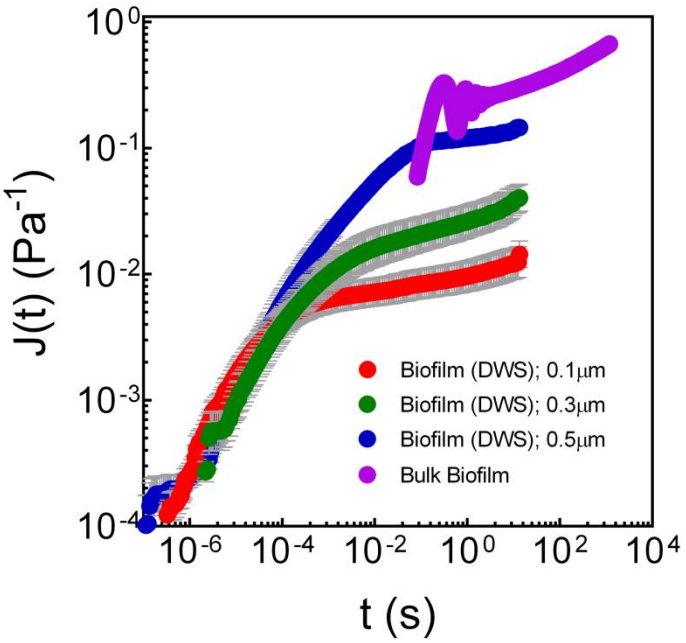

Figure 4.2. Biofilm creep compliance measured using probes of different sizes

Creep compliance, J(t) of biofilms obtained from DWS microrheology using probes of size 0.1 μm, 0.2 μm and 0.5 μm and from the bulk biofilm mechanical rheometry[38].

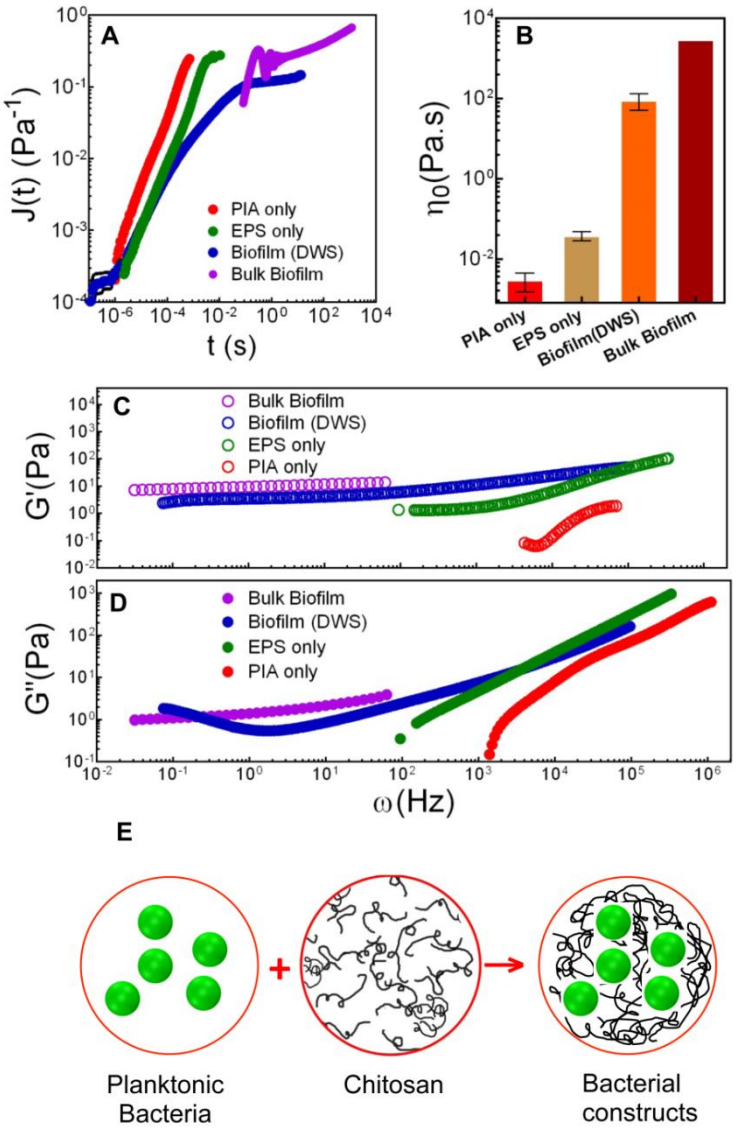

Figure 4.3. Mechanical properties of *S. epidermidis* biofilms and its constituent polymers

(**A to D**) Creep compliance, J(t) **(A)**, viscosity, η_0, **(B)**, storage modulus, G', **(C)** and loss modulus, G", **(D)** of PIA(0.016 g/mL), EPS (containing PIA at 0.016 g/mL) and cultured *S. epidermidis* biofilms. Bulk biofilm data are from (7) **(E)** Process to create biofilm-like bacterial constructs.

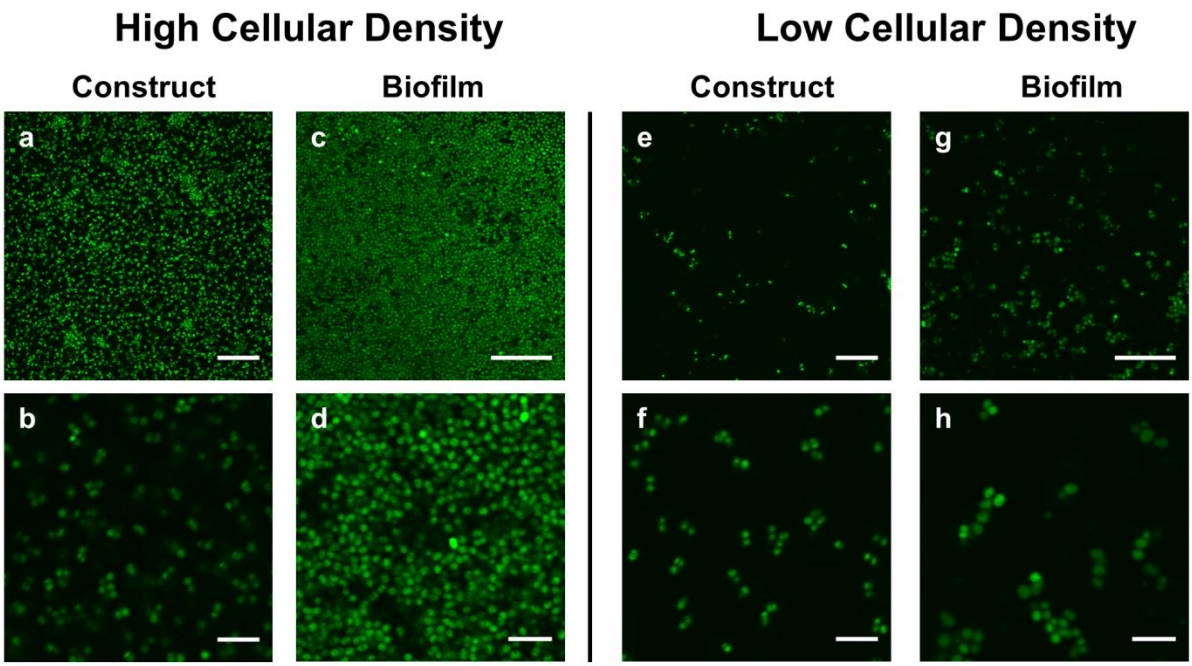

Figure 4.4. Confocal images of high and low cellular density *S. epidermidis*-chitosan constructs and biofilms

Left half compares high cellular density constructs (pH = 4.3) and high-density biofilms; right half compares low cellular density constructs (pH = 5.3) and low-density biofilms. First and second rows: CLSM images of (**a** and **b**) high cellular density bacteria-chitosan constructs; (**c** and **d**) high-density biofilms, (**e** and **f**) low cellular density constructs, and (**g** and **h**) low-density biofilms. Scale bars, 20 μm (**a**, **c**, **e**, and **g**) and 5 μm (**b**, **d**, **f**, and **h**). **(All the confocal images in this figure were obtained by Elizabeth Stewart, and is co-first author of this work)**

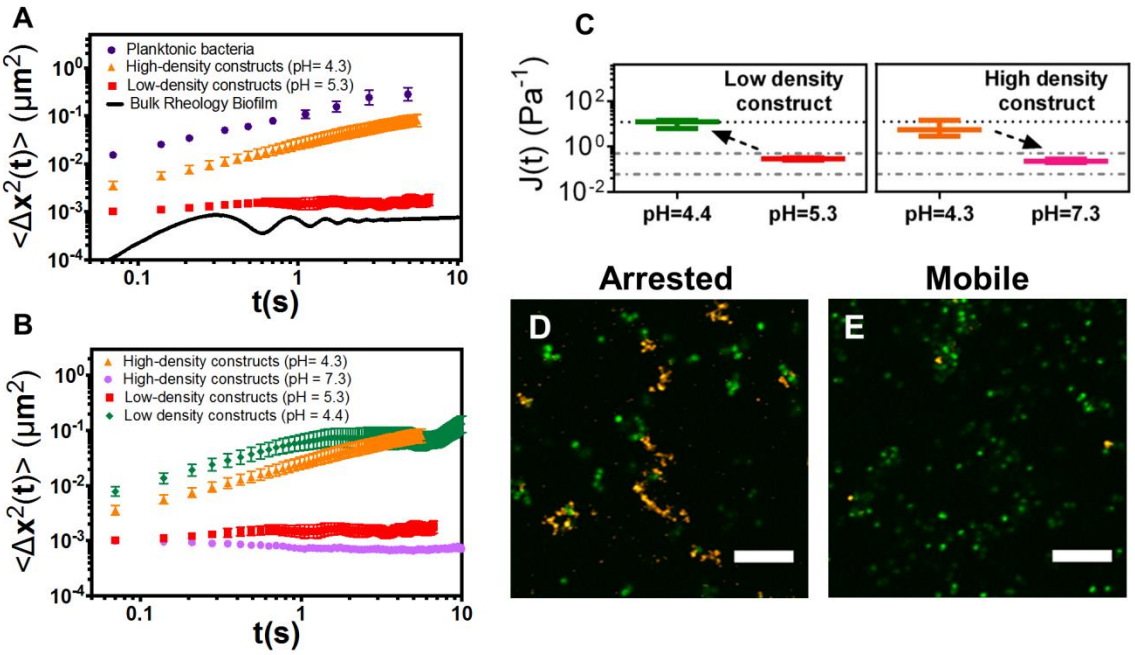

Figure 4.5. Effect of pH on dynamics of high and low cellular density bacterial constructs and chitosan

(A) $\langle \Delta x^2(t) \rangle$, of planktonic bacteria and bacteria in high (pH = 4.3) and low (pH = 5.3) cellular density constructs compared with biofilm $\langle \Delta x^2(t) \rangle$ inferred from ref (7). **(B)** $\langle \Delta x^2(t) \rangle$ of high and low cellular density constructs before and after pH change. **(C)** J(t) of high and low-density constructs before and after pH changes; arrows indicate the direction of pH change. The upper dotted line is J(t) of planktonic cells. The dotted dashed lines bound the J(t) observed for *S. epidermidis* biofilms (7). **(D)** CLSM image of cells and 0.05 wt. % chitosan at pH = 5.3. **(E)** CLSM image of cells and 0.3 wt. % chitosan at pH = 4.3. Scale bars, 10 μm. **(MSD measurements in (A,B) and confocal images (D,E) were obtained by Elizabeth Stewart, and is a co-first author of this work)**

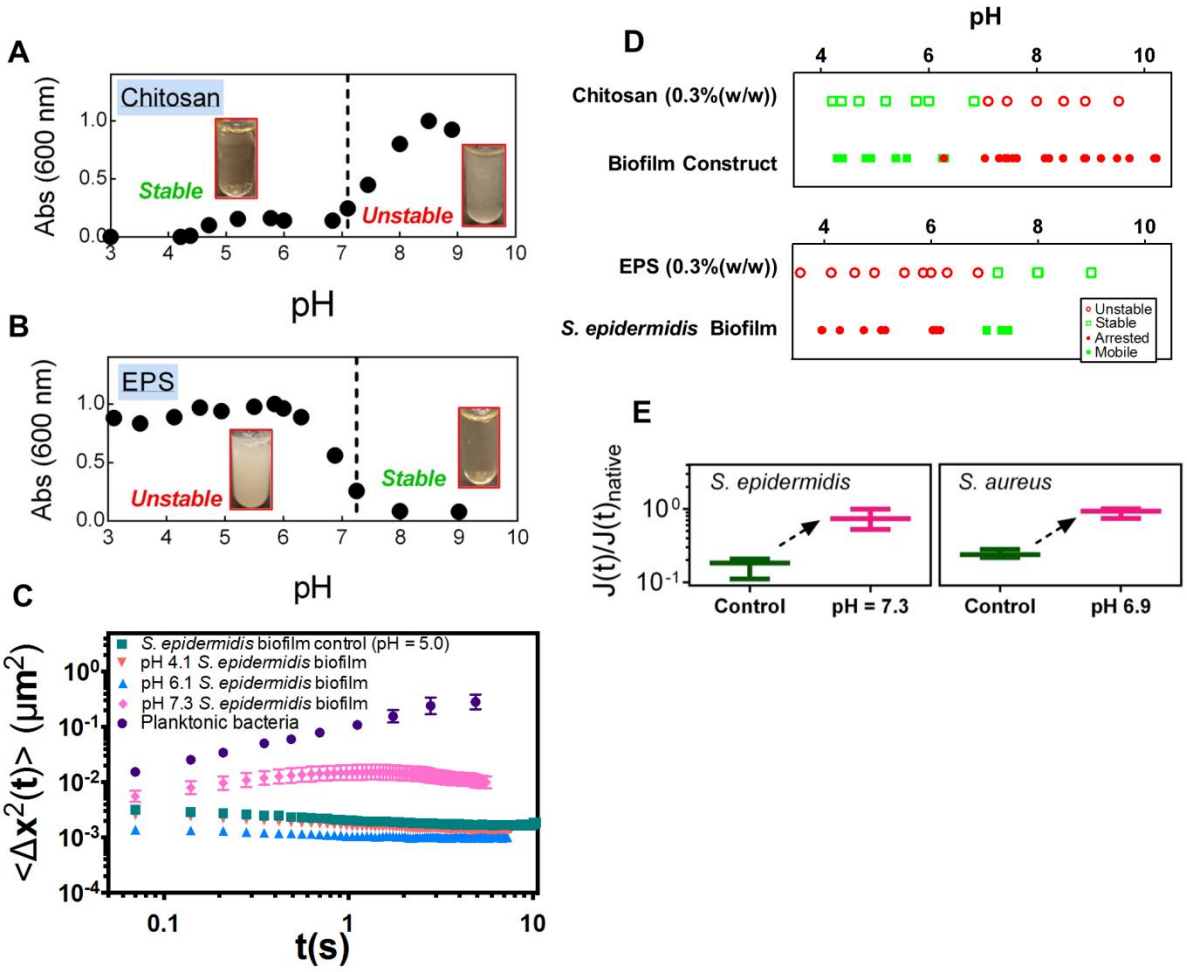

Figure 4.6. **Effect of pH on the stability/mobility of chitosan, EPS, and natural biofilms**.

Absorbance versus pH of 0.3 wt. % chitosan (**A**) and 0.3 wt. % *Staphylococcal* biofilm EPS (**B**) in TSB. (**C**) $\langle \Delta x^2(t) \rangle$ of *S. epidermidis* planktonic bacteria, 18-hour biofilm, and 18-hour biofilms with pH adjusted to 4.1, 6.1, and 7.3. (**D**) Comparison of 0.3 wt. % chitosan stability and the mobility of 0.3 wt. % bacterial-chitosan constructs, as well as the stability of 0.3 wt. % EPS and the mobility of 18-hour *S. epidermidis* biofilms at pH 4-10. (**E**) Normalized J(t) of *S. epidermidis* and *S. aureus* biofilms at their native growth condition and after increasing the pH to 7.3 and 6.9, respectively. **(MSD measurements in (C) and biofilm and construct phase stability for (D) were done by Elizabeth Stewart**

4.5 References

1. Pavlovsky, L., Younger, J. G. & Solomon, M. J. In situ rheology of Staphylococcus epidermidis bacterial biofilms. *Soft Matter* **9,** 122 (2013).
2. Costerton, J. W., Stewart, P. S. & Greenberg, E. P. Bacterial biofilms: a common cause of persistent infections. *Science (80-.).* **284,** 1318–1322 (1999).
3. Hall-Stoodley, L., Costerton, J. W. & Stoodley, P. Bacterial biofilms: from the natural environment to infectious diseases. *Nat. Rev. Microbiol.* **2,** 95–108 (2004).
4. Böl, M., Ehret, A. E., Bolea Albero, A., Hellriegel, J. & Krull, R. Recent advances in mechanical characterisation of biofilm and their significance for material modelling. *Crit. Rev. Biotechnol.* **33,** 145–71 (2013).
5. Guelon, T., Mathias, J. & Stoodley, P. in *Biofilm Highlights* (Flemming, H.-C., Wingender, J. & Szewzyk, U.) **5,** 111–139 (Springer Berlin Heidelberg, 2011).
6. Shaw, T., Winston, M., Rupp, C. J., Klapper, I. & Stoodley, P. Commonality of elastic relaxation times in biofilms. *Phys. Rev. Lett.* **93,** 98102 (2004).
7. Stewart, E. J., Satorius, A. E., Younger, J. G. & Solomon, M. J. Role of Environmental and Antibiotic Stress on Staphylococcus epidermidis Biofilm Microstructure. *Langmuir* **29,** 7017–7024 (2013).
8. Xavier, J. B., White, D. C. & Almeida, J. S. Automated biofilm morphology quantification from confocal laser scanning microscopy imaging. *Water Sci. Technol.* **47,** 31–37 (2003).
9. Bridier, A., Dubois-Brissonnet, F., Boubetra, A., Thomas, V. & Briandet, R. The biofilm architecture of sixty opportunistic pathogens deciphered using a high throughput CLSM method. *J. Microbiol. Methods* **82,** 64–70 (2010).
10. Birjiniuk, A. *et al.* Single particle tracking reveals spatial and dynamic organization of the Escherichia coli biofilm matrix. *New J. Phys.* **16,** 85014 (2014).
11. Galy, O. *et al.* Mapping of bacterial biofilm local mechanics by magnetic microparticle actuation. *Biophys. J.* **103,** 1400–8 (2012).
12. Hidalgo, G. *et al.* Functional tomographic fluorescence imaging of pH microenvironments in microbial biofilms by use of silica nanoparticle sensors. *Appl. Environ. Microbiol.* **75,** 7426–7435 (2009).
13. Flemming, H.-C. & Wingender, J. The biofilm matrix. *Nat. Rev. Microbiol.* **8,** 623–633 (2010).
14. O'Gara, J. P. ica and beyond: biofilm mechanisms and regulation in Staphylococcus epidermidis and Staphylococcus aureus. *FEMS Microbiol. Lett.* **270,** 179–88 (2007).
15. Costerton, J. W. *The biofilm primer*. **1,** (Springer, 2007).
16. Klapper, I. & Dockery, J. Mathematical Description of Microbial Biofilms. *SIAM Rev.* **52,** 221 (2010).
17. Dorken, G., Ferguson, G. P., French, C. E. & Poon, W. C. K. Aggregation by depletion attraction in cultures of bacteria producing exopolysaccharide. *J. R. Soc. Interface* **9,** 3490–3502 (2012).
18. Schwarz-Linek, J. *et al.* Polymer-induced phase separation in suspensions of bacteria. *EPL (Europhysics Lett.* **89,** 68003 (2010).
19. O'Toole, G., Kaplan, H. B. & Kolter, R. Biofilm Formation as Microbial Development. *Annu. Rev. Microbiol.* **54,** 49–79 (2000).

20. Mckenney, D. *et al.* The ica Locus of Staphylococcus epidermidis Encodes Production of the Capsular Polysaccharide / Adhesin. *Infect. Immun.* **66,** 4711–4720 (1998).
21. Rohde, H., Frankenberger, S., Zähringer, U. & Mack, D. Structure, function and contribution of polysaccharide intercellular adhesin (PIA) to Staphylococcus epidermidis biofilm formation and pathogenesis of biomaterial-associated infections. *Eur. J. Cell Biol.* **89,** 103–111 (2010).
22. Ganesan, M. *et al.* Molar mass, entanglement, and associations of the biofilm polysaccharide of Staphylococcus epidermidis. *Biomacromolecules* **14,** 1474–81 (2013).
23. Sadovskaya, I., Vinogradov, E., Flahaut, S., Kogan, G. & Jabbouri, S. Extracellular Carbohydrate-Containing Polymers of a Model Biofilm-Producing Strain , Staphylococcus epidermidis RP62A. *Infect. Immun.* **73,** 2007–3017 (2005).
24. Smith, L. R. & Gilkerson, E. Quantitation of Glycosaminoglycan Hexosamine Using 3-Methyl-2-Benzothiazolone Hydrazone Hydrochloride. *Anal. Biochem.* **98,** 478–480 (1979).
25. Lu, Q. & Solomon, M. Probe size effects on the microrheology of associating polymer solutions. *Phys. Rev. E* **66,** 1–11 (2002).
26. Seefeldt, K. F. Multiple Light Scattering Studis of Attractively Interacting and Polydisperse Colloidal Suspensions. (2003).
27. Hulst, H. C. & van de Hulst, H. C. *Light scattering: by small particles*. (Courier Dover Publications, 1957).
28. Weitz, D. A. & Pine, D. J. Diffusing-wave spectroscopy. *Dyn. Light Scatt.* 652 (1993).
29. Ladd, A., Gang, H., Zhu, J. & Weitz, D. Temporal and spatial dependence of hydrodynamic correlations: Simulation and experiment. *Phys. Rev. E* **52,** 6550–6572 (1995).
30. Dasgupta, B., Tee, S.-Y., Crocker, J., Frisken, B. & Weitz, D. Microrheology of polyethylene oxide using diffusing wave spectroscopy and single scattering. *Phys. Rev. E* **65,** 1–10 (2002).
31. Xu, J., Viasnoff, V. & Wirtz, D. Compliance of actin filament networks measured by particle-tracking microrheology and diffusing wave spectroscopy. *Rheol. Acta* **37,** 387–398 (1998).
32. Ninomiya, K. An extrapolation method for estimating steady-flow viscosity and steady state compliance from creep data. *J. Phys. Chem.* **67,** 1152 (1962).
33. Cerca, F. *et al.* Staphylococcus epidermidis biofilms with higher proportions of dormant bacteria induce a lower activation of murine macrophages. *J. Med. Microbiol.* **60,** 1717–1724 (2011).
34. Lindgren, J. K. *et al.* Arginine deiminase in Staphylococcus epidermidis functions to augment biofilm maturation through pH homeostasis. *J. Bacteriol.* **196,** 2277–2289 (2014).
35. Wang, F. *et al.* Development of luminescent pH sensor films for monitoring bacterial growth through tissue. *Adv. Healthc. Mater.* **3,** 197–204 (2014).
36. Hsiao, L. C., Kang, H., Ahn, K. H. & Solomon, M. J. Role of shear-induced dynamical heterogeneity in the nonlinear rheology of colloidal gels. *Soft Matter* **10,** 9254–9259 (2014).
37. Scheffold, F., Skipetrov, S. E., Romer, S. & Schurtenberger, P. Diffusing-wave spectroscopy of nonergodic media. *Phys. Rev. E* **63,** 61404 (2001).

38. Pavlovsky, L., Younger, J. G. & Solomon, M. J. In situ rheology of Staphylococcus epidermidis bacterial biofilms. *Soft Matter* **9,** 122–131 (2013).
39. PINEab, D. J. *et al.* Dynamical correlations of multiply scattered light.
40. Kaplan, P., Yodh, A. & Pine, D. Diffusion and structure in dense binary suspensions. *Phys. Rev. Lett.* **68,** 393–396 (1992).
41. Sinha, S. K., Freltoft, T. & Kjems, J. Observation of power-law correlations in silica-particle aggregates by small-angle neutron scattering. *Kinet. Aggreg. Gelation* **19842,** 87–90 (1984).
42. Varadan, P. & Solomon, M. J. Shear-Induced Microstructural Evolution of a Thermoreversible Colloidal Gel. 2918–2929 (2001).
43. Wilking, J. N., Angelini, T. E., Seminara, A., Brenner, M. P. & Weitz, D. a. Biofilms as complex fluids. *MRS Bull.* **36,** 385–391 (2011).
44. Zaccarelli, E. Colloidal gels: Equilibrium and non-equilibrium routes. *J. Phys. Condens. Matter* **19,** 323101 (2007).
45. Rinaudo, M. Chitin and chitosan: properties and applications. *Prog. Polym. Sci.* **31,** 603–632 (2006).
46. Anthonsen, M., Varum, K., Hermansson, a, Smidsrod, O. & Brant, D. Aggregates in acidic solutions of chitosans detected by static laser light scattering. *Carbohydr. Polym.* **25,** 13–23 (1994).
47. Peniche, C. & Argüelles-Monal, W. Chitosan based polyelectrolyte complexes. in *Macromol. Symp.* **168,** 103–116 (Wiley Online Library, 2001).
48. Mao, H.-Q. *et al.* Chitosan-DNA nanoparticles as gene carriers: synthesis, characterization and transfection efficiency. *J. Control. Release* **70,** 399–421 (2001).
49. Squires, T. M. & Mason, T. G. Fluid mechanics of microrheology. *Annu. Rev. Fluid Mech.* **42,** 413 (2009).
50. Breedveld, V. & Pine, D. J. Microrheology as a tool for high-throughput screening. *J. Mater. Sci.* **38,** 4461–4470 (2003).

CHAPTER 5

Extending the method of cavitation rheology to specimens of microscale volumes‡

5.1 Abstract

We provide a derivation relating the critical cavitation pressure, P_c, to the elastic modulus, E, of a soft material of arbitrary volume. The equation will be used for cavitation rheometry to measure the elastic modulus for specimens as small as 1 μL. Cavitation rheometry is a technique to obtain the elastic moduli of a sample by measuring the pressure necessary to create a cavity within it[1]. The application of the technique was restricted to samples of volumes larger than the initial cavity dimension. We extend the technique using *ab inito* hyperelasticity modeling to obtain a governing equation relating pressure and deformation in materials of finite thickness. The equation is validated with experiments on cavitation in viscoelastic polyethylene oxide solutions of varying volume. **(Part of the text presented in this chapter is re-printed with permission from Pavlovsky, L., Ganesan, M., Younger, J.G. and Solomon, M.J. *Applied Physics Letters* 105 (2014))**

‡ The experimental data appearing in this section was performed by Leonid Pavlovsky and is re-printed with permission from Pavlovsky, L., Ganesan, M., Younger, J.G. and Solomon, M.J. *Applied Physics Letters* 105 (2014)

5.2 Introduction

The elastic moduli, *E*, is a material property frequently measured for viscoelastic soft matter. Commonly used techniques such as bulk rheometry, microfluidics and microrheology often require expensive instrumentation (e.g. atomic force microscopy microrheology[2]), intricate processing routines (e.g. diffusing wave spectroscopy[3]), special procedure concerns (e.g. probe stability in microrheology[4]), long experimentation times (e.g. microrheology methods require ~ 1 h just to collect raw data[5]) or are limited by sample type (e.g. microfluidic rheometers are rapid, portable and easy to use, however they cannot probe solid like samples). Collectively, these techniques do not readily cater to a portable, easy to use and rapid measurement of modulus of solid and liquid like samples at a wide range of volumes.

The technique of cavitation rheometry, introduced by Zimberlin et al.,[6] is - rapid, easy to setup and operate, portable, inexpensive and has been used to probe materials of modulus up to 40 kPa[7]. Briefly, a syringe of radius R_i is used to induce cavitation in the material of interest using air as the cavitation fluid[8]. The critical pressure, P_c, required to cause cavitation, is related to *E*, through the theory of hyperelasticity (equation 1)[8]. A hyperelastic material is described by a rate independent constitutive model, where the applied stress is related to strain through a density functional[9,10]. Modeling the material to be Neo-hookean, Kundu et al.,[8] provide the following 'cavitation equation' relating P_c to *E* and the surface energy γ [1]:

$$P_c = \frac{5E}{6} + \frac{2\gamma}{R_i} \quad (1)$$

Thus, measuring P_c using syringes of different R_i, a linear fit of P_c vs $2/R_i$ would yield E and γ as slope and intercept. However, by virtue of the derivation of equation (1), the technique, in its current state, has two limitations.

First, since a Neo-hookean model was used, the application of this technique was restricted to elastic solids[1,11]. In a study led by Pavlovsky et al.[7] we addressed this restriction by showing that, for viscoelastic fluids, since cavitation rheometry pertains to a strain rate approaching the frequency independent regime of the material complex moduli, estimating E using the Neo-hookean model was within acceptable error[7].

The second limitation, addressed in this chapter is that, equation (1) is valid only for "thick-walled" spherical shells. That is, for samples whose thickness is large relative to the initial radius of the cavity, R_i[12]. Note that equation (1) is independent of sample dimension. That is, the formation and growth of a cavity is independent of how far the material wall is from the expanding cavity. Thus, equation (1) would presumably apply for samples ranging from milliliters of soft matter to biological materials such as biofilms that are only ~10^2 μm thick[13]. However, when studying bovine eye lens, Cui et al., found that for R_i = 5 μm, comparable to the size of the eye lens, the P_c measured was significantly less than that predicted by equation (1) and resulted in a 69% deviation in E estimated from cavitation and a standard dynamic mechanical analysis[14]. In this chapter, we derive a generalized form of equation (1) and institute a 'modified cavitation equation' demonstrating the necessity to incorporate a variable for sample dimension. Using polyethylene oxide (PEO) as model viscoelastic media, we experimentally demonstrate the validity of our equation.

5.3 Cavitation in the thick and thin shell limit

We begin by outlining the derivation of equation (1). The discussion will setup the framework to proceed with the generalized formulation.

5.3.1 Cavitation in a thin wall spherical shell

We derive an expression relating inflation pressure P to deformation λ of a thin walled spherical shell. A thin shell is similar to a balloon, with external radii $r_0 + d$, where r_0 is the inner radius and d is the thickness such that $d << 1$. Consider an incompressible spherical balloon of un-deformed radius r_0 and wall thickness d_0 (Fig. 5.1A). Let an inflation pressure P act normally along the inner wall causing the balloon to expand equibiaxially (equal extension along the '2' and '3' direction in Fig. 5.1B) to result in the radius and thickness in the deformed state to be λr_0 and d_0/λ^2 (Fig. 5.1B). This is chosen to satisfy incompressibility. That is, If λ_1, λ_2 and λ_3 represent the deformation along the principal axis, for incompressibility, the Jacboian of the deformation matrix F = $diag(\lambda_1^2, \lambda_2^2, \lambda_3^2)$ equals 1[9,10]. Thus,

$$\lambda_2 = \lambda_3 = \lambda \quad (2a)$$

$$\lambda_1 = \left(1/\lambda_2^2\lambda_{31}^2\right)^{1/2} = 1/\lambda^2 \quad (2b)$$

The force acting on the inner wall is given by $P.Area = P\pi(\lambda r_0)^2$ [12,15]. The force due to the circumferential stress t is given by $t.Area = t(2\pi\lambda r_0)(d_0/\lambda^2)$. Under equilibrium, equating the two we obtain

$$P = \frac{2t}{\lambda^3}\left(\frac{d_0}{r_0}\right) \quad (3)$$

We now relate t in terms of λ. The Neo-hookean strain energy density function, U_{NH}, is given as[10]:

$$U_{NH} = \frac{E}{6}\left(\sum_{i-=1}^{3} \lambda_i^2 - 3\right) \quad (4)$$

Let, τ_1, τ_2 and τ_3 be the principal components of the Cauchy stress along the '1', '2' and '3' direction. Then[16],

$$\tau_i = \lambda_i \frac{\partial U_{NH}}{\partial \lambda_i} - p \quad (5)$$

Where, p is the arbitrary hydrostatic pressure required for equilibrium in incompressible materials[16]. In equibiaxial extension, the stress along the '1' direction, τ_1, is balanced by the hydrostatic pressure, p, to maintain equilibrium. Here, we would expect P to balance τ_1. However, under the thin shell assumption, since $r_0 >> d_0$, P becomes negligibly small compared to τ_1 that it is still effectively zero and is balanced by p[15]. So, from equations (2,4,5), we obtain

$$\tau_1 = \left(\frac{E}{3}\right)\lambda_1^2 - p \ = 0 \Rightarrow p = \left(\frac{E}{3}\right)\lambda_1^2$$

$$\tau_2 = \tau_3 = \left(\frac{E}{3}\right)\lambda_2^2 - p \quad (6)$$

Thus, from equations (2, 3,6) we get

$$P = \frac{2}{3} E \frac{d_0}{r_0}(\lambda^{-1} - \lambda^{-7}) \quad (7)$$

Equation (7) is the pressure-deformation relation for inflation of thin wallded spheres, plotted in Fig. 5.1C. We find that the pressure rapidly increases for low deformations, and once it reaches a critical value, P_c, it decreases with increase in λ. This reflects a limited range of applicability of this model strain energy function; details of which is given in Ogden[9].

5.3.2 Cavitation in a thick walled spherical shell

We view this problem as the inflation of concentric thin-walled balloons [12,15]. The wall thickness in the un-deformed and deformed state is chosen as *dr* and d*r*/λ^2. The thick shell assumption is that the outer boundary of the specimen is sufficiently far from the needle, and is therefore unperturbed by deformation due to cavity formation (Fig. 5.2A). That is at r $\rightarrow \infty$, $\lambda \rightarrow$ 1. Thus, equation (5) in differential form becomes

$$dP = \frac{2}{3} E \frac{dr}{r} (\lambda^{-1} - \lambda^{-7})$$

Gent[12] identified that the wall thickness d*r*/λ^2 of the shell in the deformed state is due to an increment $d(\lambda r)$ in the radius of the strained state. This gives us a relationship between *dr* and $d\lambda$ as

$$dr = \frac{r\lambda^2}{1-\lambda^3} d\lambda$$

$$dP = -\frac{2E}{3} (\lambda^{-2} + \lambda^{-5}) d\lambda$$

The limits of integration are: at λ, pressure is *P* and at the far surface (*r* = ∞), where λ ~ 1, the pressure is *P* = 0. Integrating the above we obtain $P = E\left(\frac{5}{6} - \frac{2}{3\lambda} - \frac{1}{6\lambda^4}\right)$, which at infinite deformation, $\lambda \rightarrow \infty$, yields $P_c = \frac{5E}{6}$ (8), which is same as that proposed by Kundu et al.,[8] in equation (1). The contribution of surface energy, $2\gamma/R_i$ is evident through the Young-Laplace equation[17]. However, throughout our formulation, we neglect the contribution of surface energy. Figure 5.2B shows the pressure-extension curve for the equibiaxial expansion of a thick walled

spherical shell under internal loading. At infinite deformation, pressure reaches a critical value P_c ~ 5E/6.

If the upper limit of integration was not 1, then the pressure would be a function of both internal and external radius of the sample. In this next section, we establish the derivation of the inflation of a spherical shell of arbitrary thickness.

5.4 Inflation of a spherical cavity in a Cauchy elastic material

We derive the relation between the inflation pressure P and extension ratio λ for a spherical shell of finite thickness comparable to the size of the initial cavity (Fig. 5.3A).

5.4.1 Formulation of the problem

Consider the sphere described by a closed system in spherical co-ordiantes

$$B_0 = \{(R, \Theta, \Phi) \,|A \leq R \leq B; 0 \leq \Theta \leq 2\pi;\ 0 \leq \Phi \leq 2\pi\ \}$$

Where (R,Θ,Φ) are the co-ordinates of the material before deformation. Let this system be inflated by an internal pressure *P* that maps B_0 symmetrically into a finite ball b_0 injectively

$$b_0 = \{(r, \theta, \phi) \,|a \leq r \leq b; \theta = \Theta;\ \phi = \Phi\ \}$$

Applying incompressibility criterion we have

$$r^3 - R^3 = a^3 - A^3 = b^3 - B^3 \quad (9)$$

Using spherical symmetry and incompressibility, the deformation can be written as $r = f(R)R$ where[18,19]

$$f(R) = \left(1 + \frac{a^3 - A^3}{R^3}\right)^{1/3} = \lambda \quad (10)$$

The deformation gradient tensor in spherical co-ordinates for deformation from B_0 to b_0 is given by[18]

$$F = \frac{\partial b_0}{\partial B_0} = \begin{pmatrix} f(R) + Rf(\dot{R}) & 0 & 0 \\ 0 & f(R) & 0 \\ 0 & 0 & f(R) \end{pmatrix} = \begin{pmatrix} \lambda^{-2} & 0 & 0 \\ 0 & \lambda & 0 \\ 0 & 0 & \lambda \end{pmatrix}$$

The above satisfies the incompressibility condition where $\lambda_r\lambda_\theta\lambda_\phi = \lambda^{-2}\lambda\lambda = 1$. The advantage of the incompressibility constraint is that we can immediately get the deformation field $f(R)$ which is not possible if the material was compressible. Here, λ_1, λ_2, λ_3 are λ_r, λ_θ, λ_ϕ respectively. From equation (4,5), the principal component of the Cauchy stress are

$$\tau_1 = \tau_{rr} = \frac{E}{3}\lambda^{-4} - p \quad (11)$$

$$\tau_2 = \tau_{\theta\theta} = \tau_{\phi\phi} = \tau_3 = \frac{E}{3}\lambda^{2} - p \quad (12)$$

In the absence of any body forces, the equilibrium condition[16] $\nabla.\tau = 0$ in the current configuration b_0 reduces to

$$\frac{\partial \tau_{rr}}{\partial r} + \frac{2}{r}(\tau_{rr} - \tau_{\theta\theta}) = 0 \quad (13)$$

With boundary conditions $\tau_{rr} = -P$ at $r = a$ and $\tau_{rr} = 0$ on $r = b$. Where, $r = a$ and $r = b$ represent the inner and outer wall of the sphere

5.4.2 Solution of the boundary value problem

We define some variables here $\lambda_a = a/A$ and $\lambda_b = b/B$. From incompressibility assumption, we obtain that

$$\lambda_b = \left(\left[\left({\lambda_a}^3 - 1\right)\left(\frac{A}{B}\right)^3\right] + 1\right)^{1/3} \quad (14)$$

We then obtain one more useful relation that

$$\frac{\partial \lambda}{\partial R} = \left(1 + \frac{a^3 - A^3}{R^3}\right)^{-\frac{2}{3}}\left(\frac{a^3 - A^3}{R^4}\right) \quad (15)$$

Which, after re-arrangement simplifies to

$$\frac{\partial \lambda}{\partial R} = \frac{\lambda^{-2} - \lambda}{R} \quad (16)$$

Furthermore, we obtain a relation between λ and the radius in the deformed state *r* as

$$\frac{\partial r}{\partial \lambda} = R + \lambda \frac{\partial R}{\partial \lambda} \quad (17)$$

$$\frac{\partial r}{\partial \lambda} = R\left(\frac{\lambda^{-2}}{\lambda^{-2} - \lambda}\right) \quad (18)$$

Thus, we re-write the momentum balance, using equation (11-17) after some modification in terms of λ to obtain

$$\frac{\partial \tau_{rr}}{\partial \lambda} = \frac{2\lambda^{-1}}{\lambda^3 - 1}(\tau_{rr} - \tau_{\theta\theta}) \quad (19)$$

From equation (11,19) we obtain the following partial differential equation for the hydrostatic pressure *p*:

$$\frac{\partial p}{\partial \lambda} = \frac{E}{3}\left(\frac{2\lambda - 4\lambda^{-2} + 2\lambda^{-5}}{\lambda^3 - 1}\right) \quad (20)$$

We can integrate the above equation to get an explicit relation for *p* in terms of λ upto a constant. Using the boundary condition at the inner wall, that is $\tau_{rr} = -P$ at $r = a$ or $\lambda = \lambda_a$, we get expression for *p* to be equal to

$$p = \frac{2E}{3}\left(\frac{1}{4\lambda^4} - \frac{1}{\lambda}\right) + \frac{E}{3}\left(\frac{1}{2\lambda_a^4} + \frac{2}{\lambda_a}\right) \quad (21)$$

The principal Cauchy stress can now be obtained as

$$\tau_{rr} = \frac{E}{6\lambda^4} + \frac{2E}{3\lambda} - \frac{E}{3}\left(\frac{1}{2\lambda_a^4} + \frac{2}{\lambda_a}\right) - P \qquad (22)$$

Since at the outer wall, $r = b$ or $\lambda = \lambda_b$, we have $\tau_{rr} = 0$, the above equation becomes

$$P = \frac{E}{6\lambda_b{}^4} + \frac{2E}{3\lambda_b} - \frac{E}{3}\left(\frac{1}{2\lambda_a^4} + \frac{2}{\lambda_a}\right) \qquad (23)$$

Equation (23) represents the relationship between the inflation pressure *P* to the inner and external deformation of the material. Thus, for a given initial inner or outer radii, we can find the dimensions of the body *a* and *b* after deformation due to a known value of *P*. Now, we show that this formulation tends to the thin walled and thick walled spherical shell problem

5.4.3 Inflation of a Thin wall spherical shell

Consider $B = A(1+\varepsilon)$, where ε is small enough that higher orders can be neglected. Let the material be deformed by λ such that post deformation $a = \lambda A$. Using incompressibility, we obtain

$$b = \lambda A\left(1 + \frac{\varepsilon}{\lambda^3}\right) \qquad (24)$$

Here, $\lambda_a = a/A = \lambda$, and using the binomial approximation, $\lambda_b = \lambda(1+\varepsilon(1/\lambda^3 - 1))$. Equation (20) becomes

$$p = \frac{E}{3}\int_{\lambda} \left(\frac{2\lambda - 4\lambda^{-2} + 2\lambda^{-5}}{\lambda^3 - 1}\right) d\lambda + C \qquad (25)$$

Which implies

$$\tau_{rr} = \frac{E}{3\lambda^4} - \frac{E}{3}\int_{\lambda} \left(\frac{2\lambda - 4\lambda^{-2} + 2\lambda^{-5}}{\lambda^3 - 1}\right) d\lambda - C \qquad (26)$$

Using the boundary condition, and fundamental properties of definite integrals, we can write the above equation as

$$-P = \frac{E}{3\lambda_a^4} - \frac{E}{3\lambda_b^4} - \frac{E}{3}\int_{\lambda_a}^{\lambda_b}\left(\frac{2\lambda - 4\lambda^{-2} + 2\lambda^{-5}}{\lambda^3 - 1}\right)d\lambda \qquad (27)$$

It can be seen that λ_b-λ_a ~ *b*-*a* is of the order of ε. Thus, using the mean value theorem for integrals, we write the above equation as

$$-P = \frac{E}{3\lambda_a^4} - \frac{E}{3\lambda_b^4} - \frac{E}{3}(\lambda_b - \lambda_a)\left(\frac{2\lambda - 4\lambda^{-2} + 2\lambda^{-5}}{\lambda^3 - 1}\right) \qquad (28)$$

Using equation (28) and the expression for λ_a and λ_b in terms of λ and ε and tedious algebra, we obtain the expression relating P to λ for a thin walled spherical cavity as

$$P = \frac{2E\varepsilon}{3}\left(\frac{1}{\lambda} - \frac{1}{\lambda^7}\right) \qquad (30)$$

The above equation is the same as what was derived earlier equation (7).

5.4.4 Inflation of a thick wall spherical shell

This is a relatively straightforward. In this case, the external wall of the material is at *r* = ∞, that is both *B* and *b* tend to ∞. In this case, as *r*, $R \to \infty$ or $\lambda_b \to 1$, we have $\tau_{rr} \to 0$. The deformation of the inner dimension still remains the same, that is $\lambda_a = a/A = \lambda$.

Thus, going back to equation (27) we get

$$-P = \frac{E}{3\lambda^4} - \frac{E}{3} - \frac{E}{3}\int_{\lambda_a=\lambda}^{\lambda_b=1}\left(\frac{2\lambda - 4\lambda^{-2} + 2\lambda^{-5}}{\lambda^3 - 1}\right)d\lambda$$

The above equation is immediate to solve, thus giving us the relation between P and λ for the inflation of a thick walled cavity, and this equation is same as that obtained earlier

$$P = E\left(\frac{5}{6} - \frac{2}{3\lambda} - \frac{1}{6\lambda^4}\right) \quad (31)$$

Figure 5.3B is the pressure-extension curve for samples of varying thickness according to equation (23). We find that this curve is significantly dependent on sample thickness. As the thickness ~ 1, the curve approximates to Fig. 5.1C; while for samples of infinite thickness, the curve approximates to Fig. 5.2B where P/E approaches a plateau of ~5/6. To develop the modified cavitation equation, we plot the thickness dependent maximum in pressure, P_c, against thickness (Fig. 5.4). Figure 5.4 shows that beyond a thickness of 45 units, P_c becomes independent of thickness and approaches a value ~5/6. As thickness or material volume drops below about 45, we find that P_c drops strongly as a function of thickness. Here, thickness is the ratio of the distance of the sample's wall from the needle outer diameter to the needle inner diameter. We fit the points (obtained by numerically solving equation (21)) to a power law to obtain the modified cavitation equation as[7]:

$$P_c = \frac{5E}{6}\left[\frac{6a}{5}\left(\frac{R_i + H}{R_i}\right)^b + 1\right] \quad (32)$$

Here, a = -0.8558 and b = -0.6547. Thus, we prove that cavitation rheometry, that is, the measured critical pressure, indicating onset of cavitation in a material, is significantly dependent on the sample thickness, and equation (1) is applicable only for sufficiently large sample volumes. We now experimentally demonstrate this in Fig. 5.5. Cavitation was induced in polyethylene oxide solutions (4%(w/w) , 10^6 g/mol PEO) of varying sample volumes and the measured critical pressure is plotted against the sample volume. The circular points denote the

small volume experiments while the squares are the large volume, or thick-shell experiments. We find that P_c varies with material volume, with smaller volumes of PEO exhibiting cavity formation at smaller critical pressures than the relatively large volume solutions. Thus, the behavior is as predicted by equation (32) which was used to fit the data with *E* as the variable parameter. The good agreement between E measured from Fig. 5.5 using equation (32) and that measured using mechanical rheometry was verified in Pavlovsky et al.[7]

In conclusion, here we derived a governing equation for cavitation rheometry that extends its working scope to materials of volumes as small as 1μL. However, to further extend the scope of this technique, the following are required 1) Equation (32) was developed under a Neo-hookean framework. However, this is only a model strain energy function. More robust and broad ranged models have been developed which can be incorporated in this derivation. 2) Here, we did not consider the impact of viscosity by working within a rate independent energy density function. Thus, incorporating viscosity into the derivation would further broaden the scope of equation (32) by accounting for viscous dissipation effects.

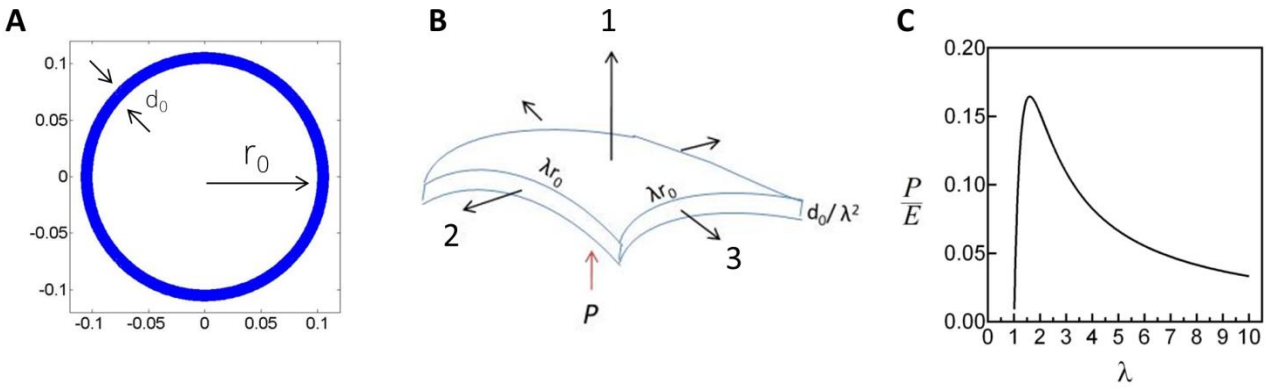

Figure 5.1. Inflation of a thin walled spherical shell

(L to R) Schematic of equibiaxial extension of a section of a thin walled spherical material of undeformed radius and thickness r0 and d0 respectively. Here, λ is the deformation or stretch ratio.(Middle) A diagram of a thin wall shell with inner diater r0 and thickness d0. (Right) Pressure-stretch curve for a thin walled material of arbitrary r0 and d0 such that d0<<<1.

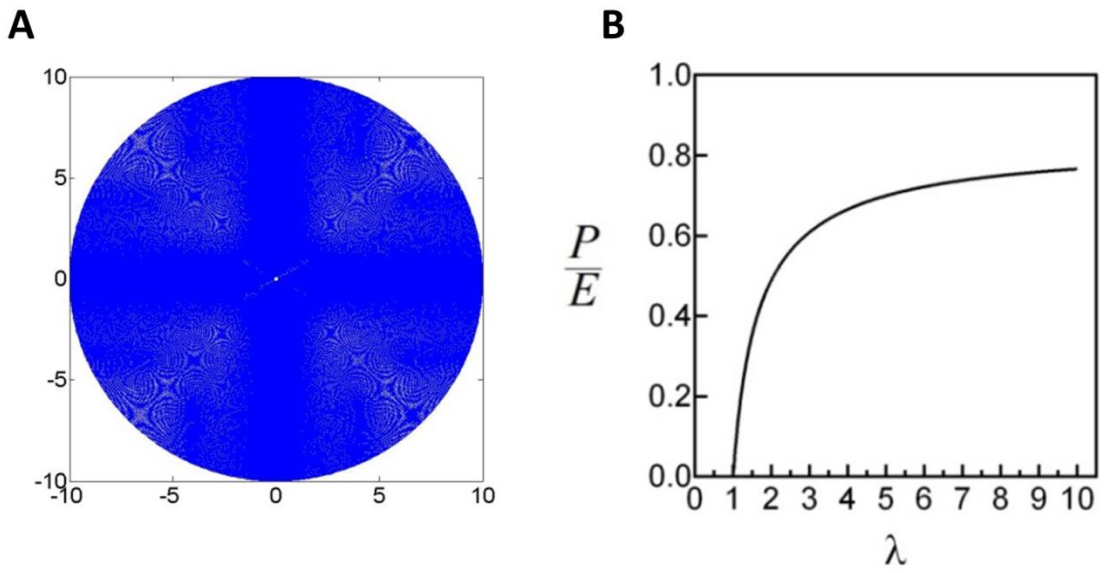

Figure 5.2. Inflation of a thick-walled spherical shell

(A) Schematic of a thick walled spherical shell, with inner radius <<<wall thickness; **(B)** The pressure extension curve for a thick walled material where at infinite extension, the pressure reaches a plateau of ~5E/6

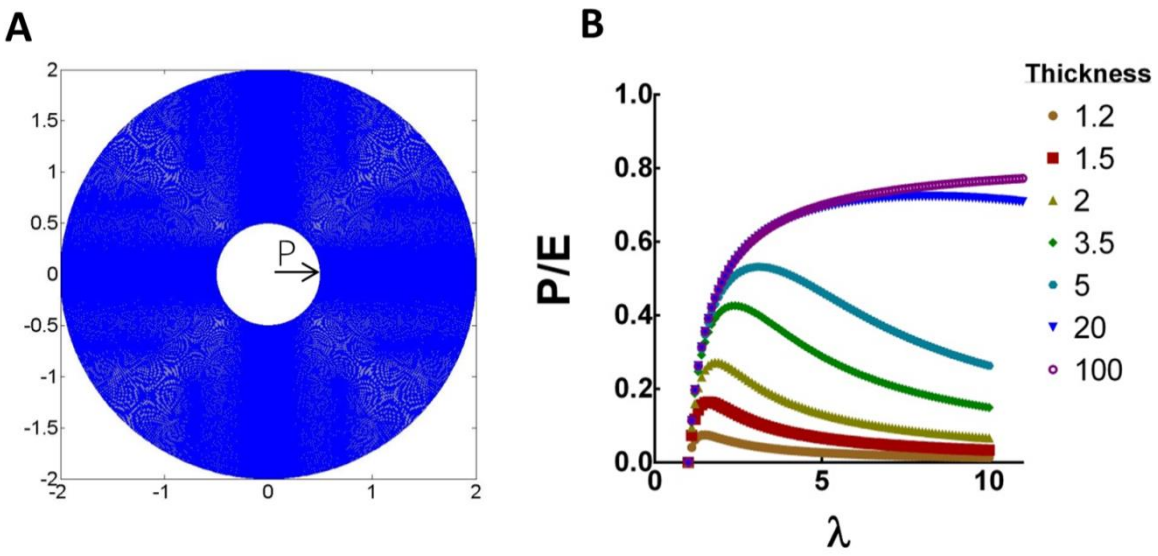

Figure 5.3. Inflation of a spherical shell of arbitrary thickness

(A) Schematic of a spherical shell of finite thickness; **(B)** Pressure deformation curves of materials of various thickness. Note that, for very thin materials, the curve is similar to that observed in Fig. 1 and for thick materials, the curve is similar to that observed in Fig 5.2.

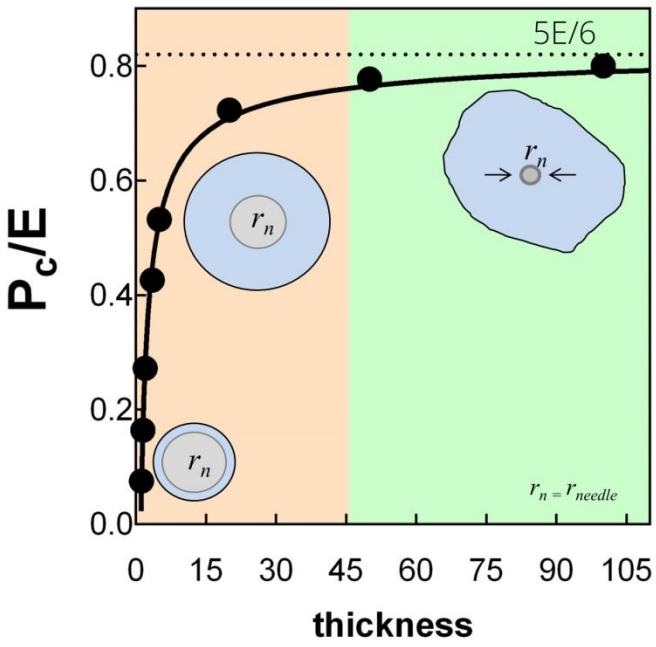

Figure 5.4. Dependence of critical pressure versus material thickness

The dependence of critical pressure P_c as a function of thickness. P_c was taken as the maximum of P vs λ curves from Fig 5.3B. We find that the Pc becomes independent of thickness only for thickness greater than about 45. For thin materials, P_c is a strong function of material thickness. The solid line is a fit of the points and is the modified cavitation equation from now on.

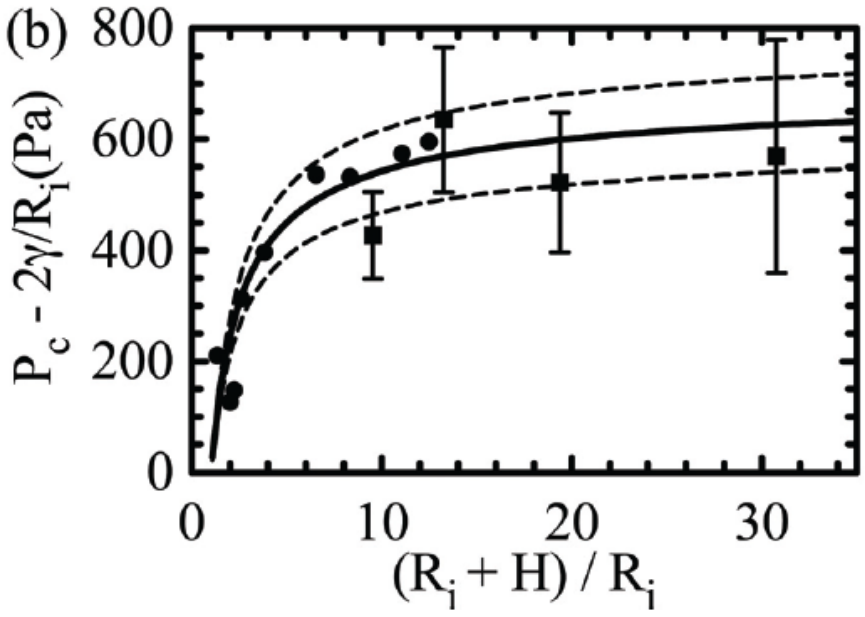

Figure 5.5. Cavitation rheometry of PEO of varying volumes

P_c with surface energy contribution subtracted, plotted as a function of PEO sample dimension. The circles and squares refer to experimental data, the solid line is the fit according to equation (32) and the dashed lines are the 95% confidence intervals. **(The experimental data in the plot were all taken by Leonid Pavlovsky and is reproduced with permission from Pavlovsky, L., Ganesan, M., Younger, J.G. and Solomon, M.J. *Applied Physics Letters*, 105, (2014))**

5.5 References

1. Zimberlin, J. A., Sanabria-delong, N., Tew, G. N. & Crosby, A. J. Cavitation rheology for soft materials. 763–767 (2007). doi:10.1039/b617050a
2. Jalili, N. & Laxminarayana, K. A review of atomic force microscopy imaging systems: application to molecular metrology and biological sciences. *Mechatronics* **14,** 907–945 (2004).
3. Weitz, D. A. & Pine, D. J. Diffusing-wave spectroscopy. *Dyn. Light Scatt.* 652 (1993).
4. Cicuta, P. & Donald, A. M. Microrheology: a review of the method and applications. *Soft Matter* **3,** 1449 (2007).
5. Lu, Q. & Solomon, M. Probe size effects on the microrheology of associating polymer solutions. *Phys. Rev. E* **66,** 1–11 (2002).
6. Zimberlin, J. A., Mcmanus, J. & Crosby, A. J. Cavitation rheology of the vitreous : mechanical properties of biological tissue. 3632–3635 (2010). doi:10.1039/b925407b
7. Pavlovsky, L., Ganesan, M., Younger, J. G. & Solomon, M. J. Elasticity of microscale volumes of viscoelastic soft matter by cavitation rheometry. *Appl. Phys. Lett.* **105,** 114105 (2014).
8. Kundu, S. & Crosby, A. J. Cavitation and fracture behavior of polyacrylamide hydrogels. 3963–3968 (2009). doi:10.1039/b909237d
9. Ogden, R. W. *Non-linear elastic deformations*. (Courier Dover Publications, 1997).
10. Treloar, L. R. G. *The physics of rubber elasticity*. (Oxford University Press, 1975).
11. Zimberlin, J. A., McManus, J. J. & Crosby, A. J. Cavitation rheology of the vitreous: mechanical properties of biological tissue. *Soft Matter* **6,** 3632–3635 (2010).
12. Gent, A. N. Elastic instabilities in rubber. *Int. J. Non. Linear. Mech.* **40,** 165–175 (2005).
13. Stewart, E. J., Satorius, A. E., Younger, J. G. & Solomon, M. J. Role of Environmental and Antibiotic Stress on Staphylococcus epidermidis Biofilm Microstructure. *Langmuir* **29,** 7017–7024 (2013).
14. Cui, J., Lee, C. H., Delbos, A., McManus, J. J. & Crosby, A. J. Cavitation rheology of the eye lens. *Soft Matter* **7,** 7827–7831 (2011).
15. Alan, G. Engineering with rubber: how to design rubber components. (2001).
16. Holzapfel, G. A. *Nonlinear solid mechanics*. **24,** (Wiley Chichester, 2000).
17. Gent, A. N. & Tompkins, D. A. Nucleation and growth of gas bubbles in elastomers. *J. Appl. Phys.* **40,** 2520–2525 (1969).
18. Green, A. E. & Zerna, W. Theoretical elasticity.
19. Chung, D.-T., Horgan, C. O. & Abeyaratne, R. The finite deformation of internally pressurized hollow cylinders and spheres for a class of compressible elastic materials. *Int. J. Solids Struct.* **22,** 1557–1570 (1986).

CHAPTER 6

Conclusions and Future Work

6.1 Concluding Remarks

In this dissertation, we quantified the polymeric and rheological properties of the polysaccharide intercellular adhesin (PIA) of *Staphylococcus epidermidis* biofilms. The goal of performing these measurements was to understand the contribution of PIA towards the bulk viscous and elastic modulus of the overall biofilm.

In Chapter 2, we identified that PIA has a molar mass of ~200 kDa as opposed to 30 kDa that was believed to be true for more than a decade. We saw that PIA exhibited a pH dependent self-association and complexation with a model albumin at concentrations consistent with that found *in situ*. These fundamental results laid the foundation for subsequent characterization of PIA in the following chapters.

We measured the rheology of PIA in Chapter 3. Here, we established the range for PIA concentration within shaker grown biofilms to vary between 0.1 – 5.0 wt. %. Within that range, PIA was found to be purely viscous upto a concentration 1.6 wt. %, beyond which, it displayed a viscoelastic rheology. The nature of this transition concentration is as yet unclear. Furthermore, at PIA concentrations greater than 1.6 wt. %, a polymeric composite, consisting of bovine serum albumin and λ DNA, that simulated the biofilm EPS, was about 50 fold more elastic than PIA alone. These data highlight the different rheological phenomena that describe PIA viscoelasticity

at different concentrations and yields scaling laws that serve as inputs in multicomponent modeling of biofilms. Furthermore, they provide an insight that the contribution of PIA towards biofilm viscoelasticity ranges from viscous contribution at concentrations less than 1.6 wt. %, to a viscoelastic contribution either on its own or through complexation with other biofilm matrix macromolecules at PIA concentrations greater than 1.6 wt. %. The important insight is that, while PIA can facilitate the overall viscous modulus of a biofilm, it does not generate, even in the presence of proteins and nucleic acids, the elasticity observed in mature biofilms.

Finally, in Chapter 4, we combine the results from the preceding chapters to deconstruct the rheology of the biofilm. For this, we measured and compared the rheology of *S. epidermidis* biofilms, its EPS and PIA across a frequency range of 10^{-1} – 10^{5} Hz. We self-assembled an artificial biofilm system that exhibited mechanical properties similar to a naturally occurring biofilm. Collectively, we found that the short time response of the biofilm is likely mediated by the EPS polymers, while the onset of long time plateau in creep was due to a physicochemical interaction between polymers and bacterial cells. This study identified that modifying the pH of the biofilm growth environment resulted in disrupting the elasticity of the biofilm.

Our findings collectively addressed several gaps that were present in our understanding of *S. epidermidis* biofilms, namely - PIA molar mass, *in situ* concentration, interaction with proteins, viscoelasticity, and contribution towards biofilm rheology and finally, its role in mediating the onset and dispersal of biofilm viscoelasticity. The findings on PIA solution properties (Chapter 2) and rheology (Chapter 3) will potentially serve as material data for large scale simulations of biofilm growth and detachment while the results on physicochemical factors mediating onset and dispersal of biofilm mechanics (Chapter 4) will serve towards development of biofilm remediation methods.

6.2 Future Work

6.2.1 Solution properties of PIA

PIA is a unique naturally occurring polymer with a β-1,6 instead of the more commonly occurring β-1,4 glycosidic linkage, and possessing hydrophilic, hydrophobic and hydrogen bonding moieties on the same chain[1]. The interplay between the associative hydrophobic/hydrogen bonding groups and the water solubility of the hydrophilic parts lead to interesting solution behavior that requires further study. The following examples highlight this.

In Chapter 2, the A_2 of PIA in water, obtained using batch mode SLS, was negative, indicating a poor solvent behavior while the scaling exponent of r_g versus M_w, obtained using SEC-MALLS, was greater than 0.5, indicating a good solvent behavior. An explanation for this competing observation could be that while the hydrophilic moieties favor solubility, the hydrophobic groups, which are greater in number, do not favor solubility in aqueous solutions. Thus, batch mode SLS, which reports averaged solution properties, yields an overall bad solvent behavior; while SEC-MALLS, that accounts for individual contribution from each size fraction, reports a good solvent behavior. Validating this proposition requires – i) batch mode light scattering on PIA eluents from a SEC column to identify which fractions exhibit a good and bad solvent behavior; ii) molecular dynamic simulations to get an insight into the conformation of the polymer as mediated by these interaction sites.

Another example reflecting the complex solution behavior of PIA is seen from its self-association at pH < 6. The self-association of PIA is thought to be due to hydrophobic interactions mediated by the methyl groups. However, at pH less than the pKa (~ 6.2) of the amine groups, PIA is expected to be protonated, which promotes its binding with the negatively

charged bovine serum albumin at pH < 6 (see Chapter 2, 4). Thus, at that pH, one would presume the repulsion between the NH_3^+ groups on the same chain would inhibit self-associations. This argument contradicts the observed onset of self-association in PIA at pH < 6. A likely explanation is that, while hydrophobic associations might occur at all pH, the protonation of the amine groups at pH < 6 further enhances self-association due to interactions between the NH_3^+ groups and the anionic succinates present in the chain[1,2]. Thus, while we report observations of self-associative behavior, precisely quantifying the nature of these interactions as either inter or intramolecular or hydrophobic or hydrogen bonding necessitates the following studies – i) the impact of destabilizing factors such as urea or guanidine salts, that are known to disrupt hydrogen/hydrophobic effects in polymers, on the solution and rheological properties of PIA is to be studied ; ii) to validate the claim that protonation of amine groups favors binding with anionic succinates on the same chain or complexation with negatively charged albumins, the behavior of PIA in the presence of positively charged proteins, at pH < 6, is to be tested. We note that, the formation of aggregates in acidic solutions of N-acetylglucosamine polymers is not yet clearly understood.

Finally, in Chapter 4, we find that the pH dependence of the behavior of biofilm EPS and chitosan, in tryptic soy broth (TSB) media, are exactly reversed. That is, EPS exhibits instability at pH < 7, while chitosan exhibits instability only at pH > 7. Since EPS is a composite consisting of PIA, proteins and DNA, and that TSB itself contains peptides that create instabilities in the EPS (see Appendix), the instability at pH < 7 observed in EPS can be explained to be due to a combination of self-association and complexations of PIA with EPS and TSB proteins at that pH. On the other hand, the onset of an unstable phase in chitosan at pH > 7 in TSB is not easily explained. In water, chitosan is known to form aggregates, or become unstable, and complex

with albumins at acidic pH[3,4]. Thus, the reversal in its behavior specifically in a growth media requires further investigation. The nature of this physicochemical interaction requires being investigated using molecular dynamics simulations or nuclear magnetic resonance techniques that can provide insight into how polysaccharides arrange themselves in the presence of proteins. The findings of such a study would help understand how this phase instability then enables the polymers to trap cells into large viscoelastic volumes as identified in Chapter 4.

In this dissertation, measurements of PIA chain stiffness such as persistence and contour length were not done. These parameters can be calculated from Casassa-Holtzer or Kratky-Porod plots using low-angle static light scattering measurements[5]. Quantifying these properties would shed light on conformational properties of PIA, that is, if PIA is a Gaussian chain, wormlike or semiflexible chain or a rigid rod. Small-angle X-ray scattering is an instructive next step towards studying secondary and tertiary structural properties of PIA.

6.2.2 Rheology of staphylococcal extracellular polymers

In Chapter 3, we measured the rheology of PIA and showed that its viscosity scaling beyond a concentration of 1.6 wt. %, briefly followed theoretical predictions for both semidilute entangled non-interacting polymers and multi-sticker associative polymers that form large aggregates. However, the range of concentrations studied in this work precluded a precise identification of the nature of this viscoelasticity in PIA. Furthermore, while the congruence in storage and loss modulus, as observed here at PIA concentrations gtreater than 4.8 wt. %, if often attributed to an onset of gelation, there is a significant lack of insight if physical or chemical crosslinking drives this behavior in PIA. To understand these further, rheology

measurements of PIA at higher concentrations is essential. Furthermore, techniques such as small angle neutron scattering coupled with rheometry would provide simultaneous structural and rheological information of PIA at different deformation conditions. These studies will enable an understanding of the nature of PIA viscoelasticity – whether it is entanglements, or associations or gelation. Such a study is imminently required to be able to suggest suitable polymer network models (either based on physical entanglements or associations or gelation) for constitutive modeling of PIA. As a pre-requisite, to enable such detailed rheological studies, a scale up in the PIA purification process or development of laboratory synthesis of PIA is required to obtain large quantities of the polymer.

In this work, our focus was to identify if PIA complexes with proteins and if it exhibited a synergistic rheology in their presence. However, under special conditions, polysaccharides and proteins interact to result in gel like complex called coacervates. Formation of coacervates in biofilms is an interesting possibility that needs attention through light scattering and microrheology measurements of PIA in the presence of varying protein concentration and pH. Furthermore, the impact of salts on the rheological properties of PIA and its complexes with proteins are essential. Such a study would provide insight into understanding the non-monotonic trend seen in biofilm elasticity with increasing salt content in the growth media. Another environmental variable that can impact polymer rheology is temperature. Studying the impact of temperature, on potentially reducing the viscoelasticity of the biofilm EPS will be useful to support treatment procedures such as hyperthermia therapy, where in, a body tissue is exposed to slightly elevated temperatures to kill microbial cells. Thus, Chapter 3 provides motivation towards studying the role of polymer-polymer interactions or agents that are disruptive to such interactions on the biofilm rheology.

6.2.3 Theoretical studies for cavitation rheometry

The Neo-hookean function used here is only a model hyperelastic framework. It has functional limitations, particularly at high deformations. The pressure versus deformation plot (see Chapter 5) indicates that infinite deformation would occur once the pressure crosses its maximum value. However, in real materials, beyond a certain deformation, a plastic regime sets in where a sharp increase in pressure versus deformation occurs, that is not predicted by the Neo-hookean model. Thus, to enable cavitation rheometry to be used as an *in vivo* diagnostic tool, we need to use more realistic hyperelastic models that have been developed for biological materials. Furthermore, by using a strain energy density functional, the role of viscosity was not considered in our study. To use this technique for viscoelastic materials, viscous dissipation has to be accounted for. For this, a generalized framework, of the Rayleigh-Plesset type, but with a viscoelastic constitutive model has to be used as the starting point in the derivation. In addition, cavitation can often lead to high strain rates that can result in non-isotropic deformations, such as necking. In such a case, spherical symmetry arguments will no longer hold. Thus, a theoretical analysis on the onset of instabilities or the lack thereof is to be analyzed. Thus, while cavitation rheometry is an attractive, rapid and cheap method, significant modeling and theoretical studies are required to ensure that the calculation of elastic modulus from critical pressure follows the right physics as dictated by the material under study.

6.3 References

1. Rohde, H., Frankenberger, S., Zähringer, U. & Mack, D. Structure, function and contribution of polysaccharide intercellular adhesin (PIA) to Staphylococcus epidermidis biofilm formation and pathogenesis of biomaterial-associated infections. *Eur. J. Cell Biol.* **89,** 103–111 (2010).
2. Mack, D. *et al.* The intercellular adhesin involved in biofilm accumulation of Staphylococcus epidermidis is a linear beta-1,6-linked glucosaminoglycan: purification and structural analysis. *J. Bacteriol.* **178,** 175–83 (1996).
3. Anthonsen, M., Varum, K., Hermansson, a, Smidsrod, O. & Brant, D. Aggregates in acidic solutions of chitosans detected by static laser light scattering. *Carbohydr. Polym.* **25,** 13–23 (1994).
4. Schatz, C., Viton, C., Delair, T., Pichot, C. & Domard, A. Typical physicochemical behaviors of chitosan in aqueous solution. *Biomacromolecules* **4,** 641–648 (2003).
5. Denkinger, P. & Burchard, W. Determination of chain stiffness and polydispersity from static light-scattering. *J. Polym. Sci. Part B Polym. Phys.* **29,** 589–600 (1991).

APPENDIX A

Solution Properties of biofilm extracellular polysaccharides in bacterial growth media

The impact of constituents of a bacterial growth media on the solution properties of biofilm polysaccharides is studied. The extracellular polysaccharides within a biofilm are typically surrounded by several components that are contained in its growth media environment, in addition to other bacterial excreta[1,2]. Such components include salts (e.g. NaCl and K_2HPO_4 in tryptic soy broth (TSB)), peptide sequences (e.g. digest of casein in LB Broth (LBB) or gelatin in Brain heart infusion broth (BHI)), sugar molecules (e.g. dextrose in TSB), host proteins (e.g. albumins in blood) and traces of minerals, vitamins[3]. In addition, due to bacteria metabolism, the growth environment within a biofilm has pH ranging between 4.5 – 7.5[4–6].

Thus, polysaccharides synthesized by the biofilm bacteria are excreted into a complex solvent environment consisting of varying pH, salts and peptide molecules (Fig. A.1) [7]. Polysaccharides are known to self-aggregate at acidic pH[8,9], undergo pH dependent complexation with peptides[10–12] and albumins[13,14] that display strong correlation to presence of salts[15]. Thus, the growth media composition potentially plays a vital role in mediating the solution properties of the extracellular polysaccharides, which subsequently affects the collective microstructure of the biofilm. Here we investigate this proposition to understand how a growth environment promotes biofilm formation by altering the properties of the extracellular polymers.

Properties of staphylococcal extracellular polymers in growth media solvents

Using extracellular polymers (EPS) synthesized by *Staphylococcus epidermidis*, we show that different growth media have a significant impact on the solution behavior of the EPS.

EPS was extracted from shaker grown biofilm Vuong et al[16] and diluted in a solvent of tryptic soy broth with 1 wt.% glucose (TSBG) to the required final concentration (see Chapter 4). Solution behavior at different pH was studied by measuring the absorbance (λ = 600 nm, GENESYS 20, Thermo Scientific).

Figure A.2A shows the changes in absorbance of *S. epidermidis* EPS at different pH in TSBG. At all concentrations studied, significant pH dependence in absorbance was seen with the onset of turbidity at pH < 6.5. The turbidity decreased by about 15 % at pH < 5 for all concentrations. Onset of turbidity at pH < 6 was found in LBB and BHI as well, which are also frequently used for culturing *S. epidermidis* biofilms (see Fig. A.2B). Figure A.2C shows photographs of EPS (at 0.05 wt. %) in TSBG at different pH. Around the vicinity of pH ~ 6, consistent with that found *in situ* biofilms, we identify the formation of stringy precipitates that appear to re-dissolve partially at pH < 6 and completely at pH > 7. Formation of stringy precipitates was not observed in water (data not shown). Therefore, Fig. A.2 summarizes that the growth media has a unique impact on the solution behavior of biofilm extracellular polymers at different pH and concentrations. It is to be noted that the EPS studied here is a composite consisting primarily of a partially de-acetylated N-acetylglucosamine polymer (~ 65 %) and smaller amounts of proteins and nucleic acids (~ 35 %). Following Stewart, Ganesan et al. (see Chapter 4), we attribute the turbidity to be due to thermodynamic phase instability in the polymer. We hypothesize that the components of bacterial growth media are opportune that the solvent is a thermodynamic bad solvent for the EPS which prevents the polymers from

dissolution thus promoting biofilm formation by instead enabling the polymers to bind to the cell wall.

Solution properties of a model polysaccharide in growth media

To validate our claim we identify the specific component of the growth media that induces the most drastic change in solution behavior observed in Fig. A.2. For this, we tracked the evolution in hydrodynamic radius (R_H) of a model polysaccharide versus pH in water containing different components of TSBG.

We chose chitosan, as used earlier by Stewart, Ganesan et al. (see Chapter 4) to mimic the glycosaminoglycan contained in *S. epidermidis* EPS. We work with a dilute concentration (less than the overlap concentration of chitosan[17]) to track the properties of a single polymer chain and avoid possible concentration dependent aggregation. The solution property was tracked by measuring the hydrodynamic radius (R_H) using dynamic light scattering (DLS) at a fixed scattering angle of 90° (ALV CGS3, ALV Langen, Germany).

To ensure chitosan is a suitable model polymer, we check if it exhibits similar pH dependent changes in TSBG. Figure A.3A shows that at different chitosan concentrations, the R_H increases with pH. Beyond a critical value, pH_c, the solution became turbid, indicating the onset of an unstable phase. DLS measurements were not performed for $pH > pH_c$ as the solution was multiple scattering. The variation of pH_c with chitosan concentration is shown as an inset. Thus, in relevance to the biofilm, the local pH ranges *in situ* presumably impacts the solution property of the EPS differently based on the local polymer concentration *in situ*.

We now investigate the different components of TSBG on their role in impacting chitosan R_H. The components of TSBG are tryptone (20 g/L), K_2HPO_4 (2.5 g/L) and NaCl (5 g/L). In Figure A.4, we track the change in R_H for chitosan versus pH in water containing each of the above components. The presence of 5 g/L NaCl caused < 10% change in the R_H of chitosan at all pH studied (see Fig. A.4A). On the other hand, in 2.5 g/L K_2HPO_4, the R_H of chitosan decreased by ~ 25 % with increase in pH. As a control, the behavior in pure water is also plotted. We find that in the presence of salts, the R_H of chitosan is ~ 30% higher than in the absence of salts, which is typical since salts drives aggregation. K_2HPO_4 is known to precipitate chitosan in aqueous solutions[18]. This could potentially indicate that while K_2HPO_4 is added as a buffering agent in growth media, the presence of the HPO_4^{2-} ions could inhibit these polysaccharides from going into solution.

Figure A.4B shows the pH dependence of chitosan R_H in water containing different amounts of tryptone. We find that for tryptone concentration ≤ 2 g/L, the change in R_H of chitosan with pH was negligible. However, at a tryptone concentration of 10 g/L, chitosan exhibited a dramatic 250 % increase in R_H at pH > 5. To test its behavior at higher tryptone concentration, we measured the absorbance, as the opacity of the solution resulted in multiple scattering. Fig. A.4C shows this result. At 2 g/L no change in absorbance was noted at all pH studied. However, in solutions of 10 g/L and 20 g/L tryptone the absorbance increased ~ 10^2 fold at pH > 4. The formation of stringy precipitates in 20 g/L tryptone, as seen in EPS, is shown as photographs. Tryptone or TSBG on its own, does not exhibit any change in absorbance with pH (data not shown).

Thus, amongst the different components of TSBG growth media, in comparison to the salts, the presence of peptides was found to be most significant in mediating the solution

behavior of the model EPS polysaccharide at pH > 5. The phenomena driving the formation of stringy materials, indicative of phase instability in the presence of tryptone is as yet unclear.

Impact of pH change for *S. epidermids* biofilms

Earlier, we observed that changing the pH of the solvent mobilized bacteria in *S. epidermidis* biofilms (see Chapter 4). Here, we show that, it is precisely the re-dissolution of surface attached extracellular polysaccharides at higher pH that results in the biofilm bacteria to become mobile.

We grew *S. epidermids* biofilms in TSBG following Stewart et al.[19], and after 18 h growth, the supernatant was replaced by filtered DI water buffered to different pH, and the culture was set aside for 4 h at room temperature. The concentrations N-acetylglucosamine (GlcNAc), extracellular proteins and DNA, in the supernatant was then measured using the Smith-Gilkerson assay[20] and the NanoDrop (Thermo Scientific) respectively.

When the pH of the solvent was increased beyond 7, we saw that there was a significant release of glycosaminoglycans, proteins and nucleic acids from cell surfaces into the supernatant (see Fig. A.5). This can be attributed to the re-dissolution of the biofilm EPS at higher pH (as seen in Fig. A.2A). That is, if the solvent was modified such that it favored polymer dissolution, or was no longer a thermodynamic bad solvent, then, the biofilm structure is disrupted, induced by dissolution of the extracellular polymers, resulting in adhered bacteria to become mobile.

Thus, we identified that the presence of peptide sequences in the growth media induce a form of instability in biofilm polysaccharides at different pH. Furthermore, this instability was essential for biofilm formation, since, inducing polymer stability by changing solvent pH caused

loss of surface attached polymers from the biofilm resulting in the mobilization of biofilm bacteria. Further experiments at different chitosan concentrations followed by molecular dynamic simulations are necessary to understand the precise role of peptides such as tryptone in affecting the structure of polysaccharides at different pH. Collectively, the findings will provide an insight to understand how the growth environment contributes to biofilm formation, which can subsequently support development of novel biofilm removal techniques.

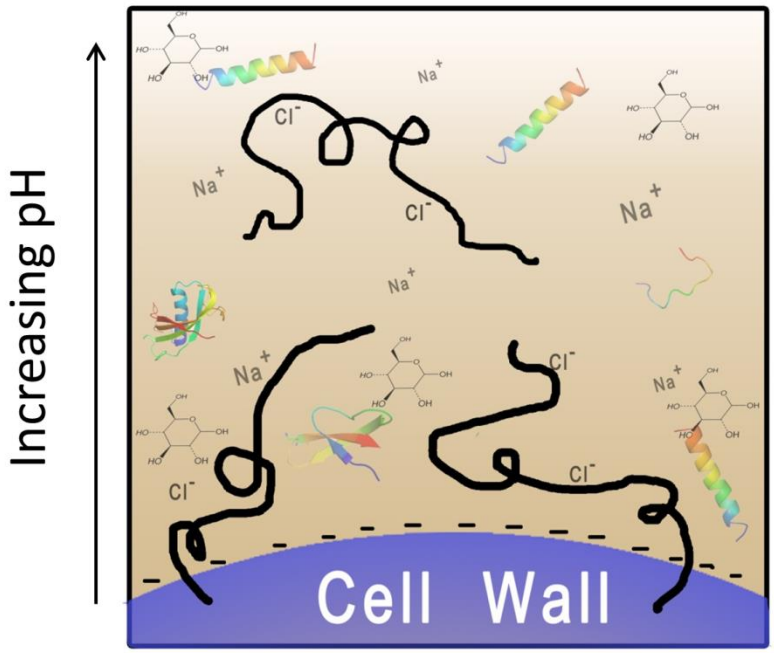

Figure A.1. A schematic depicting a biofilm polysaccharide (solid black curve) being released into the growth environment that contains cationic and anionic molecules (depicted with Na^+ and Cl^- as example), peptides (depicted as multi-colored coils) and sugar molecules (represented as glucose molecules) . The presence of pH microenvironment is depicted by a gradient in the surrounding color

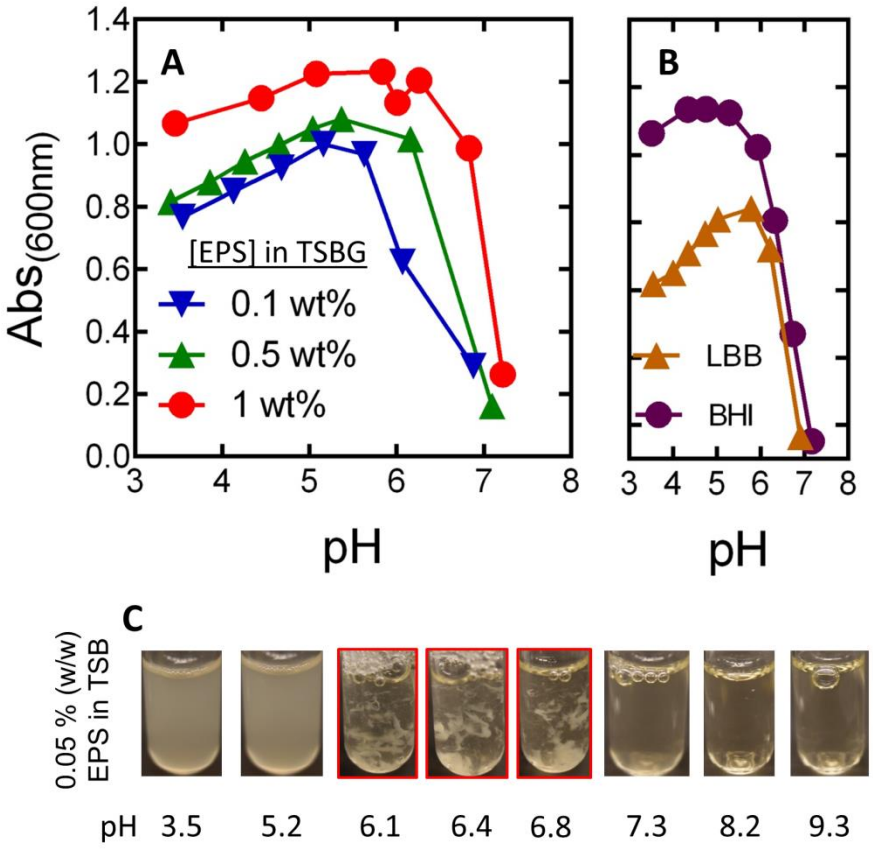

Figure A.2. (A) Absorbance vs. pH of *S. epidermidis* EPS at different concentrations, [EPS], in TSBG growth media. **(B)** Absorbance vs. pH of *S. epidermidis* EPS at 0.1 wt. % in growth media LBB and BHI. **(C)** Photographs of 0.05 wt .% EPS in TSBG media at different pH. Formation of stringy precipitates is indicated by a red border.

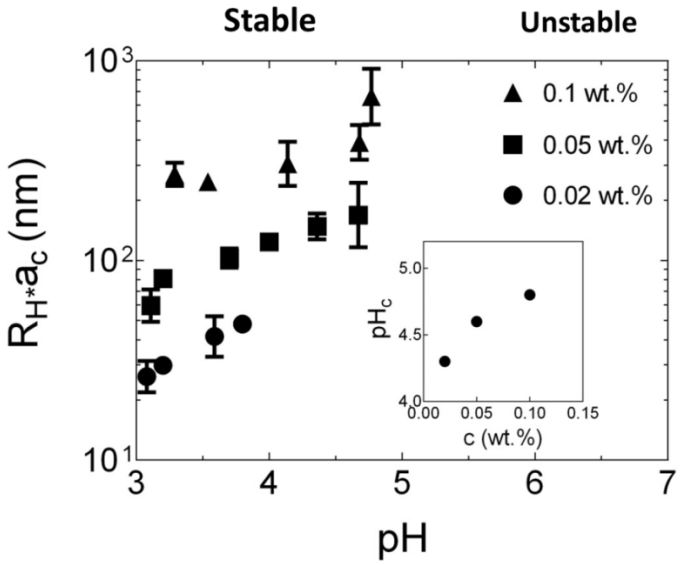

Figure A.3. R_H vs. pH for chitosan at different concentrations in TSBG growth media. The curves are scaled by an arbitrary factor a_c for better clarity. (inset) Critical pH, pH_c, marking onset of turbidity as a function of chitosan concentration.

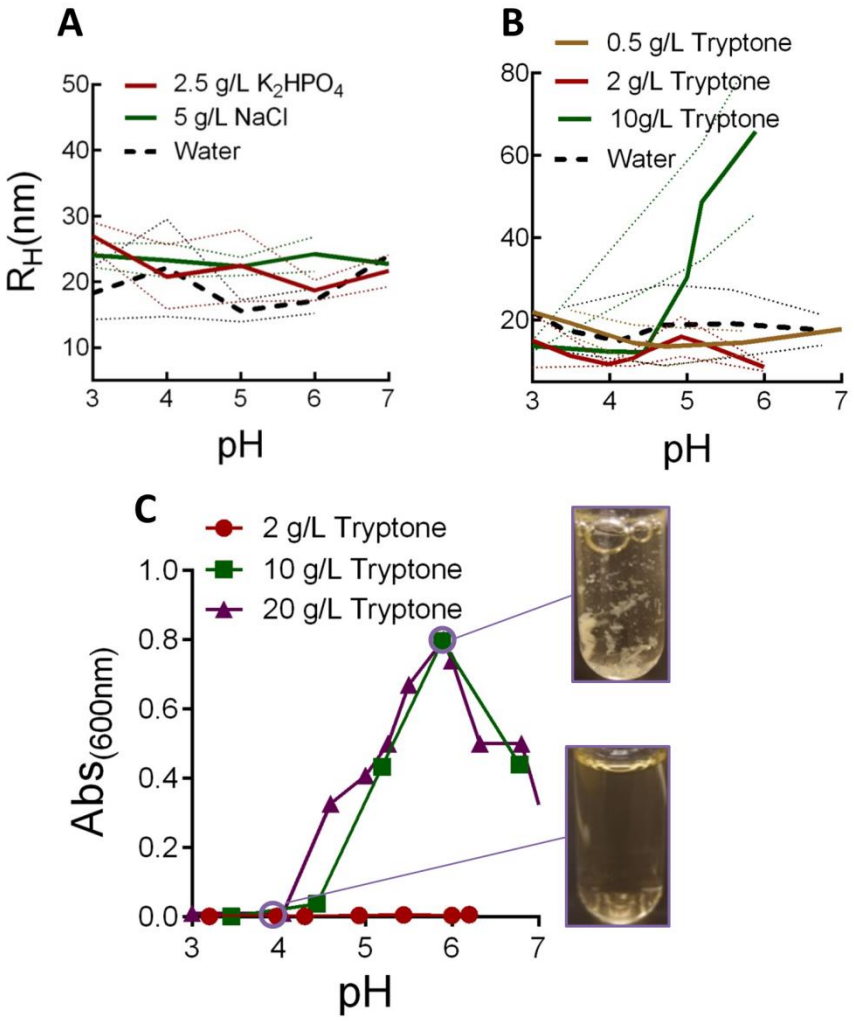

Figure A.4. (A) R_H vs pH for 0.1 wt.% chitosan in water, 2.5 g/L K_2HPO_4 and 5 g/L NaCl. **(B)** R_H vs pH for 0.1 wt. % chitosan in water containing different concentrations of tryptone. **(C)** Absorbance vs. pH for 0.1 wt. % chitosan in water containing different concentrations of tryptone. The photographs pertain to chitosan solutions in 20 g/L tryptone.

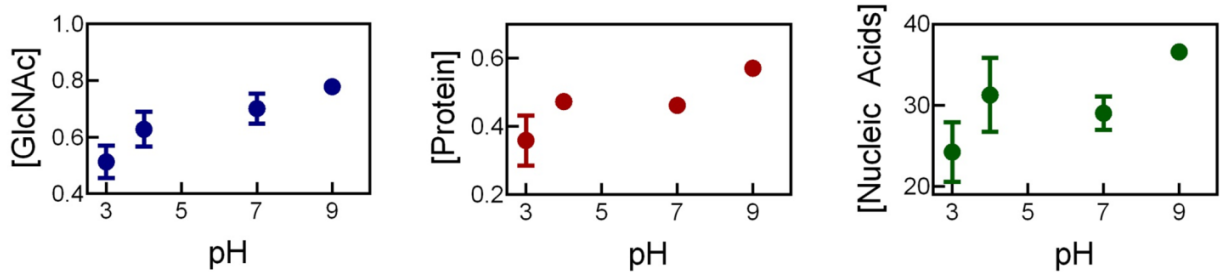

Figure A.5. Concentrations of N-acetylglucosamine, GlcNAc (mM, left), extracellular protein (mg/mL, middle) and extracellular DNA (ng/μL, right) in the supernatant water that was used to re-suspend *S. epidermidis* biofilms as a function of pH.

References

1. Flemming, H.-C. & Wingender, J. The biofilm matrix. *Nat. Rev. Microbiol.* **8,** 623–633 (2010).
2. Sutherland, I. W. The biofilm matrix--an immobilized but dynamic microbial environment. *Trends Microbiol.* **9,** 222–7 (2001).
3. Atlas, R. M. *Handbook of microbiological media*. **1,** (CRC press, 2004).
4. Lindgren, J. K. *et al.* Arginine deiminase in Staphylococcus epidermidis functions to augment biofilm maturation through pH homeostasis. *J. Bacteriol.* **196,** 2277–2289 (2014).
5. Wang, F. *et al.* Development of luminescent pH sensor films for monitoring bacterial growth through tissue. *Adv. Healthc. Mater.* **3,** 197–204 (2014).
6. Ganesh, a. B. & Radhakrishnan, T. K. Fiber-optic sensors for the estimation of pH within natural biofilms on metals. *Sensors Actuators B Chem.* **123,** 1107–1112 (2007).
7. Beveridge, T. J., Makin, S. A., Kadurugamuwa, J. L. & Li, Z. Interactions between biofilms and the environment. *FEMS Microbiol. Rev.* **20,** 291–303 (1997).
8. Schatz, C., Viton, C., Delair, T., Pichot, C. & Domard, A. Typical physicochemical behaviors of chitosan in aqueous solution. *Biomacromolecules* **4,** 641–648 (2003).
9. Anthonsen, M., Varum, K., Hermansson, a, Smidsrod, O. & Brant, D. Aggregates in acidic solutions of chitosans detected by static laser light scattering. *Carbohydr. Polym.* **25,** 13–23 (1994).
10. Herasimenka, Y. *et al.* Interaction of antimicrobial peptides with bacterial polysaccharides from lung pathogens. *Peptides* **26,** 1127–1132 (2005).
11. Zhang, L., Furst, E. M. & Kiick, K. L. Manipulation of hydrogel assembly and growth factor delivery via the use of peptide–polysaccharide interactions. *J. Control. release* **114,** 130–142 (2006).
12. Seal, B. L. & Panitch, A. Physical polymer matrices based on affinity interactions between peptides and polysaccharides. *Biomacromolecules* **4,** 1572–1582 (2003).
13. Kayitmazer, A. B., Strand, S. P., Tribet, C., Jaeger, W. & Dubin, P. L. Effect of polyelectrolyte structure on protein-polyelectrolyte coacervates: coacervates of bovine serum albumin with poly(diallyldimethylammonium chloride) versus chitosan. *Biomacromolecules* **8,** 3568–3577 (2007).
14. Gurov, A. N., Gurova, N. V, Leontiev, A. L. & Tolstoguzov, V. B. Equilibrium and non-equilibrium complexes between bovine serum albumin and dextran sulfate—I. Complexing conditions and composition of non-equilibrium complexes. *Food Hydrocoll.* **2,** 267–283 (1988).
15. Wang, X., Lee, J., Wang, Y.-W. & Huang, Q. Composition and Rheological Properties of β-Lactoglobulin/Pectin Coacervates: Effects of Salt Concentration and Initial Protein/Polysaccharide Ratio. *Biomacromolecules* **8,** 992–997 (2007).
16. Vuong, C. *et al.* A crucial role for exopolysaccharide modification in bacterial biofilm formation, immune evasion, and virulence. *J. Biol. Chem.* **279,** 54881–54886 (2004).
17. Rinaudo, M., Milas, M. & Dung, P. Le. Characterization of chitosan. Influence of ionic strength and degree of acetylation on chain expansion. *Int. J. Biol. Macromol.* **15,** 281–285 (1993).
18. LeHoux, J.-G. & Dupuis, G. Recovery of chitosan from aqueous acidic solutions by salting-out: Part 1. Use of inorganic salts. *Carbohydr. Polym.* **68,** 295–304 (2007).

19. Stewart, E. J., Satorius, A. E., Younger, J. G. & Solomon, M. J. Role of Environmental and Antibiotic Stress on Staphylococcus epidermidis Biofilm Microstructure. *Langmuir* **29,** 7017–7024 (2013).
20. Smith, L. R. & Gilkerson, E. Quantitation of Glycosaminoglycan Hexosamine Using 3-Methyl-2-Benzothiazolone Hydrazone Hydrochloride. *Anal. Biochem.* **98,** 478–480 (1979).